DISSERTATION

MYOCARDIAL AFTERLOAD REGULATES ATRIOVENTRICULAR VALVE DEVELOPMENT IN ZEBRAFISH

Submitted by

Neha Ahuja

Graduate Degree Program in Cell and Molecular Biology

In partial fulfillment of the requirements

For the Degree of Doctor of Philosophy

Colorado State University

Fort Collins, Colorado

Summer 2020

Doctoral Committee:

Advisor: Deborah Garrity

Danial Sloan
Don Mykles
Ronald Tjalkens

ABSTRACT

MYOCARDIAL AFTERLOAD IS A KEY REGULATOR OF ATRIOVENTRICULAR VALVE DEVELOPMENT IN ZEBRAFISH

The incidence of congenital heart disease (CHD) is estimated to be 1% of all human births. CHD of the heart valves occurs in over 50% of CHD cases. Despite significant clinical interest, the molecular mechanisms that govern valve development remain poorly elucidated. As the heart develops, blood flow and blood pressure increase rapidly to support the growing demands of the embryo. Our group has previously shown that pressure at the developing atrioventricular valve dramatically increases through development. Consequently, we hypothesized that afterload—defined as the pressure the ventricle must overcome in order to pump blood through the body—may be a cue that cardiac valve cells read and respond to build a valve leaflet. Here, we present a zebrafish model in which afterload has been increased through the use of vasopressin, a vasoconstrictive drug. We first show that application of vasopressin reliably produces an increase in afterload without directly acting on cardiac tissue in zebrafish embryos. To evaluate cardiac function and valve leaflet dynamics, we took a quantitative live-imaging approach. Consistent with pathology seen in adult human patients with clinically high afterload, we see defects in both form and function of the valve leaflets. To identify the cause of this functional defect, we utilized in situ hybridization to evaluate makers of cell differentiation for both valve leaflet cells and the adjacent myocardial cells. Our results suggest that this valve defect is due to changes in atrioventricular myocyte differentiation and signaling, rather than pressure directly acting on the valve leaflet cells. We next took a transcriptomics approach to identify regulators of atrioventricular myocyte differentiation and identified a subset of differentially expressed transcription factors that are putatively responsible

for sensing afterload. Together, our results show that afterload regulates the physiological and molecular state of the developing valve.

ACKNOWLEDGMENTS

I would like to thank my advisor, Dr. Deborah Garrity. I would not have been able to complete my PhD without your invaluable advice and mentorship. I have very much enjoyed my time working in your lab. Additionally, I would like to thank my committee members for their support and feedback throughout my graduate career.

I would also like to thank several undergrads that have worked on this project with me, especially Sam Ecket, Hailey Stapleton, Logan Bowey, Mary Mitchell, Uyakhan Masakazu, Ebonne Alexander, and William Hostetter. I would especially like to thank Paige Ostwald and Brandon Hylton. It was a privilege to mentor you when you were undergrads, and watching you grow and develop as scientists has been one of the most rewarding experiences of my career. I am excited to see what the future holds for you!

I would especially like to thank my family and friends for their support through my graduate career. I am especially grateful to my parents for instilling a love of science and education in me, and grateful to my brother, Nilesh Ahuja, for his unconditional support. I would also like to thank my partner, CJ Duran. I would not have made it through this year without all of you!

TABLE OF CONTENTS

ABSTRACT ii
ACKNOWLEDGMENTS iv
Chapter 1: Biomechanical Cues Direct Valvulogensis 1
Summary 1
Congenital Heart Defects 2
Incidence of Congenital Heart Defects 3
Types of CHD 4
Treatment of CHD 7
Causes of Congenital Heart Defects 9
Structure and function of mature valves 11
Valve Development 13
Linear Heart Tube Development 14
Endocardial Cushion Formation 16
Mesenchymal Cells Populate the Endocardial Cushions 22
Neural crest cells contribute to the development of the semilunar valves 23
Valve Extracellular Matrix Remodeling 25
Biomechanical inputs in heart development 26
Shear Stress 27
Pressure as a hemodynamic cue in valve development 33
Concluding Remarks 45
Dissertation Aims 46
Chapter 2: Myocardial Afterload Regulates Atrioventricular Valve Cell Differentiation 49
Summary 49
Introduction 50
Methods 53
Results 55
Vasopressin Actively Elicits Vasoconstriction in Zebrafish Embryos 55
Increased Afterload Alters Cardiac Function and Growth 57
Increased Afterload Induces Cardiac Hypertrophy and Alters Sarcomere Abundance 66
Increased Afterload Induces Retrograde Flow and Alters AVJ Mechanics 69
Increased Afterload Alters Myocardial AVJ Cell Specification 70
Increased Afterload Alters Endocardial AVJ Cell Specification 71

Discussion 72
Chapter 3 – Retrograde flow regulates valve development through klf2a 77
Summary 77
Introduction 78
Methods 80
Results 84
Onset of Klf2a expression at the atrioventricular junction accords with the period of high retrograde flow 84
Increases in RF and shear stress cause an elongation of the valve leaflet 87
Disturbed Hemodynamic Cues Lead to Increased ECM Production in Endocardial Cushions 91
Klf2a overexpression partially phenocopies vasopressin application 92
Increasing retrograde flow between 32-40 hpf is sufficient to increase ECM production and cause valve defects 96
Discussion 97
Chapter 4: Identification of Regulators of AVJ myocyte development 101
Summary 101
Introduction 101
Methods 105
Results 108
Conclusions 117
References 118
APPENDIX 1: Supplemental Material for Chapter 2 138
APPENDIX 2: Supplemental Material for Chapter 3 155
APPENDIX 3: Supplemental Material for Chapter 4 161

Chapter 1: Biomechanical Cues Direct Valvulogensis

Summary

The vertebrate embryonic heart initially forms with two chambers, a ventricle and an atrium, separated by the atrioventricular junction. Localized genetic and biomechanical information guides the development of valves, which function to ensure unidirectional blood flow. If the valve development process goes awry, pathology associated with congenital valve defects can ensue. Congenital valve defects (CVD) are estimated to affect 1-2% of the population and can often require a lifetime of treatment. Despite significant clinical interest, molecular genetic mechanisms that direct valve development remain incompletely elucidated. Cells in the developing valve must contend with a dynamic hemodynamic environment. A growing body of research supports the idea that cells in the valve are highly sensitive to biomechanical forces, which cue changes in gene expression required for normal development or for maintenance of the adult valve. This review will focus on mechanotransductive pathways involved in valve development across model species. We highlight current knowledge regarding how cells sense physical forces associated with blood flow and pressure in the forming heart, and summarize how these changes are transduced into genetic and developmental responses. Lastly, we provide perspectives on how altered biomechanical cues may lead to CVD pathogenesis.

Congenital Heart Defects

Congenital heart defects (CHD) are defects that occur when the heart fails to form properly and are a leading cause of infant mortality (Q. Yang et al., 2006). The incidence of CHD is estimated to be 1% of all human births ("Congenital Heart Defects," 2017). CHD of the heart valves occurs in over 50% of CHD cases. Heart valves prevent blood from flowing backwards into the heart. The prognosis for patients who have severe valve defects is grim. Often, the only treatment option available is valve replacement surgery, which carries an extremely high mortality rate—estimated to be 28% for neonates (Woods et al., 2012). Despite the clinical prevalence of CHD, the molecular mechanisms that lead to their pathogenesis remain elusive.

Vertebrate hearts have two sets of valves; the first set is located in between the upper chambers (atria) and lower chambers (ventricles) at the atrioventricular junction (AVJ). Atrioventricular valve development starts early in fetal development. Shortly after gastrulation is completed, the heart forms as a linear tube consisting of an outer myocardial (muscle) layer and in inner endocardial layer. The inner endocardial layer is in direct contact with blood flow, while the outer myocardial layer contracts to drive the heartbeat (Francesco Boselli, Freund, & Vermot, 2015). At four weeks of pregnancy, the valves begin developing. The first step in this process is endocardial cushion formation. Myocardial cells (myocytes) at the AVJ began secreting extracellular matrix proteins which assemble as a scaffold and create an enlarged local separation of the myocardial and endocardial layers. Endocardial cells then invade this space to form the endocardial cushions (Combs & Yutzey, 2009). The endocardial cushions then remodel into valve leaflets through continuing cell division and secretion of proteins. Small aberrations in this process can lead to pathology.

In this section, I will describe the prevalence of CHD, the current treatments for CHD and their associated risks, as well as what is known about the genetic and developmental basis for CHD.

Incidence of Congenital Heart Defects

There is some debate about the exact incidence of CHD, in part due to the diverse set of defects that can qualify as CHD. Some lesions are relatively minor and can heal on their own, while others require immediate surgery. Defects that are minor during infancy may become exacerbated during adulthood; it is estimated that 35% of patients will not present symptoms of CHD until after infancy (Mason, Kirby, Sever, & Langlois, 2005). In developed countries, estimates of the incidence of congenital heart disease ranges between 0.8% to 5% of all live births. The large variation in these estimates may be due to study design—some studies only include patients that need immediate surgery, while others end their evaluation at infancy and thus may not count patients whose symptoms present later in life. The current American Heart Association estimate for the incidence of CHD is eight of every thousand live births in the United States; of these affected individuals, six out of ten will have CHD severe enough to require immediate surgery (Van der Bom et al., 2011).

One of the most informative comprehensive studies regarding CHD epidemiology was conducted by Gilboa et al., in 2010. This group utilized death certificate data from 1999 to 2006 to calculate CHD mortality by age, sex, and race. During this period, they identified 41,494 CHD-related deaths and 27,960 CHD-directed deaths (Gilboa, Salemi, Nembhard, Fixler, & Correa, 2010). CHD-mortality was highest among infants, but mortality for all groups declined about 24% during this period. Notably, non-Hispanic blacks had an increased risk of mortality compared to non-Hispanic whites, though it is uncertain whether these differences are due to socio-economic reasons or underlying genetic differences. Males had a much higher risk of mortality as compared to females for all groups reported. While this could again be due to socioeconomic factors, it is intriguing to note that the prevalence of congenital heart defects present in males and females differs. For example, mitral valve prolapse is more likely to occur in females, while aortic valve stenosis is more likely to occur in males (Gilboa et al., 2010). As

more CHD patients survive to adulthood, long-term studies may provide valuable insight into the management of CHD.

Types of CHD

Clinically, CHD has been classified into three categories based on the frequency of care required: mild, moderate and severe (Warnes et al., 2008). Patients with a severe CHD have a poor prognosis and are recommended to follow up at an adult congenital heart disease center regularly (Table 1). Patients in this category have diseases including – but not limited to -- atresia of either the pulmonary, mitral, or tricuspid valve, transposition of the great arteries, or cyanotic congenital disease. One study evaluated survival rates among patients that had surgically-corrected severe CHD from 1980 to 2009, in an effort to better gauge patient outcomes. They found that 19% of their patients died during this time period, and that survival rates were markedly lower compared to the general population (Greutmann et al., 2015). Patients in the mild category have CHD require little to no intervention by a pediatric cardiac specialist and patients with moderate CHD should be seen periodically at congenital heart disease centers.

The state of congenital heart defect treatment is such that patients who survive initial surgery have a high likelihood of entering adulthood – approximately 96% of patients who survive their first year will be alive at age 16 (van der Bom et al., 2011). However, patients with all types of CHD have decreased life expectancy compared to the general population; as of 2007, the median age of death for patients with CHD was 57 years old (van der Bom et al., 2011). The vast majority of these deaths were due to arrhythmia, followed by congestive heart failure (Pillutla, Shetty, & Foster, 2009). There is significant clinical need for research that addresses long-term care of patients with CHD, as well as basic science research that evaluates the progression of congenital heart defects in aging models.

The following section will briefly describe the physiology of common congenital heart defects in each clinically relevant category.

Tricuspid Atresisa. Tricuspid atresia is a severe defect that occurs in the tricuspid valve, which is located in between that right atrium and the right ventricle. Atresic valves develop such that they block blood flow from the right atrium to the right ventricle, and consequently prevent blood flow to lungs (Ghodke, Kalkekar, & Radke, 2014). While there are several causes of tricuspid atresia,

Transposition of the Great Arteries (TGA). TGA is a complex defect which occurs when either of the two great arteries (the pulmonary artery or the aorta) are attached to the wrong ventricle. For example, the aorta maybe attached to the right ventricle, leading to deoxygenated blood being pumped to the body (Gutgesell, Garson, & McNamara, 1979).

Single Ventricle. Single ventricle syndrome is a condition where only one ventricle develops, leading to mixing of oxygenated and deoxygenated blood. This

particularly severe condition requires three separate surgeries to repair (d'Udekem et al., 2012).

Ebstein's Anomaly. Ebstein's anomaly occurs when one or more of the leaflets of the tricuspid valve is displaced, impeding closure between the two right-sided chambers. This is considered a moderate to severe defect (Jost et al., 2007).

Atrioventricular Canal Defect. This mild defect occurs when a hole forms in the center of the heart, allowing the mixing of blood between all four cardiac chambers (Pettersen, 2019).

Absent Pulmonary Valve. This mild defect occurs when the pulmonary valve – between the right ventricle the pulmonary arch—fails to develop (Wu et al., 2015).

Isolated Congenital Mitral Valve Disease. This disease includes a number of malformations of the mitral valve (Stellin et al., 2000).

Table 1.1 Types of Congenital Heart Defects

Category	Type	Incidence	Treatment	Mortality without treatment	Mortality with treatment	References
Severe	Tricuspid Atresia	2 in every 10,000 births	Fontan Procedure	90% at ten years	40% at 20 years	(Ghodke et al., 2014; Sittiwangkul, Azakie, Van Arsdell, Williams, & McCrindle, 2004)
	transposition of the great arteries	30 in every 100000 live births	Arterial Switch Operation, Prostaglandin	50% at 1 month	10% at 20 years	(Gutgesell et al., 1979; Villafañe et al., 2014)
	single ventricle	4-8 in every 10,000	Multiple Surgical Procedures	usually fatal with in the first month	39% at 10 years	(d'Udekem et al., 2012; O'Leary, 2002)
Moderate	Ebstein's Anomaly	1 out of 200,000 live births	Repair or replacement of valve	60% at 1 month	18% at 20 years	(Jost et al., 2007)
	Atrioventricular Canal Defect	3 out of every 10,000 births	Surgical Repair	46% at 6 months of age	17% at 10 years	(Pettersen, 2019)
	Absent Pulmonary Valve	3 out of every 10,000 births	Surgical Procedure dependent on defect	death between 3 and 6 months of life	19% at 20 years	(Wu et al., 2015; Yong et al., 2014)
Mild	Isolated Congenital Mitral Valve Disease	5 out of every 100,000	Surgical Repair or Replacement	highly variable and dependent on severity	4% at 12 years	(Remenyi & Gentles, 2012) (Stellin et al., 2000)

Treatment of CHD

Treatment of CHD is done primarily through surgical correction. It should be noted complete correction of the defect is rare; instead, most corrections are palliative – that is to say, the correction does not restore normal cardiac function but rather is the best available option to extend life. These surgeries often leave behind residua and sequela, or structural abnormalities resulting from surgery. Common complications include arrhythmia, valve regurgitation, and heart failure. In addition to these sequela, surgical patients are at an increased risk for endocarditis. The following section will describe common surgical procedures and their associated outcomes.

Fontan Procedure. The Fontan procedure was first developed to treat patients with tricuspid atresia in 1968. Subsequently, this surgical technique is most commonly used as part of a suite of palliative surgeries required for patients with single ventricle syndrome. The Fontan procedure involves creating a separate circulatory pattern to avoid nonfunctional regions to the heart. For example, in patients with a hypoplastic left ventricle – wherein the left ventricle in underdeveloped and unable to pump blood to the body – the inferior vena cava is rerouted to connect to the pulmonary artery directly, allowing deoxygenated blood from the body to directly proceed to the lungs. This allows the right ventricle to become the main pump for the body and blood to bypass the damaged left ventricle entirely (Cześniewicz & Kusa, 2017).

While the Fontan procedure has dramatically improved outcomes for patients with either atresia or single ventricle syndrome (Table 1), the surgery is palliative and patients consequently develop a variety of complications. In patients with Fontan circulation, pulmonary vascular resistance is added to the venous return circuit, dramatically increasing resistance on single pumping ventricle. This will, in time, cause the ventricle to degrade. Additionally, due to higher chronic systemic venous pressure, all organic systems in the body are exposed to chronic venous congestion, leading to multisystem organ failure. Indeed, Fontan-associated liver disease results from alterations of the liver structure to due to Fontan circulation. More

work needs to be done to understand best practices for adult patients that have undergone the Fontan procedure during infancy, especially as surgical techniques become more advanced and lead to patients surviving longer (Kim et al., 2018).

Arterial switch operation (ASO). ASO is a procedure developed to treat patients with transposition of the great arteries. At birth, patients are usually given prostaglandin, which works to keep the ductus arteriosus (the fetal connection between the pulmonary artery and aorta) open and allow a temporary increase in blood flow (Gutgesell et al., 1979). During this procedure, neonates are hooked up to a heart-lung machine while the surgeon transects the pulmonary artery and the aorta and ligates them back into their correct places. Despite being an open-heart surgery, ASO has an extremely low perioperative mortality rate of less than 2% (Villafañe et al., 2014).

Because ASO is a relatively new operation (first performed in 1975), there is little data available on long-term complications and outcomes. While we know that ASO dramatically reduced patient mortality (Table 1), it has become apparent that further complications can occur later in life. The most common complication involves coronary artery blockage. In TGA, the location of the coronary arteries on the aortic root is highly variable, and coronary arteries must be transferred to the neoaorta. This can be technically difficult, and coronary artery obstruction is a/the leading cause of death among patients that have undergone ASO (Breinholt & John, 2019). Additionally, pulmonary valve complications are exceedingly common. Because the pulmonary valve is not designed to withstand high pressures associated with aortic circulation, it is thought that the excessive burden placed on the pulmonary valve from being connected to the neoarota can cause valve dysfunction. Pulmonary valve stenosis is the most common cause of reoperation in ASO patients, with a severe stenosis being present among 10-30% of patients (Choi et al., 2010). Despite these complications, prognosis for patients with ASO remains relatively positive.

Balloon Dilation. Balloon dilation is a technique used to repair congenital valve defects, most commonly pulmonary valve stenosis. In this technique, a catheter with an inflatable balloon is inserted through the patient's groin. The catheter is threaded all the way through the patient's heart, and the balloon is deployed at the pulmonary valve. The inflated balloon serves to open the stenoic valve and works to restore normal blood flow patterns. Indeed, long-term survivability is excellent, with preliminary studies indicating patients exhibit average life expectancies comparable to the rest of the population. However, balloon dilation is not without its risks – approximately 20% of patients require cardiac re-intervention (Voet et al., 2012). In a study that evaluated outcomes of infants with tetralogy of Fallot and pulmonary stenosis who had undergone the balloon dilation procedures, 57% of patients developed pulmonary valve regurgitation 5 years after the procedure (Hofferberth et al., 2018). Despite suboptimal long-term outcomes, balloon dilation remains standard of care due its non-invasive nature and because it does not preclude later, more robust intervention.

Transcatheter Valve Replacement. Transcatheter valve replacement is used to treat patients that have severe, isolated valve defects. It is a relatively new surgical technique, first used in the year 2000. Transcatheter valve replacement, similar to balloon angioplasty, involves inserting a catheter into the patient's groin and guiding it to heart. When in position, an umbrella-like device will deploy and release the replacement valve. Due to challenges regarding growth of the valve concomitant with the child, valve repair is almost always preferred.

Causes of Congenital Heart Defects

Congenital heart defects have complex etiology; the genetic cause for CHD can only be identified in approximately 30% of cases. Complicating our understanding of the underlying genetics of CHD is the large variation in penetrance and expressivity associated with the disease. For example, some individuals with known pathological gene variants display no overt phenotype. However, studies indicate that a family member with CHD represents a 5-fold

increased risk factor for the disease. Indeed, co-occurrence rates between siblings are approximately 4.1% (Kuo et al., 2017). These lines of evidence suggest that despite having complex etiology, congenital heart defects are heritable.

Over 400 genes are associated with CHD pathogenesis. These genes include transcription factors, epigenetic modifiers, and cell signaling transducers. Many of these genes work synergistically and are connected in the same gene regulatory network, suggesting a broad network may regulate heart development (Kuo et al., 2017). Mutations in single genes appear to have variable penetrance in the human patient population, suggesting interactions between multiple genes regulate the development of CHD. Because of these higher order interactions, interest in epigenetic regulation during heart development has increased. Several studies have identified aberrant expression of epigenetic markers in human CHD patients. For example, DNA hypermethylation of several genes including *has2*, *nxk2.5,* and *mef2c* have been found in patients with varying types of CHD (Jarrell, Lennon, & Jacot, 2019). Together, this evidence suggests that shifts in networks that regulate heart development underlie CHD pathology.

Approximately half of all neonates born with Down's syndrome have a CHD. While the relationship between Down's syndrome and CHD has not been fully elucidated, two hypotheses exist to explain this high incidence. The gene-dosage hypothesis postulates that an increase in gene expression related to trisomy 21 causes the CHD. The gene-mutation hypothesis postulates that mutations at Down's syndrome associated loci can cause CHD. In support of the gene-dosage hypothesis, several candidate genes on chromosome 21 have been shown to cause increased risk for CHD. For example, collagen VI (COL6A1) is expressed in fetal hearts beginning at 5 weeks post conception. Overexpression of COL6A1 is thought to contribute to pathogenesis of atrioventricular septal defects. More work is required to identify mechanistic links between Down syndrome and CHD (H. Zhang, Liu, & Tian, 2019).

Structure and function of mature valves

Over the lifetime of an individual, valve leaflets must withstand extraordinary physical demands. Heart valves open and close as many as 40 million times a year and 3 billion times over an average lifetime. Unobstructed forward blood flow in the heart demands that leaflets (in the tricuspid and mitral valves) or cusps (in the pulmonary valve and aortic valve) maintain substantial mobility, pliability and structural integrity. Valve tissues close when mechanical forces decrease, based on their intrinsic elastic properties. For valves to prevent backflow, the cusps must stretch and mold to fully cover the orifice, and they must resist back pressure present in the downstream anatomy of the heart. All four cardiac valves display a similar three-layered architecture, which contributes to their incredible strength, durability and flexibility (Flanagan & Pandit, 2003; Schoen, 2008). Valve endothelial cells (VECs) line the entire outer surface of the valve leaflet and serve to limit inflammatory cell infiltration and lipid accumulation. The mammalian vertebrate heart has four sets of valves: the aortic and pulmonary semilunar valves separate the ventricles from circulation, whereas the mitral and tricuspid valves separate the atria from the ventricles. Each of these valve leaflets has a unique physiology and structure that allows them to meet their local hemodynamic and locational challenges (Pozzoli, Zuber, Reisman, Maisano, & Taramasso, 2018). Inside the valve, valve interstitial cells (VICs) are arranged in three layers, termed the fibrosa layer, the spongiosa layer, and the ventricularis layer. Cells in each layer produce a specialized extracellular matrix (ECM). The mammalian vertebrate heart has four sets of valves: the aortic and pulmonary semilunar valves separate the ventricles from circulation, whereas the mitral and tricuspid valves separate the atria from the ventricles. Each of these valve leaflets has a unique physiology and structure that allows them to meet their local hemodynamic and locational challenge (Pozzoli et al., 2018).

Within the fibrosa layer, densely packed collagen fibers are arranged in a circumferential orientation. Collagen fibers in the fibrosa are primarily responsible for the load-bearing

properties of heart valves. Fibrillar collagen is notable for its high tensile strength when taut, due to its intertwined triple-helix structure, but it cannot be compressed. Therefore, during systole, as the valve constricts and opens, collagen fibers adopt a crimped, corrugated, and less aligned conformation. During diastole, as the valve closes and leaflets span the orifice, collagen fibers unfold and adopt a parallel orientation.

The cyclical nature of the heartbeat requires that collagen fibers be extremely sensitive to instantaneous mechanical stretch. The spongiosa layer is organized as a porous gel matrix composed of proteoglycans interspersed with randomly oriented collagen and fine layers of elastic tissue. Proteoglycans are composed of a protein core covalently linked to smaller linear sugar polymers termed glycosaminoglycans. Due to the dense negative charges on the glycosaminoglycan side chains, proteoglycans attract and bind water abundantly. The hydrated matrix cushions compressive forces and absorbs stresses during valve closure. It also provides lubrication between the fibrosa and ventricularis layers and sustains the flexibility of the leaflets during constant valve motion.

Finally, the ventricularis is a thin layer enriched in radially-oriented elastic fibers that provide the stretchiness necessary for the leaflets to repeatedly deform and reform. Elastin is a long hydrophobic protein that coils to minimize exposure of its surface to water. When the valve is open, elastin fibers are forced into an elongated and taut configuration that provides a physical resistance. As the valve closes, tension is relieved and elastin rebounds, thus helping to restore the retracted conformation of the leaflet or cusp. The ventricularis layer is adjacent to the endothelial surface directly exposed to incoming blood flow, whereas the fibrosa layer, on the opposite side, is near the surface commonly exposed to turbulent flow just beyond the valve. Over the lifetime of the organism, the durability of the valve requires constant monitoring of the valvular ECM. The optimal amount, quality, and arrangement of collagen, elastin and glycosaminoglycans contributes to the ability of cells in the valve tissue to sense their mechanical environment and transduce that information intracellularly to mediate molecular

changes. Active function of the valve requires synthesis, remodeling and repair of ECM components, particularly collagen, elastin and glycosaminoglycans.

In the United States, valve disease has an overall prevalence of approximately 2.5% and imposes a health care burden of approximately one billion dollars per year. Treatment is often limited to surgical interventions (Lincoln & Garg, 2014). Both congenital valve disease and acquired valve disease result in ECM disorganization and VIC activation, leading to fibrotic valve leaflets that fail to ensure unidirectional blood flow. Over time, ineffectively functioning valves can lead to decreased cardiac output and cardiac failure. While the majority of valve diseases onset during adulthood, the origin of these diseases is often related to development – either through congenital malformations that grow increasingly severe with time or through the activation of normally quiescent fetal gene programs (Dirkx, da Costa Martins, & De Windt, 2013; Lincoln, Alfieri, & Yutzey, 2004). For example, Bicuspid Aortic Valve disease (BAV) is a common congenital malformation and is estimated to affect approximately 0.5-2% of people worldwide. The aortic valve usually develops with three leaflets; patients with BAV develop aortic valves with two unequal-sized leaflets. BAV is usually asymptomatic during childhood, but over time progresses to more serious conditions such as aortic valve calcification (Siu & Silversides, 2010). A greater understanding of the mechanisms that control valve development may aide our understanding of mechanisms that promote valve disease.

Valve Development

Heart valve defects occur in 20-30% of congenital heart defects, and the incidence of valve defects has been estimated as high as 5% of live births (Combs & Yutzey, 2009). As one example, BAV, the most common etiology to require an adult heart valve replacement, is caused by defects in the development of the aortic valve. Despite their physiological differences, the initial development of the four sets of valves is quite similar. The following section will describe the developmental processes that give rise to valve leaflets.

Linear Heart Tube Development

Following gastrulation, mesenchymal cells from the mesoderm migrate laterally to form separate but bilateral regions, termed the primary heart fields. Even before the heart tube forms, atrial and ventricular precursor cells already express distinct genetic programs and reside in distinct areas. Mesodermal cells from the primary heart field then migrate to the midline and coalesce into a structure termed the cardiac crescent in humans, mice and chick, and the cardiac cone in zebrafish. The cardiac crescent or cone eventually remodels to give rise to the linear heart tube (Wagner & Siddiqui, 2007), consisting of two cell layers: an outer myocardial cell layer and an inner endocardial cell layer separated by an acellular ECM termed the cardiac jelly. Valve development begins soon after linear heart tube formation.

The earliest stages of heart formation involve the specification of the cardiogenic mesoderm within the splanchnic mesoderm, in bilateral regions termed the primary heart field. This is accomplished through signals from overlying ectodermal cells as well as from a transitory cell signaling center that organizes gastrulation (termed Henson's node in chickens and mammals, the Spemann Organizer in amphibians, and Kupffer's vesicle in zebrafish). The anterior endodermal cells secrete paracrine factors such as Bone Morphogenetic Protein 2 (BMP2) and Fibroblast Growth Factors, which act as positive signals for cardiogenic mesoderm induction. Inhibitory signals such as Chordin, Noggin, and Wnt3a serve to restrict cardiac induction to a subset of the splanchnic mesoderm. This combination of signaling factors serves to induce expression of cardiogenic transcription factors such as T-box transcription factors, Tal1, and GATA. These regions of specified cardiogenic mesoderm are termed the bilateral primary heart fields (Wagner & Siddiqui, 2007).

Cardiac progenitor cells must translocate from the bilateral heart fields to the body midline and reassemble to form the cardiac crescent (or cone). The migratory process is facilitated by endocardial cells and their associated extracellular matrix. Current research suggests that endocardial cells originate from a specific population of mesodermal cells within

the primary heart field (Haack & Abdelilah-Seyfried, 2016). Migration from the heart field to midline and subsequent fusion is regulated by a combination of paracrine signaling and extracellular matrix proteins. For example, knockdown of the paracrine factor *vegfa* or its receptor leads to failure of endocardial tube fusion in zebrafish (Fish et al., 2011). Additionally, it is thought that expression of the myocardial gene *Tmem2* creates an extracellular matrix environment that facilitates endocardial cell migration (Totong et al., 2011).

After endocardial cells assemble into a midline endocardial tube, myocardial cells are recruited around the endocardial cells to form a two-layered heart tube. In contrast to endocardial cells – which migrate as individual cells – evidence from zebrafish embryos indicates that myocardial cells migrate as a sheet (Trinh & Stainier, 2004). This process is regulated by ECM components, such as fibronectin, as well as by communication from the adjacent endodermal cells. For example, disruption of platelet-derived growth factor (PDGF) through mutation of its receptor, *pdgfra*, prevented myocardial migration towards the midline in zebrafish embryos. The PDGF ligand is expressed by endodermal cells at the midline of the embryo and acts as an instructive cue to direct myocardial cell migration (Bloomekatz et al., 2017). Fibronectin is a multi-domain glycoprotein that gradually assembles into an insoluble fibrillar matrix by binding other fibronectin proteins, and ECM components including collagens, proteoglycans and integrins. Knockdown of fibronectin prevents myocardial cell migration in zebrafish embryos and mouse embryos (George, Baldwin, & Hynes, 1997; Trinh & Stainier, 2004). In zebrafish *cloche* mutants, which lack the endocardial cells that produce fibronectin, the myocardial cells still initiate migration, but are unable to assemble into a cardiac cone at the midline (Holtzman, Schoenebeck, Tsai, & Yelon, 2007). This observation suggests that signals from endocardial cells facilitate the directional migration of myocardial cells, though the molecular mechanisms behind the process are unclear. The correct completion of this process results in the formation a two-layered heart tube.

Endocardial Cushion Formation

After formation of the linear heart tube, the heart initiates cardiac looping and ballooning. During these processes, the linear heart tube grows in cell number and begins to fold into an S-shape that evolves into a two-chambered heart. Concomitantly, the endocardial cushions, which are thickened mounds of specialized ECM in association with endocardial cells, accumulate at the atrioventricular junction and at the outflow tract. The endocardial cushions, in association with adjacent endocardial cells, give rise to the valve leaflets at these two locations (Combs & Yutzey, 2009). The following sections describes current knowledge regarding development of the endocardial cushions (Figure 1).

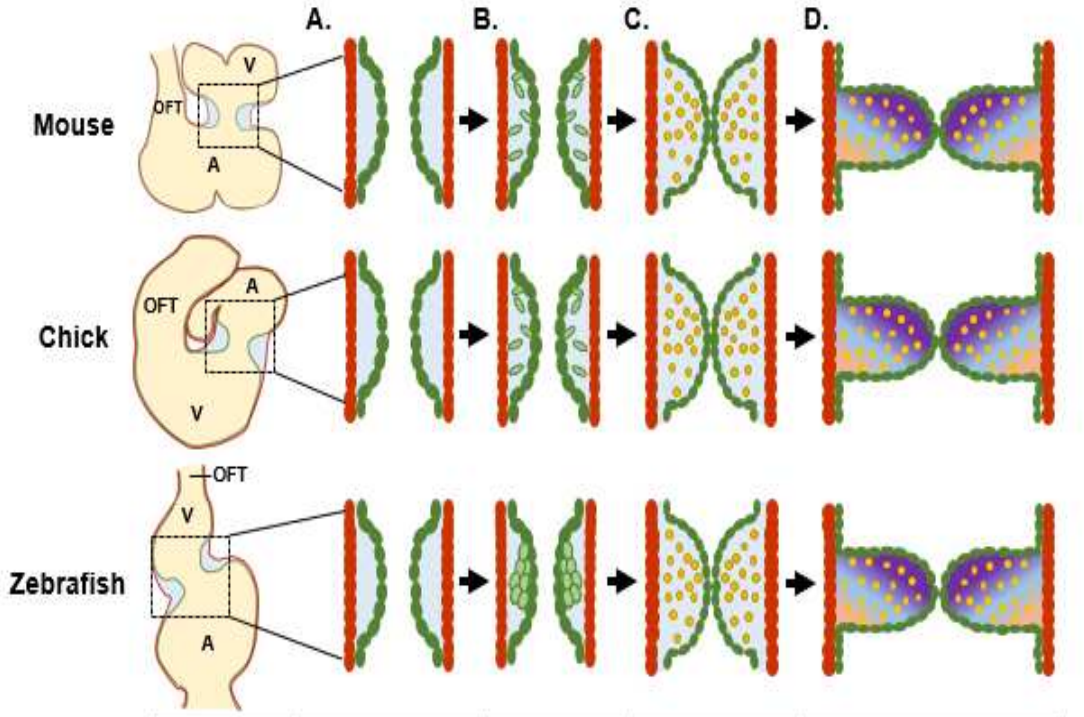

	Cardiac Jelly Accumulation	Endocardial Migration	Mature Cushions	Stratified Valve Leaflets
Mouse	E9	E9.5	E12.5	E14.5 - Birth
Chick	HH12	HH16	HH22	HH28 - 36
Zebrafish	36 hpf	72 hpf	96 hpf	Day 5- Day 16

Figure 1.1 Atrioventricular valve development across species. **A)** Valve development begins as cardiac jelly accumulates between the myocardial (red) and endocardial cell layers. **B)** Endocardial cushions (ECs, in green) are created as endocardial cells invade the cardiac jelly following epithelial to mesenchymal transition (mouse, chick) or via a local invagination of the endocardium (zebrafish). **C)** ECs mature as the mesenchymal cells differentiate into valve interstitial cells (VICs, in yellow) as the cushions begin to function to occlude retrograde flow. **D)** Valve leaflets form from remodeled ECs, as VICs proliferate, stratify, and differentially modify the ECM. Gradient represents three layers of stratified ECM. A, atrium; V, ventricle; OFT, outflow tract. Figure created using BioRender.

The first step in the formation of the endocardial cushions is the accumulation of the cardiac jelly at the atrioventricular canal. The cardiac jelly is a layer of ECM located between the endocardial and myocardial layers. Initially, the cushions consist primarily of a hydrated network of proteoglycans (such as versican) and glycosaminoglycans (such as hyaluronan). Over time, structural proteins such as collagen and fibronectin are deposited as well. Disruptions of ECM proteins results in defective endocardial cushion formation. For example, knockdown of *hyaluronan synthase 2* – the enzyme that synthesizes hyaluronan – results in fewer valve-forming cells at the atrioventricular junction in zebrafish embryos (Patra et al., 2011). In addition, morpholino knockdown of *fibronectin 1b* results in defective endocardial cell clustering at the atrioventricular junction (Emily Steed et al., 2016). Similarly, murine embryos with mutations in fibronectin showed defective endocardial cushion formation and lacked differentiated cushion cells (Astrof, Crowley, & Hynes, 2007). While the exact function of atrioventricular junction accumulation of cardiac jelly in valve development is not known, current models suggest that the ECM creates a permissive environment that allows further progression of endocardial cushion development (Bakkers, 2011).

As the ECM at the atrioventricular junction differentiates, the adjacent endocardial cells proliferate and migrate into the cardiac jelly to populate the endocardial cushions. In mammalian hearts, this event is accomplished through an endothelial-to-mesenchymal transition (EMT), a complex event involving over 100 genes. Activated endothelial cells reduce their endothelial markers, gain mesenchymal markers such as alpha smooth muscle actin (a-SMA), and release their contacts with neighboring cells. Soon, endothelial cells delaminate from the endocardial layer, acquire a mesenchymal phenotype, and invade the cardiac jelly. Once in the cardiac jelly, these cells proliferate and differentiate into VICs, which gradually stratify to give rise a functional valve leaflet. In zebrafish, leaflet formation initiates with a local invagination of the intact AV endocardial layer into the cardiac jelly (Scherz, Huisken, Sahai-Hernandez, & and Stainier, 2008)(Figure 1). Once folding occurs, cells then delaminate and invade the cardiac jelly (Pestel

et al., 2016; Emily Steed et al., 2016). The signaling mechanisms mediating mammalian and zebrafish endocardial cushion formation and remodeling are quite complex, and involve extensive reciprocal communication between the endocardium and the myocardium, as well as the intersection of several signaling pathways (Combs & Yutzey, 2009).

Recent data suggests that Bone Morphogenetic Protein (BMP) pathway plays a key role in coordinating endocardial cushion development (Combs & Yutzey, 2009). BMP ligands are paracrine factors that have extensive roles in regulating cardiac morphogenesis, reviewed in (van Wijk, Moorman, & van den Hoff, 2007). Of particular importance are BMP2 and BMP4, which are secreted by the myocardial cells and which are required for induction of EMT by the overlying endocardial cells. The first evidence supporting a role for BMP in valve formation came from *in vitro* experiments in which endocardial cells were cultured upon gel monolayers. Mouse endocardial cells did not undergo EMT when cultured alone; however, when cultured with exogenous Bmp4, endocardial cells abolished PECAM expression and acquired a mesenchymal phenotype (Sugi, Yamamura, Okagawa, & Markwald, 2004). Since this seminal work in 2004, a requirement for BMP in EMT has been verified in several *in vivo* models. The mutation of *bmp4* in mouse models resulted in hypocellular endocardial cushions (van Wijk et al., 2007). Similarly, knockout of *BMP2* in mouse embryos resulted in failure of cardiac jelly expansion at the AVJ, and abrogated EMT (L. Ma, Lu, Schwartz, & Martin, 2005). In zebrafish, chemical inhibition of *bmp2/4* similarly resulted in failure of endocardial cell differentiation (Palencia-Desai et al., 2015).

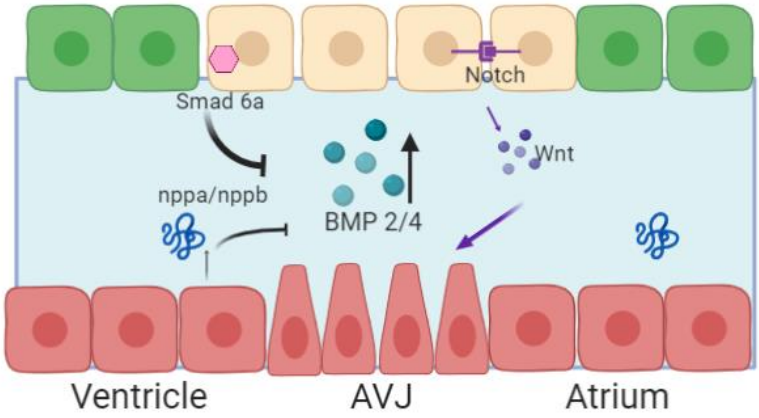

Figure 1.2: Spatiotemporal expression of BMP 2/4 is achieved through activation at the AVJ, and repression through the cardiac chambers. Red cells represent myocardial cells, green cells represent endocardial cells, yellow cells represent valve-forming endocardial cells. Blue space between the two cell layers represents the cardiac jelly. Figure created with BioRender.

The requirement for Bmp4 in endocardial cushion formation has been well established; however, several open questions remain regarding the establishment of Bmp signaling in the cardiac valve. In zebrafish, the dynamic pattern of *bmp4* expression is rather curious – *bmp4* is first expressed throughout the myocardium of the entire linear heart tube. At 36 hpf in zebrafish, *bmp4* expression retracts to the atrioventricular junction myocardium (Walsh & Stainier, 2001). Likewise, in mouse embryos, BMP2 and BMP4 are both expressed throughout the cardiac crescent, and the expression becomes restricted throughout time. Interestingly, their expression patterns diverge over time; by E12.5, BMP2 is expressed in the AVJ and outflow tract mesenchyme, while BMP4 is expressed excclusively at the OFT (Yuasa & Fukuda, 2008). The establishment of this restricted expression pattern is dependent on both paracrine signaling and extracellular matrix proteins (Figure 2).

Expression of BMP2 and BMP4 is positively regulated by canonical Wnt signaling. In mouse embryos, Notch signaling coordinates endocardial Wnt4 expression, which in turn regulates myocardial expression of BMP2 (Wang et al., 2013). In zebrafish embryos, repression of Wnt singaling through overexpression of *axin*, a protein involved in the degradation of β-catenin, abrogated *bmp4* expression at the AVJ (Verhoeven, Haase, Christoffels, Weidinger, & Bakkers, 2011). In addition to positive signaling, inhibitory signaling represses *bmp4* expression in the ventricular myocardium. Knockdown of the extracellular matrix protein, Nephronectin, in zebrafish embryos results in expanded Bmp4 signaling and impaired endocardial valve cell differentiation, suggesting that Bmp signaling can be modulated by the ECM (Patra et al., 2011). Chamber myocytes secrete Atrial neurotic peptide (anf/nppa), which serves to repress BMP expression. Additionally, Smad6, an inhibitory SMAD, is expressed in the valve endocardium, putatively as part of a negative feedback loop to control BMP signaling. Homozygous mice lacking Smad6 (Madh6) generated an excess of AVJ mesenchymal cells at the time of EMT and later developed hyperplastic valves (Galvin et al., 2000). Knockout of Smad6 resulted in dramatic reorganization of the ECM – specifically, *periostin* and *veriscan* expression were

significantly reduced in mutant mice (Sugi, Kern, Markwald, & Burnside, 2012). Together, these data highlight the complex combinatorial control that constrains the region of BMP expression and triggers further valve cell differentiation.

Mesenchymal Cells Populate the Endocardial Cushions

Endocardial cushions undergo substantive remodeling to give rise to the mature valve leaflet. This process is primarily characterized by alterations in the ECM. The ECM of endocardial cushions consists primarily of proteoglycans, while the valve leaflet ECM consists of three stratified layers: a collagen-rich layer termed the fibrosa, a proteoglycan-rich layer termed the spongiosa, and an elastin-rich layer termed the atrialis in the AV valves, or the ventricularis in semilunar valves (Combs & Yutzey, 2009; Hulin et al., 2019). Heart valve development is characterized by increasing complexity and organization within the ECM. As mesenchymal cells populate the endocardial cushions, they proliferate, migrate, differentiate into fibroblastic interstitial cells and remodel the ECM.

Surprisingly, EMT-derived mesenchymal cells continue to express cadherin-based adherens junctions including N-cadherin and Cadherin-11 at their surface for a brief period while colonizing the cardiac jelly. Mesenchymal cells display a collective migration and intercellular communication that is important to this process. Mice with Cadherin-11 deleted valve cells completed EMT successfully, but were unable to migrate collectively, showed defects in protrusion formation and failed to populate the cushions evenly (Bowen, Zhou, Sung, & Butcher, 2015). Downstream of Cadherin-11, RhoA activity supports the migratory behavior and traction force required for morphogenesis.

How endocardial cells choose to become VICs is a topic of intense interest. Studies in zebrafish embryos indicate this cell fate decision is regulated by *Nuclear Activated T-Cell Factor (NFAT*), as well as an EMT-promoting transcription factor, *twist1b* (Gunawan, Gentile, Gauvrit, Stainier, & Bensimon-Brito, 2020). By 144 hpf in zebrafish embryos, cells in the ECM of the atrioventricular valve no longer express the endocardial marker *fli1a*, but actively express *hhex,*

a marker for VICs. Lineage tracing experiments using the photoconvertible transgene kaede in conjunction with reporter lines for either neural crest (*sox10*), endocardium (*kdrl*), or epicardium (*tcf2i*) demonstrated that VICs predominately originate from the endocardial lineage with a small contribution from the neural crest. As early as 38 hpf, *nfat* is specifically expressed in the atrioventricular junction endocardium. Lineage tracing of photoconverted cells at 38 hpf revealed that *nfat*-expressing endocardial cells give rise to approximately 80% of the VICs present at 86 hpf. Knockout of *nfat1* in zebrafish embryos abrogated VIC formation and decreased proliferation by 72 hpf in the valve endocardium. Interestingly, *nfat1* mutants displayed a significant decrease in the expression of *twist1b.* Overexpression of a dominant negative *twist1b* allele prevented valve leaflet entirely. Taken together, this demonstrates that endocardial cells make decisions regarding VIC cell fate early on in cardiac development, and that this process requires NFAT (Gunawan et al., 2020).

Recent work in mice demonstrated that following EMT, mesenchymal cells activate expression of the Sox9 transcription factor in the population of cells that differentiate as VICs (Gallina & Lincoln, 2019). In embryonic stages, Sox9 is not expressed in VECs, and thus may provide a genetic handle to identify additional genes required in VIC differentiation. A critical role for Sox9 in proliferation of valve precursor cells was suggested by targeted loss of function mice, which display severely hypoblastic endocardial cushions(Lincoln, Kist, Scherer, & Yutzey, 2007). Sox9 has later embryonic roles in ECM remodeling later in valve development, and following birth, becomes expressed in VECs as well as maturing VICs(Gallina & Lincoln, 2019).

Neural crest cells contribute to the development of the semilunar valves

Neural crest cells contribute to the development of the outflow tract and consequently the development of the aortic and pulmonary valves. At E8.5 in mouse embryos, cardiac neural crest cells delaminate from the neural tube and migrate to the outflow tract, where they differentiate into smooth muscle cells that contribute to the aortic arch. By E10.5, endocardial cells lining the outflow tract undergo EMT and begin to invade the outflow endocardial cushions.

Concomitantly, neighboring cardiac neural crest cells migrate in bilateral columns into the outflow cushions, where they give rise to a portion of the VICs (Plein, Fantin, & Ruhrberg, 2015). Defective neural crest cells produced by loss-of-function mutation of the Pax6 transcription factor led to the development of dysmorphic, nonfunctional semilunar valves (Jain et al., 2011). Similarly, laser ablation of neural crest cells in quail embryos at HH8 led to dysmorphic valves (P. Ma et al., 2016). Defects in neural crest cells are strongly associated with a host of CHDs -- including DiGeorge's Syndrome, Noonan's syndrome and bicuspid aortic valve disease – extensively reviewed in (Keyte & Hutson, 2012). Together, this data strongly suggests that presence of neural crest cells in the outflow tract is essential for proper semilunar valve development.

Reciprocal signaling from neural crest cells and other neighboring cell types in the heart field may aid the patterning of semilunar valves. Neural crest cells are thought to aid in the development of valve leaflet ECM as well as facilitate apoptosis of mesenchymal cells in later stages of gestation. Deletion of *Pax3*, a neural crest cell marker, resulted in abnormal hypercellular and thickened aortic valve leaflets in mouse embryos at E17.5. As neural crest cells migrate into the outflow tract, they pass by cells of the secondary heart field, presenting an opportunity for paracrine or juxtacrine signaling. Tissue-specific deletion of *notch1* from the secondary heart field phenocopied the malformed valves and altered neural crest cell patterning of *pax3* mutants (Jain et al., 2011). Likewise, tissue-specific deletion of *notch1* from endocardium resulted in a similar bicuspid aortic valve phenotype, whereas deletion of *notch1* from neural crest did not produce an obvious phenotype (Koenig et al., 2016). Together, this data highlights intracellular communication via *notch1* as a key regulator of neural crest cell migration and valve leaflet formation.

The presence of neural crest cells may provide an instructional cue that aids in defining the geometry of the tricuspid valve leaflet. At E10.5 in mouse embryos, neural crest cells within the cardiac outflow cushions were distributed throughout the circumference of the cardiac jelly, and

were beginning to aggregate. Condensation refers to the process of aggregated cells becoming aligned and attached via cell:cell contacts. By E11.5, two distinct condensed clusters were evident, termed the superior and inferior cushions. Mice bearing a dominant negative mutation of *ROCK* (a Rho Kinase) showed uneven positioning of neural crest cells in cardiac jelly, followed by disruptions in the condensation process and ultimately, abnormal aortic valve leaflet morphology. Specifically, when dominant negative *ROCK* mutation resulted in fewer or hypoplastic neural crest cell clusters, the aortic valves developed a bicuspid valve leaflet phenotype. When the same mutation resulted in multiple patchy, aberrant cell clusters, the aortic valve adopted a quadriscuspid phenotype. Together, this data strongly suggests that proper positioning of neural crest cells directs the formation of the outflow cushions, and each individual valve leaflet (Phillips et al., 2013).

Several signaling pathways control the differentiation and activity of the valvular neural crest, including the *Bmp4*, *Fgf8*, and *Hippo* pathways (Manderfield et al., 2015; J. Zhang et al., 2010). Recently, *Krox20,* a transcription factor that regulates collagen, was identified as a cell-autonomous factor that regulates neural crest cell apoptosis. Fate mapping studies using Krox20^{Cre} transgenic mice demonstrated that Krox20 is specifically expressed in the subpopulation of neural crest cells that invade the arterial valve cushions. By E18.5, homozygous Krox20 mutant mice display dysmorphic, hypercellular aortic valve leaflets with disorganized ECM and a partially penetrant bicuspid valve phenotype. Interestingly, endothelial-derived VICs were present in normal numbers, but neural-crest derived VICs were increased approximately 1.8 fold in Krox20 mutants as compared to stage-matched wildtype embryos. Together, this data demonstrates that *Krox20* is a key transcription factor regulating neural crest cell behavior and valve leaflet formation (Odelin et al., 2018).

Valve Extracellular Matrix Remodeling

After formation of the VICs, valve leaflets must remodel their existing ECM into the trilayered adult valve leaflet structure. The mechanisms that control this process during

development are not well understood; however, some insight can be gained from the study of valve leaflets in adult humans or model organisms. Throughout infancy and adolescence, hemodynamic pressure within the heart increases as the circulatory system expands to meet increased physiological demands. Valve leaflets undergo extensive growth and remodeling in order to meet these demands (Oomen, Holland, Bouten, Kuhl, & Loerakker, 2018). Tissue growth, including changes in leaflet length, area, and thickness, incurs the production of new ECM. Tissue remodeling, however, occurs via changes in ECM structure and composition. In particular, leaflets develop thicker collagen bundles and denser collagen cross-links. These changes in collagen architecture serve to increase stiffness of the leaflets with age. In adult humans with high blood pressure, similar remodeling events are mediated by altered hemodynamics and can lead to valvular disease (Pagnozzi & Butcher, 2017). Whether leaflets in adults respond to the same mechanisms as were active in the initial valve leaflet development remains relatively uninvestigated. Mutations in either collagen or elastin are linked to a variety of severe congenital heart defects (Siu & Silversides, 2010). During late gestation, the apoptosis is used to sculpt the leaflets. A significant percent of the mesenchymal cells undergo apoptosis, leaving a valve leaflet that consists of a tri-layered ECM with relatively few VICs (Zhao & Rivkees, 2000).

Biomechanical inputs in heart development

The heart is the first organ to form and begins contractions shortly after formation of the linear heart tube. Cardiac contractions began at 22 hpf in zebrafish, 48 hpf in chicks, embryonic day 8.5 in mice, and at approximately 22 days in humans. As development progresses, heart contractions increase in force and frequency, thereby altering hemodynamic forces. Both blood pressure and heart rate increase rapidly as differentiation proceeds in zebrafish, chicken, mouse, and humans (Lindsey, Butcher, & Yalcin, 2014). Because hemodynamic factors change both spatially and temporally, they can elicit precise transcriptional responses. The following

section will review current knowledge regarding the role mechanical forces play in heart development.

Shear Stress

Conceptually, shear stress is the frictional force per unit area between laminar layers of fluid and is known as wall shear stress (WSS) at the surface of the endothelial layer as blood flows parallel to the heart wall. WSS creates a drag force on the endothelial layer and it regulates several specific aspects of normal valve development and blood vessel development, as well as pathological aspects such as fibrosis under conditions of heart failure. Both the direction and the magnitude of WSS play a role in triggering gene expression changes. This next section will describe the evidence from zebrafish, chicken, and mice that relate signals provided by WSS to the underlying molecular circuitry.

In vitro experiments first elucidated the role of WSS in heart morphogenesis. When exposed to laminar flow, cultured endothelial cells realigned in the direction of flow, and altered ECM production and gene expression. In particular, cells increased their expression of the transcription factors *Kruppel-like factor 2 (KLF2)* (X. Cui et al., 2017; Sathanoori et al., 2015). The first *in vivo* evidence for shear stress as a factor directing valve morphogenesis came from a zebrafish model in which blood flow had been occluded in the heart by the insertion of glass beads (Hove et al., 2003). Specifically, a glass bead placed at either the outflow or inflow tract of the developing zebrafish embryos prevented flows at the atrioventricular junction and the rest of the heart. Under conditions of absent flows, the endocardial cushions and the atrioventricular valve failed to form (Hove et al., 2003). Though this hemodynamic intervention is rather invasive, this work established the presence of blood flow and associated WSS required for normal valve development.

An open question in the field concerns the underlying molecular circuitry that regulates the WSS response. On a transcriptional level, the best studied response is the flow-responsive nature of *klf2* transcription. Under conditions of normal flow, chicks, mice, and zebrafish

embryos all upregulate *klf2* transcripts in response to increased shear stress, thus triggering the activation or repression of a number of downstream signaling pathways. KLF2 is required for endocardial valve cell differentiation and endocardial cushion formation in both mice and zebrafish embryos (Goddard et al., 2017; Groenendijk, Van der Heiden, Hierck, & Poelmann, 2007; Vermot et al., 2009).

The KLF2 Pathway

Much of the work that elucidated the KLF2 pathway in valve development comes from zebrafish. Due to a genome-wide duplication event, zebrafish encode two paralogs of KLF2, *klf2a and klf2b.* The flow-responsive properties of *klf2a* expression were noted in zebrafish embryos treated to alter blood viscosity (Vermot et al., 2009). The *gata1* and *gata2* transcription factors are required for hematopoiesis. Morpholino knockdown of either of gene resulted in decreased hematocrit. While *gata1* and *gata2*-morpholino-injected embryos both displayed reduced blood viscosity, they differed in their specific patterns of blood flow and shear stress. *Gata1* morphants displayed increased oscillatory flow at the atrioventricular junction, whereas *gata2* morphants displayed reduced oscillatory flow. Because these knockdowns displayed similar decreases in overall blood viscosity and shear stress magnitude but display different directional flow profiles, they provide a convenient tool to probe the role that directional shear stress plays in valve development (Vermot et al., 2009).

Gata2 morphants, with decreased retrograde flow, showed defective endocardial cushion development and a failure of endocardial cells to cluster at the atrioventricular junction. These phenotypes could be recapitulated through knockdown of *klf2a* (Vermot et al., 2009). This data established *klf2a* transcription as responsive to oscillatory flows and required for valve development. Further work with a *klf2a* mutant showed that Klf2a function is required for cell clustering at the atrioventricular junction, as well as cell migration into the cardiac jelly. Intriguingly, a Tg[klf2a:H2B-eGFP] reporter line revealed that cells at the atrioventricular junction display a gradient of *klf2a*-expression. Cells initially express high levels of *klf2a*, but as they

enter the cardiac jelly *klf2a* expression becomes low. Once inside the cardiac jelly, cells acquire a putative mesenchymal phenotype and began to proliferate (Emily Steed et al., 2016). Together, these data establish that oscillatory WSS regulates *klf2a* expression, which, in turn, regulates cell migratory behavior.

In addition to its role in cell migration, Klf2a regulates multiple genetic pathways and morphogenetic events. Zebrafish studies demonstrate Klf2a positively regulates fibronectin, a critical extracellular matrix component (Emily Steed et al., 2016). In human umbilical vein endothelial cells (HUVECs), overexpression of *klf2a* produced a transcriptional profile with alterations in pathways involved in cell migration, inflammation, and stress fiber formation (Dekker et al., 2006). In mouse embryos, KLF2 expression induced WNT9b, which is required for EMT and endocardial cushion formation (Goddard et al., 2017). More work needs to be done to identify Klf2 targets in order to fully understand how Klf2 coordinates multiple morphogenetic events.

While data support the regulation of *klf2a* transcription by oscillatory WSS, how cells are able to sense oscillatory shear stress and transduce a mechanical signal into a genetic response remains an area of intense interest. One mechanism for sensation of oscillatory flow employs two mechanosensitive calcium channels, Trpv4 and Trpp2 (Heckel et al., 2015). These channels are both expressed in endocardial membranes facing the cardiac lumen. Mutation of either channel in zebrafish resulted in decreased *klf2a* expression at the AVC and altered valve morphology. It is proposed that, as these channels become activated by oscillatory flow, they trigger an influx of calcium into endocardial cells within the AVC, which in turn regulates *klf2a* expression (Heckel et al., 2015).

In addition to mechanical regulation, KLF2 expression is also regulated by molecular feedback loops. One such feedback loop elucidated in zebrafish valvulogenesis involves the proteins *Krit1* (also known as CCM1) and *heart of glass* (HEG1). The Krit1 and Heg1 proteins bind one another and are active in the formation and stabilization of endothelial cell junctions.

Heg1 expression is regulated by blood flow and *klf2a*, and consequently is expressed at the atrioventricular junction. Heg1 stabilizes expression of its binding partner, Krit1, which is expressed in a blood flow-independent manner in the endocardium. Loss of Krit1 leads to aberrant *klf2a* expression throughout the endocardium and defects in chamber and valve formation. Together, this data suggests a model wherein *klf2a* is spatially regulated by a negative feed-back loop mediated by the Krit1-Heg1 proteins (Donat et al., 2018).

Overall, the data points to a model wherein oscillatory WSS induces expression of KLF2, which subsequently mediates valve development by promoting cell migration and regulating extracellular matrix proteins. To achieve precise spatiotemporal regulation of KLF2 expression, both blood-flow dependent and independent mechanisms are used in the chamber endocardium, leading to precise control of endocardial cushion and valve leaflet formation.

. The role of cilia in sensing shear stress

Primary cilia are solitary, immotile protrusive organelles that function as mechanosensors. The stiffness of this antenna-like organelle contributes to its high sensitivity to WSS and facilitates its ability to function as a flow sensor in a variety of tissues, including Henson's node, kidney epithelium, bile duct epithelium and vascular endothelium (Marshall & Nonaka, 2006). As blood or fluid flows over vascular endothelium, primary cilia projecting from the luminal side of the cells deform/bend, eliciting the rapid opening of polycystin-2 calcium-permeable cation channel complexes and a subsequent influx of calcium ions. In this way, cells translate the mechanical stimulation of primary cilia into an intracellular calcium transient. Calcium influx regulates a variety of downstream signaling pathways leading to functional responses. For example, calcium levels indirectly activate eNOS, the enzyme responsible for production of nitric oxide (NO). NO exerts vasodilatory effects by promoting smooth muscle relaxation. Several studies now support cilia dysfunction as a causative component of several cardiac and vascular diseases (Pala, Jamal, Alshammari, & Nauli, 2018).

While the role of primary cilia in vasculature development has been well-characterized, less is known about how cilia may function in endocardial or valve development. In murine models, mutations in the cilia structural gene *ift88* result in cardiac dysfunction and hypoplastic endothelial cushions,

suggesting that WSS may act on cilia in the endocardium to facilitate endocardial cushion development (Nonaka et al., 1998; Slough, Cooney, & Brueckner, 2008). In zebrafish embryos, cilia are required for activation of notch in the endocardium (Samsa et al., 2015). The exocyst is a molecular trafficking complex required for ciliogenesis. Disruption of EXOC5, a linker protein required for exocyst integrity, produced cardiac phenotypes reminiscent of biaortic valve disease in both zebrafish and mice embryos (Fulmer et al., 2019). Together, this data highlights the fact that cilia have an evolutionarily conserved role in valve development.

The integrity of cilium itself is unable to withstand high levels of shear stress. Exposure to high WSS triggers disassembly of its internal microtubule structure, the axoneme. Accordingly, cilia are normally internalized from the cell surface in areas of high shear stress such as the atrioventricular endocardium in both chick and zebrafish embryos (Haack & Abdelilah-Seyfried, 2016). When cultured *in vitro* and in the presence of laminar flow, ciliated endothelial cells do not readily undergo EMT. In contrast, genetically modified endothelial cells that lack cilia acquire a mesenchymal phenotype when exposed to laminar flow. This data strongly suggests that absence of cilia – caused by patterns of high shear stress -- is a prerequisite for the transition to a mesenchymal status observed in endocardial cushion maturation (Ten Dijke, Egorova, Goumans, Poelmann, & Hierck, 2012).

MicroRNAs in the shear stress response

The role of microRNAs in regulating the shear stress response pathway has well been described in the vasculature (extensively reviewed in (Kumar, Kim, Simmons, & Jo, 2014; Kumar, Williams, Sur, Wang, & Jo, 2019)). In adult cardiac valve pathology, microRNAs are emerging as novel regulators of the shear stress-response. Less is known about whether or how microRNAs function to convey information about shear stress during valve development, though it is possible that the same underlying molecular circuitry is involved.

MicroRNAs are implicated in the progression of adult valve disease. For example, in calcified aortic valve disease (CAVD), the aortic valve (located between the aorta and the left ventricle) becomes gradually thicker. Over time, the aortic valve accumulates calcium deposits and obstruction of flow can occur. The aortic valve experiences low and oscillatory WSS shear on the aortic side (the fibrosa), and high WSS on ventricular side (the ventricularis). Aortic valve calcification occurs most often on the fibrosa

side while the ventricularis remains relatively unaffected, making CAVD a side-specific disease. Remarkably, several microRNAs demonstrate enriched expression in the fibrosa relative to the ventricularis in healthy tissues. *Ex vivo* experiments demonstrate that the one-sided differential expression of microRNAs is indeed linked to oscillatory shear stress, normally larger on the fibrosa relative to the ventricularis. An attractive hypothesis is that disrupted expression of side-specific microRNAs might mediate CAVD pathology. Silencing of *miR-214* by anti-miR-214 generated increased expression of TGFα1 in the fibrosa of porcine aortic valve explants, but only when exposed to conditions of oscillatory flow (Rathan et al., 2016). Thus, *miR-214* exhibits a shear-dependent functional role in the AV. Pharmaceutical inhibition of another microRNA, *miR-34a*, resulted in ameliorated aortic valve calcification in a murine model. *MiR-34a* is produced in human adult patients with CAVD (Toshima et al., 2019).

In bicuspid aortic valve (BAV) disease, the malformed geometry of the adult aortic valve results in altered hemodynamics including abnormal patterns of shear stress and more potential for turbulent flow. Bioinformatic analysis indicated that a number of microRNAs exhibit differential expression in the cusps of the bicuspid aortic valves, or in circulating serum, as a result of BAV disease (Sabatino et al., 2019). These cohorts of microRNAs may serve as clinical biomarkers specific for BAV, and analysis of their putative targets can provide insight into the biological processes they influence. Together, these data establish that shear-stress-mediated modulation of circulating microRNAs has important impacts on molecular circuits pertinent to aortic valve disease.

The role of shear stress-mediated microRNAs is increasingly evident in adult valve pathology, but their role during normal development remains understudied. A study by Banjo and colleagues (2013) demonstrates how a flow-dependent microRNA contributes to normal valvulogenesis. In zebrafish, *miR-21* acts as a shear-responsive regulator of valve development. Arresting the heartbeat for as little as 12 hours in embryogenesis was sufficient to eliminate *miR-21* expression in AVC endocardial cells, suggesting that this miR is blood-flow dependent. Levels of *pre-miR-21-1,* one of the two primary transcripts of zebrafish *miR-21*, was likewise dependent on the presence of a heartbeat, suggesting that regulation of *miR-21* biogenesis occurs at the level of transcription. Following the loss of *miR-21* expression due to heartbeat cessation, as little as 1 hour of reactivated heartbeat was sufficient to restore

pre-miR-21 to normal levels. Thus, detection of flow information and the transcriptional response can be extremely rapid. Epinephrine-induced vasoconstriction doubled the shear stress and nearly doubled *pri-miR-21* expression in whole zebrafish bodies. Conversely, knockdown of *miR-21* through morpholinos produced a valveless phenotype by 72 hpf. Morphant hearts displayed few valve-specified ALCAM expressing cells and only a single thin layer of endocardial cells in the AV canal. *miR-21* negatively regulates *sprouty2*, an inhibitor of the RTK/Ras/ERK pathway, and positively regulates several genes active in cell proliferation. Thus, *miR-21* is an important mediator of the shear-response circuitry required for valve development (Banjo et al., 2013).

Several open questions remain regarding the role of microRNAs in valve development. First, are the microRNAs that are differentially expressed in a shear-specific manner in adult valve pathology also expressed during development? If so, their tightly regulated expression may constitute one mechanism that produces physiological differences between valve leaflets. Second, how is microRNA activation by shear stress achieved? Is their expression mediated by mechanosensitive ion channels, cilia, or by deformations in the glycocalyx? These questions must be addressed to fully define the molecular circuitry underlying the shear stress – miRNA axis in valve development.

Pressure as a hemodynamic cue in valve development

While the biomechanical signals from WSS are becoming increasingly well characterized, less is known about how pressure impacts heart valve development. Pressure throughout the heart is determined by the loading state of the heart. Afterload refers to the pressure the ventricle must overcome to pump blood throughout the circulatory system. For a given cardiac output, the pressure is proportional to the flow rate times the resistance. The higher the afterload, the higher the transmural pressure throughout the heart (Pappano & Wier, 2013). In contrast, preload is defined as the degree of ventricular stretch at the end of ventricular filling. As preload increases, stroke volume and cardiac output increase concomitantly. Preload is commonly estimated by measuring left atrial pressure at the end of

diastole. Preload can be thought of as passive tension placed on the ventricle while it is filling, whereas afterload is the wall stress the ventricle experiences as it is contracting (Figure 3).

As the heart develops, both preload and afterload increase to meet the demands of the embryos (Phoon, 2001). We and others characterized the pumping dynamics of zebrafish embryos as they progress from a linear heart tube stage (30 hpf) through looping and chamber ballooning (48 hpf). At 30 hpf, the heart tube contracts in peristaltic-like fashion, with relatively low blood velocity. As development progresses, the heart transitions to independent contraction of the atria and ventricular chambers, deploying a displacement pumping mechanism (Forouhar et al., 2006; Johnson, Garrity, & Dasi, 2013). This transition in pumping mechanism is recapitulated in vertebrate model organisms and serves to increase blood velocity. As an organism grows, a larger cardiac output is required and there is more peripheral vascular resistance. As a result, ventricular pressure must also increase to maintain perfusion through the vascular beds (Bark, Johnson, Garrity, & Dasi, 2017). Indeed, hearts in chick embryos exhibit a dramatic increase in hemodynamic pressure once valve leaflets form (Yalcin, Shekhar, McQuinn, & Butcher, 2011).

The increased pressure on the valve as development proceeds suggests the hypothesis that pressure regulates developmental processes that give rise to the valve leaflet. To understand how changes in pressure results in both pathological and developmental responses, it is useful to look at how pressure elicits changes on the cellular level. Increases in afterload result in transmural pressure on the cardiac wall and valvular structures. This can be mechanically transduced through deformations of the glycocalyx, β-integrin signaling, as well as through activation of mechano-gated ion channels (Israeli-Rosenberg, Manso, Okada, & Ross, 2014; Pagnozzi & Butcher, 2017; Peyronnet, Nerbonne, & Kohl, 2016). In addition to the increase in transmural pressure, cardiac myocytes must increase contractility to compensate for the increased afterload, overall increasing tensile stress in the wall (not necessarily stretch, which is otherwise seen for preload). Initially, the capacity to increase contractility is

accomplished through alterations in sarcomere shortening fraction (LaCombe & Lappin, 2019). This alteration in sarcomere mechanics can be transduced to genetic responses through a variety of stretch sensitive and titin-mediated mechanisms (Krüger & Kötter, 2016). Over time, compensation may be achieved through the initiation of the hypertrophic gene program and remodeling of the myofibril architecture. Increases in preload are accomplished through in increases venous return. This causes an increase in tension on the atrial myocytes as they stretch to compensate for increased volume. Increases in tension can be transduced to changes in gene expression through focal adhesion kinase and other adhesion proteins (Burridge, 2017). The next section will review current knowledge regarding the role pressure plays in regulating valve development and pathology and will highlight mechanotransducive circuits involved in valve development.

Pressure in adult pathology

High afterload exerts deleterious effects in adults that lead to lead to cardiac hypertrophy and valve pathology (Davila & Forfia, 2015; Hirt et al., 2012; Levy, Larson, Vasan, Kannel, & Ho, 1996). Recently, two epidemiological studies involving millions of adult subjects definitively established an association between elevated blood pressure (hypertension) and regurgitant mitral valve disease, aortic stenosis (AS) and aortic regurgitation (AR) (Rahimi et al., 2018; Rahimi et al., 2017). Each 10 mmHg increase in blood pressure was associated with a 41% higher risk of AS and a 38% higher risk in AR. Because hypertension increases the pressure the ventricle must pump against, it can be thought of as a condition of high afterload. While these studies did not investigate the mechanisms that underlie the association, the authors postulate that high blood pressure exerts a mechanical stress. The stress of these interactions then facilitates endothelial cell damage and altered extracellular matrix. Gradually, further structural changes impede normal function of the valve. In the case of AS and AR, the aorta becomes less distensible and the aortic valve stiffens (Rahimi et al., 2018; Rahimi et al., 2017).

As mentioned earlier, although differing in geometry, human valve leaflets all share a similar structure in the fibrosa, spongiosa and ventricularis layers. Changes in the cardiac physiological environment have the potential to disrupt the valve's mechanical microenvironment at the ECM/cellular level. Collagen fibers mediate the load-bearing integrity of the valve. In healthy valves, collagen fibers in the fibrosa layer are primarily oriented along the circumference of the valve. Pant and colleagues (2018) investigated whether the arrangement of fibrous collagen proteins in the ECM of porcine tricuspid valve explants differed in a pressurized environment versus a non-pressurized environment. The study found that the presence of hydrostatic pressure increased the alignment of collagen fibers in the leaflets, suggesting that normal physiological pressure helps to maintain the collagen-based mechanical integrity of leaflets (Pant et al., 2018). Conversely, abnormal pressures might contribute to disease by adversely affecting the collagen microenvironment. Since this study did not recapitulate the cyclical/oscillatory pressure waves normally present in the heart, much remains to be learned about how (or whether) differential strain on leaflets during the course of the heartbeat impacts the collagen microenvironment.

In addition to affecting alignment of macromolecules in the extracellular matrix, pressure can affect function of the VICs themselves. Application of pathological stretch to mature porcine aortic valve explants caused VICs to up-regulate myofibroblast markers such as alpha smooth muscle actin and vimentin (Balachandran, Konduri, Sucosky, Jo, & Yoganathan, 2006). Indeed, gene expression profiling of porcine aortic VICs cultured under conditions of high pressure demonstrated large-scale transcriptional changes compared to control cells. Of note, expression of several genes in the inflammatory response pathway was altered, as well as expression of ECM proteins (Warnock et al., 2011). Taken together, these results establish the existence of a mechanotransduction pathway between pressure and the mature valve leaflet which has the ability to substantially alter gene expression.

Due to difficulties in precisely manipulating pressure without altering other hemodynamic and physiologic variable *in vivo,* few studies have attempted to examine the effect of high pressure on heart valves in whole animal models. However, analysis of heart valves in giraffes provides insights. Blood pressure in the giraffe is higher than any other mammal (approximately twice that of humans) in order to sufficiently perfuse the head tissues atop the long neck. Despite these high pressures, giraffes do not develop premature valve disease. In a study to determine how giraffes have adapted to this extreme condition, Funder and colleagues noted that the aortic valve was 70% stronger and stiffer than bovine controls. Aortic leaflets were thicker and showed higher collagen and elastin content. In addition, collagen was more compactly arranged than bovine controls. Thus, although the heart mass in giraffes is comparable to other mammals (~0.5% of body weight), giraffe hearts have adapted to their hemodynamic environment by altering the abundance and arrangement of ECM macromolecules within the leaflets (Amstrup Funder et al., 2017).

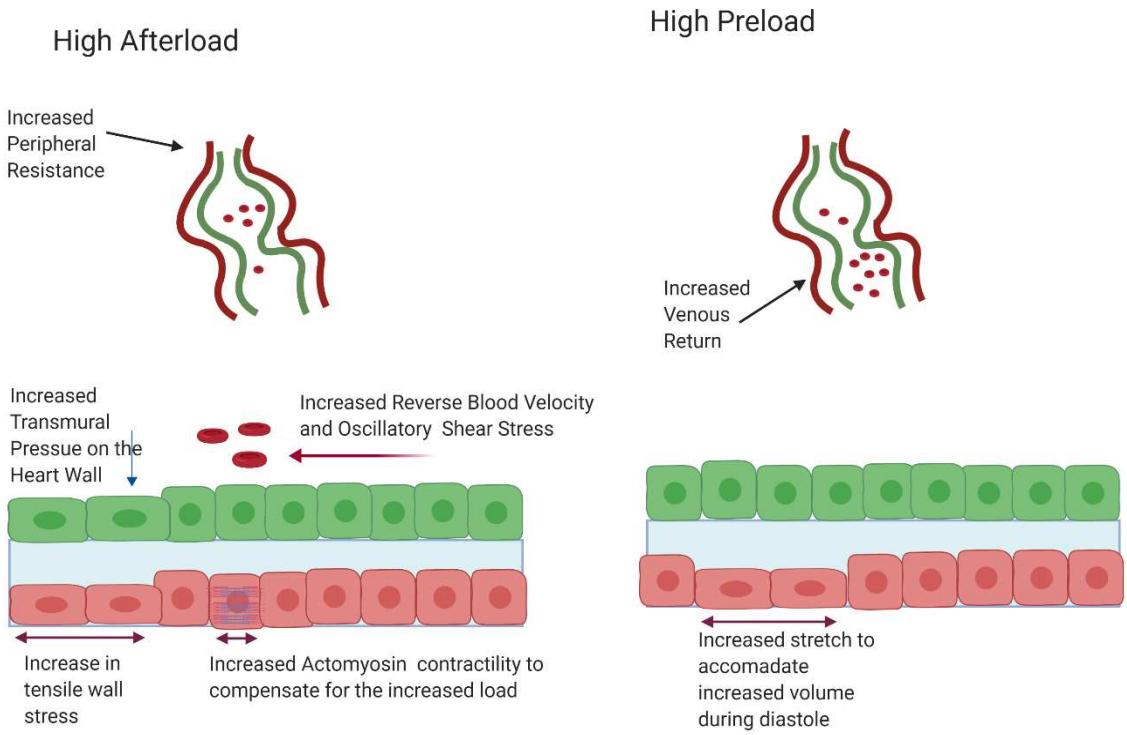

Figure 1.3: High afterload induces oscillatory shear stress, compressive pressure, and increased contractility resulting in increased tensile wall stress. High preload leads increased stretch to accommodate higher blood volumes during diastole. Figure created with BioRender.

Paracrine factors in the transforming growth factor beta (TGFβ) superfamily, including BMP-2 and BMP-4, have been implicated in the pathological response of valves to elevated cyclic tissue stress. Explanted valves placed in a bioreactor to induce physiological levels of cyclic stress expressed BMP-2 and BMP-4. Under conditions of pathological stress, expression of these genes was significantly higher, particularly in the endothelial layer on the fibrosa side of the cusps. Pathological degrees of stretch induced valves to mount an enhanced osteogenic and calcification response via a BMP-dependent mechanism, but those events could be blocked by the addition of BMP antagonists to the system. These data suggest that the endothelial layer acts as the mechanotransducer of cyclic stress, and that under conditions of elevated stretch, BMP signaling is required for the process of valve calcification (Balachandran, Sucosky, Jo, & Yoganathan, 2010). In another study, application of TGFβ to VICs *in vitro* facilitated their differentiation into myofibroblasts. The contractile valve myofibroblasts then exerted tension on the valve ECM, resulting in a dramatic realignment of fibronectin fibrils and the formation of stress fibers (Walker, Masters, Shah, Anseth, & Leinwand, 2004).

Pressure as a cue during embryonic valve development

Evidence supports the link between increased pressure and valve pathology in mature organisms, but less is known about how pressure may affect the development of the valve leaflets during embryogenesis. Much of what we do know comes from surgical procedures performed on chick embryos including outflow tract (OFT) banding (sometimes called conotruncal banding) or left atrial ligation (Madeline Midgett & Rugonyi, 2014). As its name implies, OFT banding involves suturing the developing OFT to reduce its cross-sectional area and consequently create a dramatic increase in afterload. On a physiological level, OFT banding produces cardiomyocyte hyperplasia in both chicken embryos and in guinea pigs. The left atrial ligation procedure redirects blood flow from the left atrium to the right atrium, thereby creating an increase in preload on the right side of the heart and a concomitant decrease in

preload on the left side. This model results in an underdeveloped, hypoplastic left ventricle and a compensatory hyperplastic overdevelopment of the right ventricle (Sedmera, Pexieder, Rychterova, Hu, & Clark, 1999). Similar results are seen in humans with left outflow obstruction, with some recovery seen upon removal of the obstruction (Freud et al., 2014).

The emerging theme of these studies is that alterations in the local hemodynamic environment, producing either too much or too little pressure, significantly alter the composition of the extracellular matrix (cardiac jelly) in the endocardial cushions, and affect the propensity of endothelial cells to undergo EMT and invade the cardiac jelly. OFT banding performed on chick embryos at Hamburger-Hilton (HH) stage 18 (approximately 3 days of incubation, during EMT) dramatically increased left ventricular pressure and blood flow velocity in the outflow region during the onset of EMT in the endocardial cushions. Along with these changes, researchers observed a significant increase in the number of cells undergoing EMT in the outflow tract region, and a substantial remodeling of the cardiac jelly near the cushion mesenchyme. Proteomic analysis demonstrated that several ECM proteins such as fibulin, mucin 6, and laminin underwent several fold changes in response to increased pressure (M. Midgett, López, David, Maloyan, & Rugonyi, 2017).

Interestingly, outflow tract banding at later stages (Hamburger-Hilton 21, post-EMT during ECM remodeling) resulted in smaller, dysmorphic mitral valves by Hamburger-Hilton stage 29. Dysmorphia was accompanied by a decrease in endocardial apoptosis, and dysregulation of ECM proteins such as fibulin and collagen. Expression of shear-responsive genes such as *KLF2* and *endothelial-1 (EDN1)* was elevated. *KLF2* was specifically upregulated on the atrial side of the mitral valve, while *EDN1* was increased throughout the right ventricular myocardium (Pang, Parnall, & Loughna, 2017).

Indeed, the developmental time when outflow tract banding is performed seems to be particularly relevant to how well EMT progresses in valve-forming regions. Banding at an earlier stage (Hamburger-Hamilton 15) lead to a significant decrease in OFT cushion volume,

accompanied by the production of fewer mesenchymal cushion cells. Despite higher shear rate and pressure as measured by computational fluid dynamics, expression of the shear-responsive gene *KLF2* was decreased, as measured by qPCR. Genes involved in EMT regulation, such as TGFβ, were similarly down regulated (Menon, Eberth, Goodwin, & Potts, 2015). Whether the EMT defect occurred due to changes in pressure directly affecting EMT-related pathways or whether these changes are secondary to malformation of the cardiac cushions remains unclear.

The left atrial ligation (LAL) approach offers additional perspective since it produces simultaneous but distinct effects on the left and right atrioventricular valves. The right atrioventricular valve – which experiences higher pressure in embryos that have undergone LAL – becomes more fibrotic and resembles a bicuspid valve rather than its typical tricuspid morphology. The left atrioventricular valve – which experiences abnormally low pressure - was either dysplastic, or in severe cases, resembled underdeveloped atretic valves (Sedmera et al., 1999). Other research noted endocardial fibroelastosis in chicken embryos that have undergone LAL, and increase in myofibroblast markers in the endocardial cushions, accompanied by an increase in collagen expression (Pesevski et al., 2018). In adult valve pathology, one hallmark of a diseased valve is the differentiation of VICs to myofibroblasts, concomitant with ECM remodeling (Walker et al., 2004). Just like Goldilocks, the developing valves need their surrounding pressure to be “just right”.

3.1.3. Signaling pathways involved sensing and responding to changes in pressure in valve development

Given that afterload can affect both embryonic valve development and pathology, it is of great interest to understand the molecular mechanisms that sense and respond to changes in pressure to facilitate mechanotransduction, and whether cells use the similar genetic signals as in adult valves. Because pressure in the heart is intrinsically tied to shear stress and oscillatory flow, it can be difficult to disentangle the effects of pressure from the effects of blood flow. Insight has come from *in vitro* studies that precisely manipulate explanted tissue to replicate

changes in afterload and preload. As in adult hearts, as preload increases, the stretch of individual myocytes must increase to compensate for the increase in load. An increase in stretch can trigger a cellular response to initiate transcription of target genes. Several mechanisms have been proposed to account for how load on the heart may be transduced to endocardial and myocardial cells. Increases in afterload create increased pressure on the heart wall, which may in turn distort the glycocalyx or activate mechanosenstive proteins such as integrins, ultimately leading to differential intracellular cellular responses. The next section will describe three common pressure-sensitive pathways involved in heart valve development.

Rho/Rac cascade. Rho and Rac are membrane-bound GTP-ase proteins that belong to the Ras superfamily. When activated by GTP binding, Rho and Rac activate downstream effects that alter the cytoskeletal properties of the cell. To date, more than 70 different effector molecules have been described for members of the Rho/Rac family. One of the best characterized is the Rho-associated serine/threonine kinase (ROCK); when activated, ROCK phosphorylates myosin light chain causing polymerization of myosin fibers. In addition, ROCK activates LIM kinase, which phosphorylates and deactivates the actin severing protein Cofilin. The combined effect of these transduction events is increased cellular stiffness and increased actomyosin contractility in the cell. Other downstream effectors of Rac include several cytoskeletal proteins including scaffolding proteins and tubulin. Additionally, Rac can stimulate a downstream kinase called p-21 activated kinase 1 (PAK1). Overall, Rho and Rac respond to mechanotransductive cues by mediating the cytoskeletal response to mechanical stress (Bustelo, Sauzeau, & Berenjeno, 2007; Parri & Chiarugi, 2010).

During valve development, Rho and Rac have opposing expression patterns in the cushion mesenchyme. In avian embryos at Hamburger-Hilton stage 25 (post-EMT), Rho expression and activation was relatively high as determined by ELISA and immunohistochemistry, but as development progressed, expression and activation of Rho decreased. Conversely, Rac activation was relatively low at Hamburger-Hilton stage 25, but

increased through valve leaflet remodeling stages, and ultimately reached over 2-fold greater activity by Hamburger-Hilton stage 36 (Gould et al., 2016). Inhibition of ROCK prevented flow-driven fibrous ECM accumulation and valve stiffening in explanted HH25 avian valves, demonstrating and additional function for the mechanotransductive abilities of Rho/Rac in mediating ECM dynamics (Tan et al., 2013). Finally, Rho-GTPases have been implicated in regulating valve interstitial cell phenotypes in adult valves. RhoA was upregulated in VIC nodules associated with calcified aortic valve disease. Inhibition of ROCK dramatically reduced expression of myofibroblast markers such as α-smooth muscle actin (Gu & Masters, 2011). These observations on altered valvular cell phenotype indicate yet a third way that Rho and Rac mediate changes in response to mechanotransductive cues.

Exactly how the biomechanical environment might activate Rho and Rac remains an area of open research. One mechanism for activation of these GTPases lies in regulation of GTPase associated proteins such as Guanine Nucleotide Exchange Factors (GEFs). Often, Rho GEFs associate with other cytoskeletal elements. When those cytoskeletal elements are deformed, GEFs dissociate and activate Rho. For example, under conditions of high tension, GEF-H1 is recruited to cell adhesions, where it is activated by the Focal Adhesion Kinase (FAK) pathway. GEF-H1, in turn, activates RhoA (Guilluy et al., 2011). Because Rho and Rac each associate with different GEFs, they have a large capacity to associate with different cytoskeletal proteins. Thus, Rho and Rac could conceivably mediate distinct cellular responses in response to a variety of mechanical stimuli (Lessey, Guilluy, & Burridge, 2012).

Rho and Rac have different roles in valve development, as suggested by their differential expression patterns. Overexpression of Rho is sufficient to drive AV progenitor cells to differentiate into myofibroblasts in collagen gel assays, whereas loss of Rho prevented expression of myofibroblastic genes such as alpha-smooth muscle actin and serum response factor. Conversely, RAC was found to be required for ECM compaction and fiber formation and overexpression of RAC promoted matrix compaction in collagen gel explants. Recently, RAC

proteins were found to be activated by cyclic mechanical stretch that was dependent on a GTPase Activating Protein (GAP) called FilGAP. When placed in bioreactor, atrioventricular valve cells cultured in collagen gels increased expression of RAC when exposed to cyclic stretch, but did not when exposed to absence of mechanical stress or constant mechanical stretch. In conditions of low mechanical stress, FilGAP was associated with the large cytoskeletal protein Filamin A. Filamin A connects transmembrane proteins to the actin cytoskeleton, and serves a variety of intracellular scaffolding functions. Under conditions of high mechanical stress, Filamin A undergoes a conformational change which releases FilGAP, which in turn activates Rac. In this way, high cyclic stretch mediates compaction and development of the valve ECM (Gould et al., 2016).

Nfat/calcineurin signaling. The Nfat/calcineurin signaling cascade is a mechanosensitive calcium-dependent signaling pathway implicated in cardiac valve development and hypertrophy. The mechanosensor in this pathway is calcineurin, which is a protein phosphatase consisting of a 60 kDA catalytic subunit (CnA) and a 19 kDA regulatory subunit (CnB). CnB has four EF-hand calcium binding sites; when is calcium is bound, calmodulin is recruited to the complex. Calmodulin recruitment causes a conformational change that exposes the catalytic phosphate site and yields a constitutively active phosphatase. The active form of calcineurin then removes a phosphate group from Nuclear Factor of Activated T-cells (NFAT), which translocates to the nucleus and affects transcriptional change (Parra & Rothermel, 2017).

Activation of calcineurin is regulated through calcium and cellular stretch. In cardiac cells, inactive calcineurin is tethered to the sarcomere Z-disc via interactions with LIM protein (MLP) and calsarcin. Under conditions of high mechanical stress, MLP dissociates from the Z-disc and translocates into the nucleus where it plays a role in initiating expression of hypertrophic genes. Knockout of MLP or pharmacological inhibition of MLP-calcienurin binding abrogated calcineurin activation in murine pressure overload models, confirming that the stretch-sensor MLP is strictly required for calcineurin signaling at the Z-disc (Heineke et al.,

2005; Jeong et al., 2008). In addition to its role as a mechanostransducer via scaffolding with the sarcomere, calcineurin also acts at the plasma membrane through calcium channels. Calcineurin directly binds and dephosphorylates L-type calcium channels (LTCC). Dephosphorylation increases channel activation, which results in elevated calcium levels. Because calcineurin is itself regulated by calcium, this regulatory pathway likely represents a feed forward mechanism (Frank & Frey, 2011).

The NFAT-Calcineurin pathway is required for valve development. Tissue-specific knockout of endocardial CnB using a cre-lox mouse model resulted in failure of valve development and embryonic lethality by E14.5. Prior to lethality, mesenchymal cells were present in the valve cushions; however, valve leaflets lacking CnB displayed altered extracellular matrix and failed to elongate. Notably, myocardial NFAT-signaling at E9 is required for the initiation of EMT. Pharmacological inhibition of NFAT with cyclosporin A inhibited EMT in collagen explant gel studies. This inhibition could be rescued through addition of a Vascular Endothelial Growth Factor (VEGF) inhibitor, indicating that myocardial NFAT works to suppress VEGF signaling during endocardial cushion formation (Chang et al., 2004).

Concluding Remarks

The role of mechanotransduction in regulating valve development and pathology has become increasingly appreciated over the last few years. In several cases, the field is now able link specific fluid forces with underlying molecular circuitry that is essential for valve development progressions. Several open questions remain. Firstly, much of our understanding of how hemodynamic cues operate comes from either adult organisms or from in vitro assays. This can be attributed to the difficulty of specifically manipulating only a single biomechanical cue in animal model systems, especially small embryos. The interrogation of more model

systems using sophisticated tools such as optical tweezers to precisely manipulate hemodynamic forces at the developing valve could greatly enhance our understanding of how biomechanical cues affect the valve. Secondly, our understanding of the later stages of valve development remain incomplete. More work needs to be done to elucidate the mechanisms by which VICs remodel the ECM during development, as well as into identifying cues the cause supporting structures such as the chordea tendea to form. Thirdly, the advent of RNA-seq has been highly advantageous; we now have differential gene expression data sets from several different time points and mutants that have yielded great insight into the valve development process (Barnette, VandeKopple, Wu, Willoughby, & Lincoln, 2014; Y. Cui et al., 2019; Hulin et al., 2019). The next step in this process is to generate gene regulatory networks to identify the broad network that governs valvogenesis. Insight into how mechanostransduction impacts valve formation may facilitate the design of therapeutics to treat valve disease as well as improve the engineering of tissue-derived artificial valves

Dissertation Aims

Aim 1: Determine how increasing afterload affects valve development. High afterload can cause hypertrophy and valve disease in human adults. The effect of high afterload on embryonic development is poorly understood. To better elucidate the effect of on afterload on valve development, we first established a model system in which afterload can be reliably increased. We then investigate how an increase an afterload alters cardiac chamber morphogenesis and cell differentiation.

In the circulatory system, afterload is mathematically described as $\text{Afterload}=(8\mu L)/(\pi r^4)$; where μ is the fluid viscosity, L is the length of the vessel, and r is the radius of the vessel. Because of this relationship, very small changes in the radius of the vasculature can have a dramatic impact on the resistance (and afterload) the heart encounters. We therefore chose to

use vasopressin, a potent vasoconstrictor, to increase afterload and evaluate the effects on AV valve development in embryonic zebrafish. Importantly, the external fertilization of zebrafish coupled with their short generation times allow researchers to manipulate blood flow in genetically-amenable backgrounds at the earliest stages of development.

Aim 2: Determine the effect that increased RF has on valve development. Studies in zebrafish (Danio rerio) have highlighted the contributions of retrograde flow (RF), referring to the portion of blood flow that flows backwards from the ventricle to the atrium during pre-valvular stages of development. RF functions as a discrete biomechanical cue required for atrioventricular valve development. The presence of retrograde flow promotes expression of the mechanosensitive transcription factor Kruppel-like factor 2a (*klf2a*), which is required for valve development. Taken together, these data indicate that hemodynamic cues may induce discrete transcriptional changes that regulate gene expression and cell differentiation.

While the relationship between RF and *klf2a* is well established, how RF and klf2a work together to direct cell behavior and differentiation is not well established. To address this question, we first defined the developmental period in which RF occurs. We then perturbed RF during this period through the use vasopressin. Finally, we examine how overexpression of *klf2a* alters development. Work completed in this aim helps to better understand how RF affects valve development.

Aim 3: Characterizing transcriptional changes that regulate atrioventricular myocyte development and function. At 48 hours post-fertilization, AVJ cardiomyocytes transition to a trapezoidal shape compared to cuboidal ventricular and flat atrial cardiomyocytes. AVJ myocytes secrete Bone Morphogenetic Protein 4 (bmp4), which signals adjacent endocardial cells to initiate leaflet formation. Although basic morphological steps are described, a knowledge gap exists regarding genetic mechanisms required for AVJ differentiation. We expect that a unique set of genes regulates differentiation of AVJ cardiomyocytes. To fully characterize the differentiation of these AVJ myocytes, we took an RNA-seq approach.

To isolate AVJ myocytes, we used a bmp4 reporter line [Tg(bmp4:eGFP)] that expresses eGFP in AVJ myocytes. We used Fluorescent Activated Cell Sorting (FACS) to isolate AVJ myocytes and chamber myocytes. For comparison, we isolated undifferentiated cardiomyocytes from younger embryos. Cells were used for RNA-seq. We find that AVJ cells undergo distinct transcriptional changes than chamber cells and identify putative regulator of AVJ myocyte differentiation.

Chapter 2: Myocardial Afterload Regulates Atrioventricular Valve Cell Differentiation

Summary

Aims: Heart valve development is governed by both genetic and biomechanical inputs. Prior work demonstrated that oscillating shear stress associated with blood flow is required for normal atrioventricular (AV) valve development. Other biomechanical inputs such as loading and pressure present during heart development may also impact cardiogenesis in distinct ways. Cardiac afterload is defined as the pressure the ventricle must overcome to pump blood throughout the circulatory system. In human patients, conditions of high afterload can cause valve pathology. Whether high afterload adversely affects embryonic valve development, or predisposes hearts to malfunction later in life, remains poorly understood.

The objective of this work is to develop an animal model in which embryos are subject to high cardiac afterload and investigate the resultant phenotypes and underlying molecular circuitry.

Methods and Results: Here we describe a zebrafish model exhibiting increased myocardial afterload, caused by vasopressin, a vasoconstrictive drug. We show that application of vasopressin reliably produces an increase in afterload without directly acting on cardiac tissue in zebrafish embryos. We find that increased afterload alters the rate of growth of cardiac chambers and causes remodeling of cardiomyocytes. Consistent with pathology seen in patients with clinically high afterload, we see defects in both form and function of the valve leaflets.

Conclusions: Conditions of high afterload lead to altered cardiac function and altered valve mechanics in developing embryos. Our results suggest that valve defects are due to changes in atrioventricular myocyte signaling, rather than pressure directly acting on the endothelial valve

leaflet cells. Cardiac afterload should be considered a biomechanical factor that particularly impacts embryonic valve development. (Abstract)

Introduction

Congenital heart defects (CHD) occur when the heart fails to form appropriately during the early stages of embryonic development. Approximately 8 out of every 1000 births result in a newborn with CHD.("Congenital Heart Defects," 2017) Valve pathology occurs in over 50% of all CHD cases.(Hoffman & Kaplan, 2002) Despite the prevalence of CHD, the etiology of CHD is not well understood. In fact, only approximately 20% of all CHD arise from a known genetic lesion.(Blue, Kirk, Sholler, Harvey, & Winlaw, 2012) Phenotypically-similar CHD may arise from mutations in unrelated proteins,(Buja & Butany, 2015) and conversely, identical mutations can cause a variety of distinct phenotypes.(Fahed, Gelb, Seidman, & Seidman, 2014) A likely explanation of this phenomenon is that the pathology arises not only from loss or modification of protein function, but also through alteration of the mechanical environment of the heart. Increasingly, research efforts are directed at defining biomechanical contributions to normal heart development and CHD.

Shear stress produced by blood flow within the heart lumen, contraction itself, and pressures resulting from contraction represent types of biomechanical cues that facilitate normal development of valves.(Francesco Boselli et al., 2015; Haack & Abdelilah-Seyfried, 2016) Because endothelial cells contributing to development of the AV valve are in direct contact with blood flow, they may be especially sensitive to perturbations in hemodynamics. As one example, exposure of porcine valves to physiological levels of shear stress was found to directly impact development of the striated ECM present in valve leaflets through the induction of collagen expression and even differentially affects each forming valve leaflet.(Mongkoldhumrongkul, Latif, Yacoub, & Chester, 2016)

While the biomechanical signals derived from shear stress are increasingly wellcharacterized, the impact of other potential biomechanical signals such as cardiac loading on cardiac development remain relatively uninvestigated. Afterload refers to the resistance the ventricle must overcome to pump blood throughout the circulatory system. For a given cardiac output, the pressure is proportional to the flow rate times the resistance. The higher the afterload, the higher the transmural pressure throughout the heart.(Pappano & Wier, 2013)

In the fetus, conditions of high afterload have been linked to ventricular hypertrophy and fetal hydrops.(Davey, Szwast, & Rychik, 2012) Human fetuses with decreased fetal growth demonstrate decreased cardiac output thought to be caused by increased afterload,(Verburg et al., 2008) as well as tricuspid valve regurgitation.(Davey et al., 2012) Moreover, afterload is linked to CHD as shown by work demonstrating that reduction in afterload through Hydralazine (a vasodilator) treatment can help mitigate large ventricular septal defects.(Endo, Shiraishi, & Yanagisawa, 1994),(Beekman, Rocchini, Dick II, Crowley, & Rosenthal, 1984) The impact of high afterload has been best characterized in adult organisms, where its' deleterious effects lead to valve pathology and cardiac hypertrophy.(Davila & Forfia, 2015; Hirt et al., 2012; Levy et al., 1996) Specifically, adult patients with conditions of increased afterload often experience concentric pathologic hypertrophy, in which sarcomeres are added in parallel within existing myofibrils.(Bernardo, Weeks, Pretorius, & McMullen, 2010)A better understanding of the molecular circuitry activated by the afterload-response may yield translational insights into the causes of both adult valve pathology and CHD.

Studies of how abnormal afterload might impact embryonic valve development so far have been hampered by a paucity of *in vivo* tools able to accurately and reliably induce conditions of altered loading without directly impairing cardiac contraction. Prior work has utilized models such as outflow tract (OFT) ligation in chick embryos to increase afterload.(Madeline Midgett & Rugonyi, 2014) Increasing afterload through OFT ligation resulted in a smaller mitral valve, dysregulation of shear stress-responsive genes and altered expression

of ECM markers.(Pang et al., 2017) Conversely, computational models of avian embryonic valve development predicted that increased pressure on the developing endocardial cushions would promote leaflet-like elongation. These studies demonstrate that loading can affect AV valve development.

To respond to changes in afterload, cells at the atrio-ventricular junction (AVJ) must be able to perceive changes in blood flow and pressure. Endocardial cells can sense both the direction and the magnitude of blood flow through mechanosensors.(Haack & Abdelilah-Seyfried, 2016) Monocilia present on endocardial cells are thought to bend under conditions of high flow and shear stress, leading to the activation of signaling pathways. Mouse endocardial cells lacking cardiac cilia fail to properly develop endocardial cushions and show impaired endothelial-to-mesenchymal transition (EMT).(Slough et al., 2008) Mechanosensitive ion channels can activate expression of transcription factor *klf2a* under conditions of oscillatory flow.(Heckel et al., 2015) Despite being physically separated from flow, myocardial cells also play a role in mechanotransduction. *In vitro* rat myocardial cells adapted to changes in load by undergoing hypertrophy.(Hirt et al., 2012) Myocardial cells may perceive changes in load by assessing their degree of stretch using NFAT-calcineurin or titan-mediated mechanisms.(McCain & Parker, 2011) These cells may also sense direct pressure transmitted through the cardiac wall through integrin-mediated mechanisms.(McCain & Parker, 2011) As part of their normal function, myocardial cells release paracrine signaling factors, such as BMP, that are required to signal endocardial differentiation.(Dietrich, Lombardo, Veerkamp, Priller, & Abdelilah-Seyfried, 2014) Based on these findings, it is possible that the loading state of the myocytes impacts their release of key signals required for normal valve development.

In the circulatory system, resistance is mathematically described as $Resistance = (8\mu L)/(\pi r^4)$; where μ is the fluid viscosity, *L* is the length of the vessel, and *r* is the radius of the vessel. Because of this relationship, very small changes in the radius of the vasculature can have a dramatic impact on the resistance (and afterload) the heart encounters. We therefore

chose to use vasopressin, a potent vasoconstrictor, to increase afterload and evaluate the effects on AV valve development in embryonic zebrafish.

Vasopressin is 9 amino-acid hormone that causes vasoconstriction. The zebrafish genome encodes three vasopressin receptors: *avtr$_{1a1}$*, *avtr$_{1a2}$*, and *avpr2*. *Avtr$_{1a1}$* and *avtr$_{1a2}$* are both homologues of the mammalian V1a receptor.(Iwasaki & Kenichi, 2013) The mammalian V1 receptor is expressed predominantly in smooth muscle cells surrounding peripheral vessels. Vasopressin binding triggers an intracellular cascade that increases the intracellular calcium concentration and consequently causes muscle constriction and vasoconstriction.(Daza, Lewicka, & Larhammar, 2012) The mammalian V2 receptor, which is a homolog of the zebrafish *avpr2* receptor, is expressed predominantly in the kidneys and acts to increase blood volume. Stimulation via either receptor raises blood pressure and directly increases myocardial afterload through increased vascular resistance.(Holmes, Landry, & Granton, 2004)

Here, we show that vasopressin is vasoactive in zebrafish, and demonstrate that vasopressin application produces alterations in cardiac function and growth. We find that increased afterload affects the differentiation of both endocardial and myocardial valve cells. Our data support myocardial AVJ cells as especially sensitive to alterations in afterload in normal development.

Methods

Zebrafish Husbandry and Vasopressin Application

Zebrafish were raised as per Colorado State University Animal Care and Use Protocols. Zebrafish embryos were raised at 28.5°C until 24 hpf in E3 medium, and dechorionated. Embryos were placed in a solution of Arginine-Vasopressin Acetate Salt (Sigma, catalog number V9879) diluted in E3 embryo media to a final concentration of 10 µmol/L, unless otherwise specified. Treated embryos remained in vasopressin solution for the entirety of the study.

Live Imaging

For vessel and whole heart live imaging, samples were immobilized in agarose and treated with MESAB to temporarily stop heartbeats. Quantification of vessel diameter was performed in Image J.(Rueden et al., 2017) Quantification of cardiac chamber volume and looping angle was performed as previously described.(J Yang, Hartjes, Nelson, & Xu, 2014),(Berndt, Poschmann, Stühler, Holmgren, & Bräutigam, 2014)

For live imaging of the valves, confocal microscopy was used. Embryos were treated with MESAB until cardiac contraction stopped, and then mounted in low-melt agarose in a depression slide in a tilted ventral-up orientation, such that the heart was roughly parallel to the coverslip.

Quantification of Cardiac Functional Parameters

Quantification of cardiac parameters (cardiac output, stroke volume and heart rate) was performed as previously described.(Johnson et al., 2013) Briefly, embryos were raised at 28.5°C until the appropriate time point. Fish were mounted in low melt agarose, with no MESAB. Videos were taken with a Photron Mini UX-100 camera at 1600 frames per second, across at least 3 cardiac cycles. Videos were analyzed as previously described using a line scan and spatiotemporal kymographs to quantify cell movement along the line scan.(Johnson et al., 2013)

Immunohistochemistry

Immunohistochemistry was performed on dissected zebrafish hearts as previously described.(Jingchun Yang & Xu, 2012) Briefly, hearts were dissected in an L15-10% FBS solution and then placed on a polylysine-coated slide. Hearts were fixed for 40 minutes in 4% PFA and permeabilized with a 1% solution of Triton-X. For ALCAM labelling, zn8 antibody (Hybridoma Bank) was used at 1:10 dilution. Embryos were washed 3X with PBST solution and then incubated with Alexa-546 anti-mouse IgG secondary antibody (Thermo-Fischer Cat #A-11030) at a 1:200 dilution. Hearts were mounted in50% glycerol under coverslips. Images were taken on the Zeiss LSM800 and analyzed blind.

Reverse-Transcriptase PCR

RNA was extracted from either dissected hearts or entire embryos, using TRIzol (Invitrogen) according to manufacturer's protocol and diluted in Nuclease-Free Water (Sigma). cDNA synthesis was performed using AMV reverse transcriptase (Fisher Scientific) and Oligo(dT)$_{12-18}$ primer (Invitrogen). PCR products were separated a 2% agarose gel.

Results

Vasopressin Actively Elicits Vasoconstriction in Zebrafish Embryos

To verify that vasopressin receptors are expressed embryonically in zebrafish, we performed reverse-transcriptase PCR on RNA extracted from either dissected heart tissue or whole embryos at 24, 48 or 72 hpf (Figure 1A and Supplemental Figure 1A). At all timepoints tested, the *avtr$_{1a1}$*, *avtr$_{1a2}$*, and *avpr2* receptors were all expressed in whole body samples but not in cardiac samples. This finding implies that the observed cardiac phenotypes caused by vasopressin application do not arise from direct action of vasopressin on cardiac tissue, but rather reflect biomechanical impacts arising from changes in cardiac afterload and its downstream consequences.

To measure directly whether vasopressin elicits vasoconstriction in zebrafish embryos, we transferred Tg(fli1:EGFP) embryos at 24 hours post-fertilization (hpf) to media containing 10 µM of vasopressin, and measured vessel diameters at 52 hpf by assessing the outside borders of the GFP-labeled endothelial cells (Figure 1B-D). We found that 24 hours of vasopressin exposure was sufficient to cause significant vasoconstriction of major blood vessels (18% constriction in the dorsal aorta and 25% constriction in the cardinal vein; p=0.007 for dorsal aorta, p=0.0004 for cardinal vein). Vessel radius is the major regulator of vascular resistance in the body ($(Resistance = (8\mu L)/(\pi r^4)$; where µ is the fluid viscosity, *L* is the length of the vessel, and *r* is the radius of the vessel). Thus, an 18 or 25 percent constriction in diameter corresponds to a 124% and 281% increase in resistance, respectively, with the assumptions of Hagen-Poiseuille flow. Vasopressin application did not cause detectable constriction of the

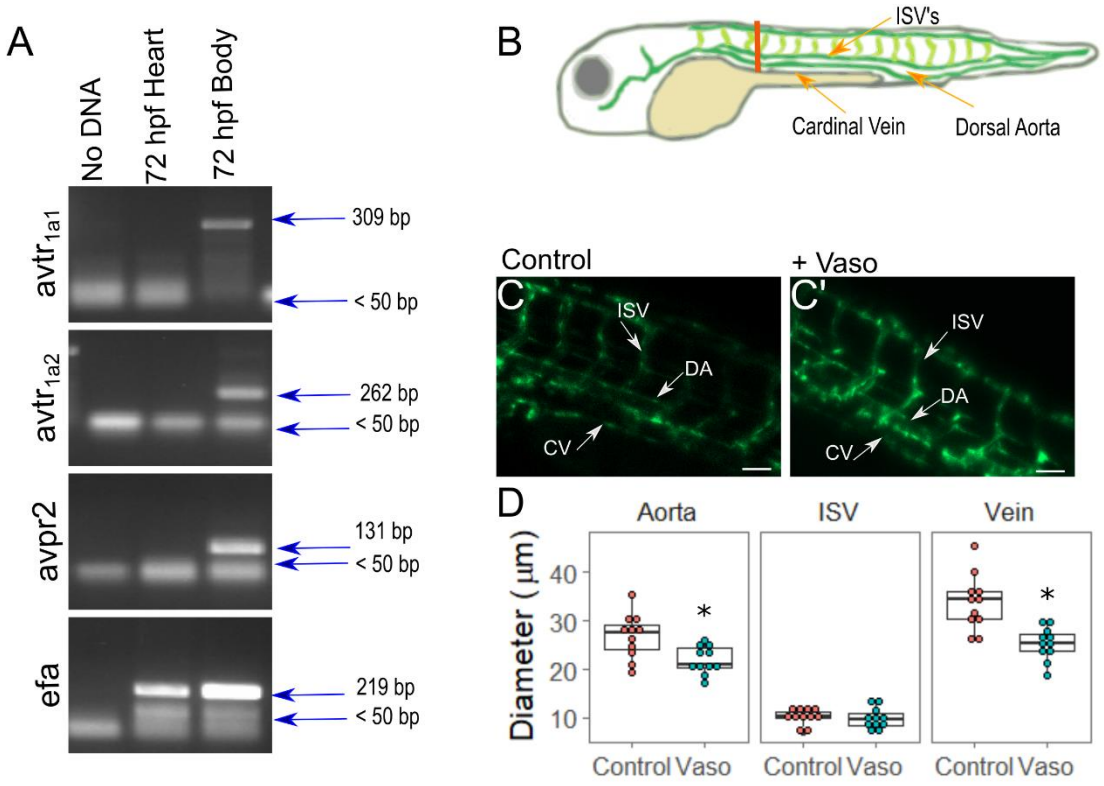

Figure 2.1: Application of vasopressin (vaso) causes vasoconstriction of major blood vessels in zebrafish by 48 hpf. A) RT-PCT of vasopressin receptors in whole body vs cardiac tissues. B) Diagram of zebrafish vasculature. C) Vasculature of control and C') vasopressin-treated embryos at 48 hpf. D) Diameter of cardinal vein (CV), dorsal aorta (DA), and intersegmental vessels (ISV). For D-E: n=11 for wildtype, n=11 vasopressin-treated embryos. Two-sided t-test was performed to validate statistical significance. * indicates $p < 0.05$. Scare bar represents 50 micrometers.

intersegmental vessels (ISVs)(p=0.43). At 52 hpf, ISVs have not yet developed smooth muscle,(Ando et al., 2016) which is consistent with their failure to constrict here. To determine the minimal length of vasopressin exposure sufficient for significant vasoconstriction, we treated 24 hpf embryos with vasopressin for shorter periods and again measured the diameter of the dorsal aorta. Embryos exposed to 4 hours of vasopressin treatment already showed significant constriction in their dorsal aorta (Supplemental Figure 1B). Among treated and untreated embryos, very few exhibited general abnormalities like hemorrhaging, or body patterning defects (<5 out of 78 embryos scored presented either defect). To assess the degree of cell death, 72 hpf embryos were treated with acridine orange, a vital dye. Vasopressin-treated embryos did not exhibit significantly more cell death than buffer-treated controls, suggesting that vasopressin treatment is not toxic to cells (Supplemental Figure 2). Together, these data establish vasopressin exposure as a reliable method to increase afterload in zebrafish embryos without directly acting on cardiac tissue.

Increased Afterload Alters Cardiac Function and Growth

We next tested the hypothesis that increased afterload impairs zebrafish embryonic cardiac function. We exposed embryos to 0, 2.5, 5, 7.5, and 10 µM doses of vasopressin beginning at 24 hpf. After 16 hours of continuous vasopressin exposure (i.e., in 40 hpf embryos), we found that increasing concentrations of vasopressin produced a dose-dependent effect on vessel constriction (Supplemental Figure 3), and therefore a dose-dependent effect on afterload. Doses of 5 µM or higher produced significant vessel constriction. To measure cardiac output, control and vasopressin-treated embryos were recorded by high-speed video. Kymograph analysis provided a measure of the velocity of red blood cells, which was then used to calculate flow rate. Parameters of cardiac function were computed from flow rate as previously described.(Johnson et al., 2013)

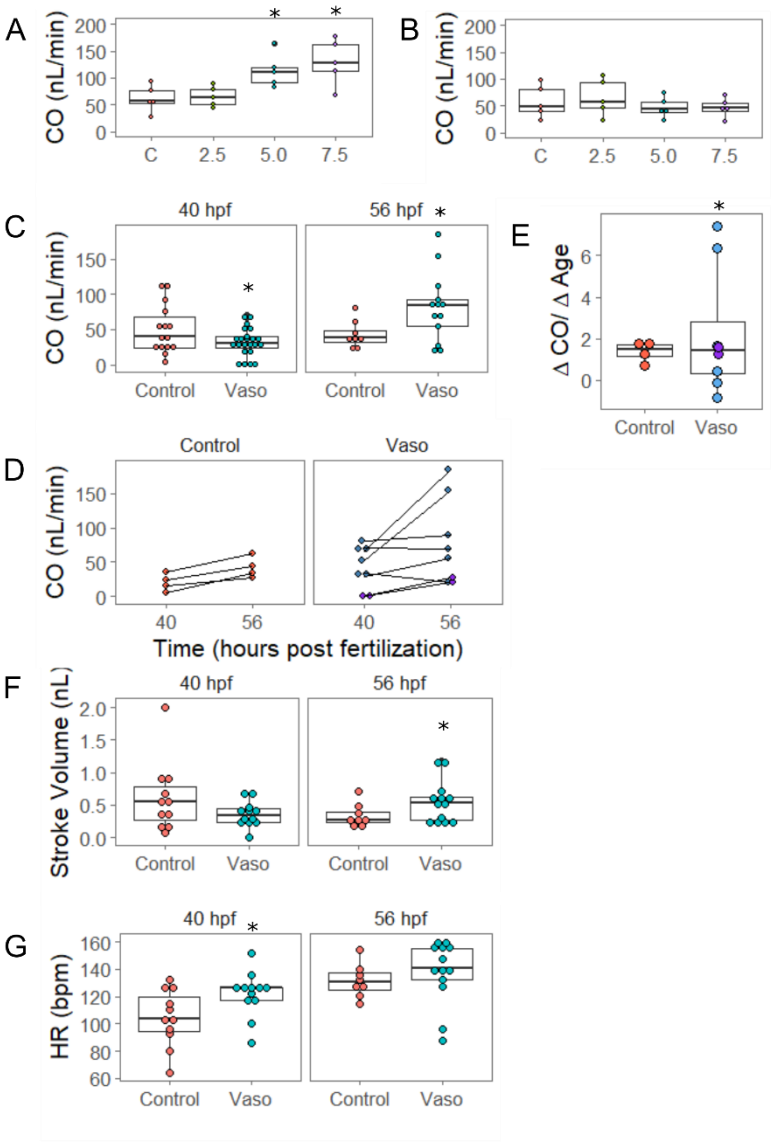

Figure 2.2: Increased pressure causes a compensatory response by 56 hpf. A) Cardiac output at 40 hpf at increasing doses of vasopressin (control, 2.5, 5, and 7.5 um). B) CO at 56 hpf at increasing doses of vasopressin. N = 5 fish per group. C) Cardiac output at 40 and 56 hpf in control and vaso-treated fish. N = 15 control, 23 vaso-treated fish at 40 hpf, 8 control and 11 vaso-treated at 56 hpf. D) Cardiac output throught time, where each colored dot represents a tracked individual fish; orange dots represent control fish, light blue dots represent mildly-affected and purple represents severely-affected fish. N = 4 control, 8 vaso. E) Rate of change for cardiac output with respect to time. F) Stroke volume and G) heart rate of control and 10 micromolar treated vaso fish. N= 11 control and 12 vaso-treated fish at 40 hpf. * indicates $p < 0.05$

At 24hpf, the heart has just formed a linear tube and is beginning to contract, but circulation is not yet robust. We measured the heart rate of embryos immediately before posure to 10 µM vasopressin, and then after 5 minutes of vasopressin exposure. There was no significant difference in heart rate post vasopressin exposure (Supplementary Figure 4, $p = 0.29$, $n = 3$ control and 3 vasopressin-treated embryos). No overt change in morphology was note. Consequently, changes noted at later time points are likely due to remodeling events and not a consequence of vasopressin-application.

At 40 hpf the constriction at the AVJ has developed, but endocardial cushion formation has not yet initiated. Analysis of embryos at this time point revealed that embryos treated with 5 µM vasopressin produced a 1.85-fold increase in cardiac output, and embryos treated with the 7.5 µM dose produced a 2.11-fold increase in cardiac output relative to controls (Figure 2A, $p=0.03$ for 5 µM, and $p=0.005$ for 7.5 µM). Because there These data clearly suggest that hearts are sensing the change in load and are implementing functional responses to meet physiological need. Given that cardiac output is the product of stroke volume times heart rate, we investigated whether either of these measures changed. The stroke volume for embryos treated with either the 5 µM or 7.5 µM dose averaged approximately 33% larger than controls, providing some explanation for the increased cardiac output, though this difference was not statistically significant (Supplemental Figure 5, $p=0.25$ for 5 µM, 0.07 for 7.5 µM). However, embryos at all doses demonstrated significant increases in heart rate equivalent to 125-135% of controls, providing a further explanation for the increased cardiac output (Supplemental Figure 6, $p=0.04$ for 2.5 µM, $p=0.007$ for 5 µM, $p=0.003$ for 7.5 µM, $p=0.04$ for 10 µM). Together, these data taken at 40 hpf suggest that moderate increases in afterload (5 and 7.5 µM doses) triggered a compensatory response of increased heart rate, resulting in an increased cardiac output.

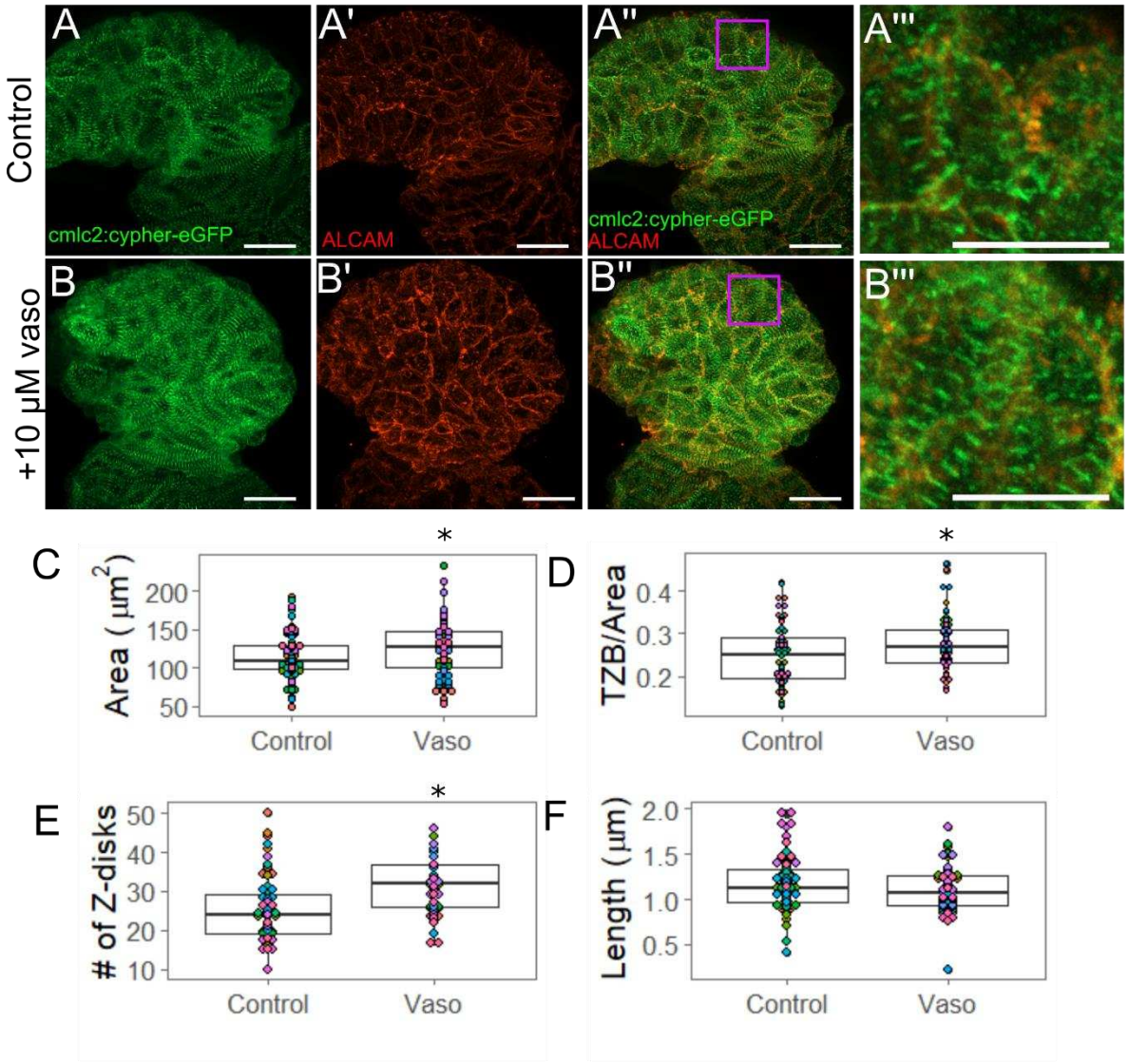

Figure 2.3: High Afterload Induces Cardiac Hypertrophy by 56 hpf. A) Control and B) vasotreated hearts showing zbands (A, B) and cell shape through ALCAM immunohistochemistry Purple box shows region of interest shown in A''' and B'''. For A-A'', and B-B'', scale bar represents 20 µm. For A''' and B''', scale bar represents 10 µm. C) Area of ventricular cells. D) Total z-band size (TZB) of sarcomeres present in each cell normalized to the area of each cell (1/µm). E) Number of z-bands per cell. F) Average length of the sarcomeres present in each cell. For control and vasotreated hearts, 14 fish were analyzed. 5 cells from the were analyzed per fish, such that 70 total cells were analyzed.. * indicates $p < 0.05$.

Embryos exposed to the 10 µM dose reacted differently than those exposed to lower doses. First, they did not achieve an increase in cardiac output by 40 hpf, but instead demonstrated a significant decrease in cardiac output (Figure 2C; control = 50.6 nL/min, vasopressin=32.26 nL/min, p=0.04 by t-test, n=15 control, and 23 vasopressin-treated embryos). A subset of the embryos treated with 10 µM vasopressin (7 out of 23 embryos) exhibited disproportionate chambers and increased looping angle (Supplemental Movie 2). These embryos were termed "severely affected," while embryos that did not exhibit these overt morphological defects were termed "mildly affected." Looping angle was evaluated by measuring the angle between the line bisecting the atrium and the line parallel to blood flow in the AVJ.(Johnson et al., 2013) Control and mildly affected embryos displayed similar looping angles (109º for control, 104º for mildly affected; n=16 control, 16 mildly affected, p=0.52 by Dunnett's test), while severely affected embryos had an average looping angle of 139º (n=7, p=0.002 against control by Dunnett's test, Supplemental Figure 7A).

To evaluate if treated chambers grew in proportion to those in control hearts, we measured the cross-sectional area of the ventricle and atrium at the end of ventricular contraction and calculated the ratio of ventricular area to atrial area. Control and mildly affected embryos displayed similar chamber area ratios (control = 0.42, mild = 0.47, p=0.25 by Dunnett's test), whereas the chamber area ratio of severely affected embryos was significantly smaller (ratio = 0.27, p=0.00013 by Dunnett's test, Supplemental Figure 7B). To further analyze this data, we plotted embryo count against the looping angle or chamber area ratio (Supplemental Figure 8). In both cases, the severely affected embryos clustered together, and the data distributions appeared bimodal (Hartigan's diptest for unimodality, p=0.03 for looping angle, and p=0.05 for chamber area ratio). Together, this data indicates that under conditions of high afterload, about two-thirds of hearts develop the correct chamber morphology and looping angle by 40 hpf, while approximately one-third of hearts were compromised.

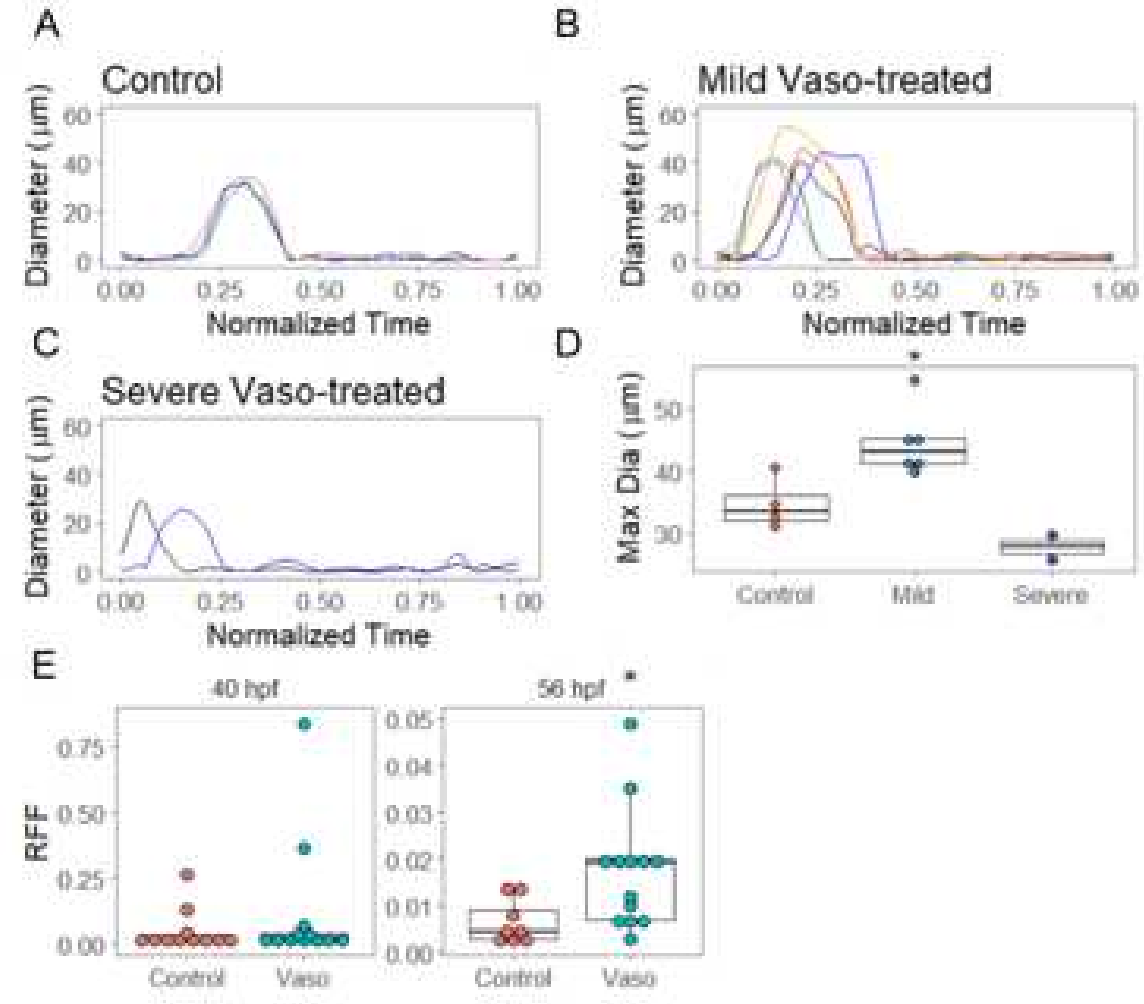

Figure 2.4: Increased afterload increases retrograde flow and alters AVJ mechanics. A) Diameter of the flow field at the atrioventricular junction in control hearts at 56 hpf. X-axis is normalized time across a cardiac cycle, where 0 corresponds to the beginning of atrial contraction and 1 represents the end of ventricular contraction. n = 4 B) Diameter analysis of vaso-treated hearts that showed hypertrophic growth between 40 and 56 hpf. n = 6 C) Diameter analysis of vaso-treated hearts at 56 hpf. These hearts showed severely altered pumping mechanics at 40 hpf. D) Maximum diameter analysis of control, vaso-treated hearts that showed altered pumping (AP) and vaso-treated hearts that showed hypertrophic growth (HH). E) Retrograde flow fraction (RFF) at 40 and 56 hpf in control and vaso-treated hearts. n = 11 control and 12 vaso-treated fish. * indicates $p < 0.05$.

To understand how increasing afterload alters overall contraction patterns in the heart, we measured the speed of the progressing contractile wave in control and 10 µM vasopressin-treated embryos at 40 hpf. In this assay, we tracked successive points of maximal chamber lumen constriction as contractile wave progressed across the length of the heart tube. The speed of the contraction wave across the cardiac cycle was plotted against normalized time; where 0 corresponds to the onset of contraction at the atrial inlet, and 1 corresponds to the completion of ventricular systole. In control embryos, the speed of contraction during atrial systole peaked at 2.4 mm/s, then slowed to 0.3 mm/s as the wave passed into the AVJ, followed by increases in speed as contraction proceeded through the ventricle (Supplemental Figure 9). In the 10 µM vasopressin-treated group, both mild embryos and severe embryos displayed similar contraction wave patterns: contraction through at the atrial inlet began with a similar speed (control average: 2.2 mm/s, vasopressin average: 2.5 mm/s, p=0.30), but the speed did not peak near the end of atrial systole as occurred in control embryos. Furthermore, the speed of the contraction wave in the AVJ itself was 2 to 3-fold increased in both mild and severe vasopressin-treated embryos, a significant difference (Supplemental Figure 10A, n= 11 control, 15 mild, and 7-severe vasopressin-treated embryos; p=0.03 for control vs mild, and p=0.003 for control vs severe by Dunnett's test) To correct for possible variability in the overall contraction speed in each heart, we normalized the AVJ speed to the maximum speed in each heart, but significant increases were still detectable (Supplemental Figure 10B). Together this data indicates that increased afterload has already altered cardiac contraction patterns by 40 hpf and specifically alters AVJ function, even in the mildly-affected group.

To investigate how increasing afterload alters embryonic pumping mechanics, we evaluated the length of endothelial closure in 40 hpf embryos. During each cardiac cycle, there exists a period during which the endothelial layers lining either side of the AVJ come into brief

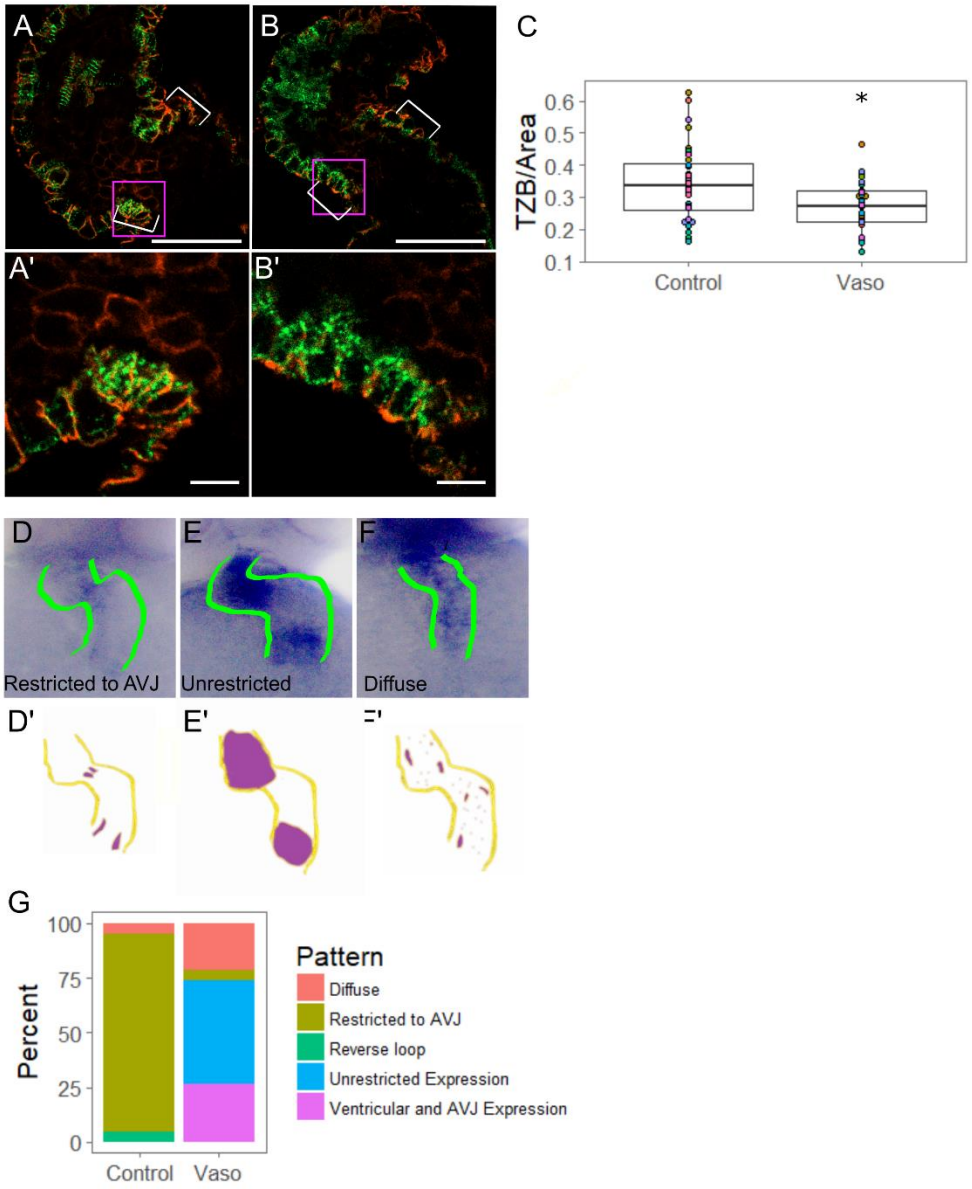

Figure 2.5: Increased pressure alters AVJ myocyte morphology and specification. A) Control and B) vaso-treated hearts showing z-bands and cell shape through ALCAM immunohistochemistry at 56 hpf. Purple box shows region of interest shown in A' and B'. For A-A-B, scale bar represents 20 µm. A') Control and B') vaso-treated hearts. Scale bar represents 10 µm. White brackets indicate AVJ. C) TZB of sarcomeres present in each cell normalized to the area of each cell (1/µm). n=36 cells for control and 33 for vaso-treated hearts. Two-sided t-test was used to assess statistical significance, * indicate $p < 0.05$. D) *In situ* hybridrization of myocardial AVJ marker *bmp4* in control and E-F) vaso-treated hearts. D'-F') Diagrams of ISH expression patterns. G) Percent of fish expressing a particular *bmp4* expression pattern. 20 fish were scored in each group.

physical contact. In control embryos, the length of endothelial closure (i.e., the extent of maximal endothelial contact in the AVJ region) approximates 77 μm at the end of ventricular systole (see Supplemental Figure 11). Previously, our group identified the length of endothelial closure as a parameter that embryonic hearts can alter to adapt to increases in pressure and limit reverse flow.(Bulk, Bark, Johnson, Garrity, & Dasi, 2016) Thus, we hypothesized that as afterload increased in relation to greater vasopressin concentrations, the length of endothelial closure would also increase. We measured the length of endothelial closure for each dose of vasopressin (from 0 to 10 μM). As predicted, vasopressin elicited a dose-responsive increase in the length of endothelial closure by 40 hpf (Supplemental Figure 11). This data suggests that hearts subjected to sustained high afterload use increased endothelial closure as one means to adapt to stressful pressure.

By 56 hpf, the chambers have undergone primary ballooning and endocardial cushion development is robust. After 32 hours of continuous vasopressin exposure (i.e., in 56 hpf embryos), we re-examined heart function to determine how well hearts had adapted to a period of sustained high afterload. Remarkably, by 56 hpf no significant differences in cardiac output were detected at any of the doses tested expect for the 10 μM, which displayed significantly increased cardiac output (Figure 2C, $p=0.04$ by Tukey's). No embryos overtly exhibited weakened contractility. Since these findings contrasted with those of 40 hpf, we hypothesized that embryo hearts have adaptive to rescue cardiac function by 56 hpf. To test this hypothesis, we tracked individual control or 10 μM vasopressin-treated embryos and assessed cardiac function at both 40 and 56 hpf. We obtained time-matched data sets for 4 control and 8 vasopressin-treated embryos, of which 2 had exhibited the severe phenotype at 40 hpf. Intriguingly, these two embryos did not display any overt morphological defects at 56 hpf (Supplemental Movie 3). Control embryos uniformly increased cardiac output between 40 and 56 hpf (n=4), while vasopressin-treated embryos exhibited much more variability in their

response (n=8; Figure 2C). Quantification of the rate of change using Bartlett's test for homogeneity of variance confirmed that vasopressin-treated embryos responded with significantly more variability than controls (Figure 2D; p=0.01), though their overall rate of change was not significantly different (p=0.27). This data indicates that at the highest tested condition of afterload, rather than continuing the downward trend in function seen at 40 hpf, by 56 hpf embryos were on average able to sustain their CO, and in some cases increase it over controls.

To better understand how embryos at the 10 µM dose had modulated cardiac output, we analyzed stroke volume and heart rate at 56 hpf. No significant differences were detected in stroke volume at 40 hpf (p=0.32 by Kruskal-Wallis). However, at 56 hpf, stroke volume was ~50% higher in vaso-treated embryos compared to controls, a significant change (Figure 2E, p= 0.04 by t-test). At 40 hpf, vaso-treated embryos had demonstrated heart rates approximately 7% higher than controls, a significant change (Figure 2F, p=0.03 by t-test), but heart rates at 56 hpf matched controls. These data suggest that increased heart rate was the initial adaptation to compensate for increased afterload at 40 hpf, but that increased stroke volume was the primary driving force that maintained (or increased) cardiac output at 56 hpf.

Increased Afterload Induces Cardiac Hypertrophy and Alters Sarcomere Abundance

Compared to the lower doses, the 10 µM treated embryos took longer to ramp up their response of increased cardiac output, as might be expected by the work needed for hearts to pump against such high resistance. We hypothesized that hearts in 56 hpf treated embryos had structurally remodeled to provide a sustainable response. The next series of experiments focusses on 10 µM treated embryos to investigate this hypothesis.

Murine models indicate that hypertrophy in the cardiac ventricle reflects an increase in myocardial cell size, while embryonic chicks undergo hyperplasia in response to conotruncal banding.(Clark, Hu, Frommelt, Dummett, & Tomanek, 1989; Maarman, 2013) To evaluate

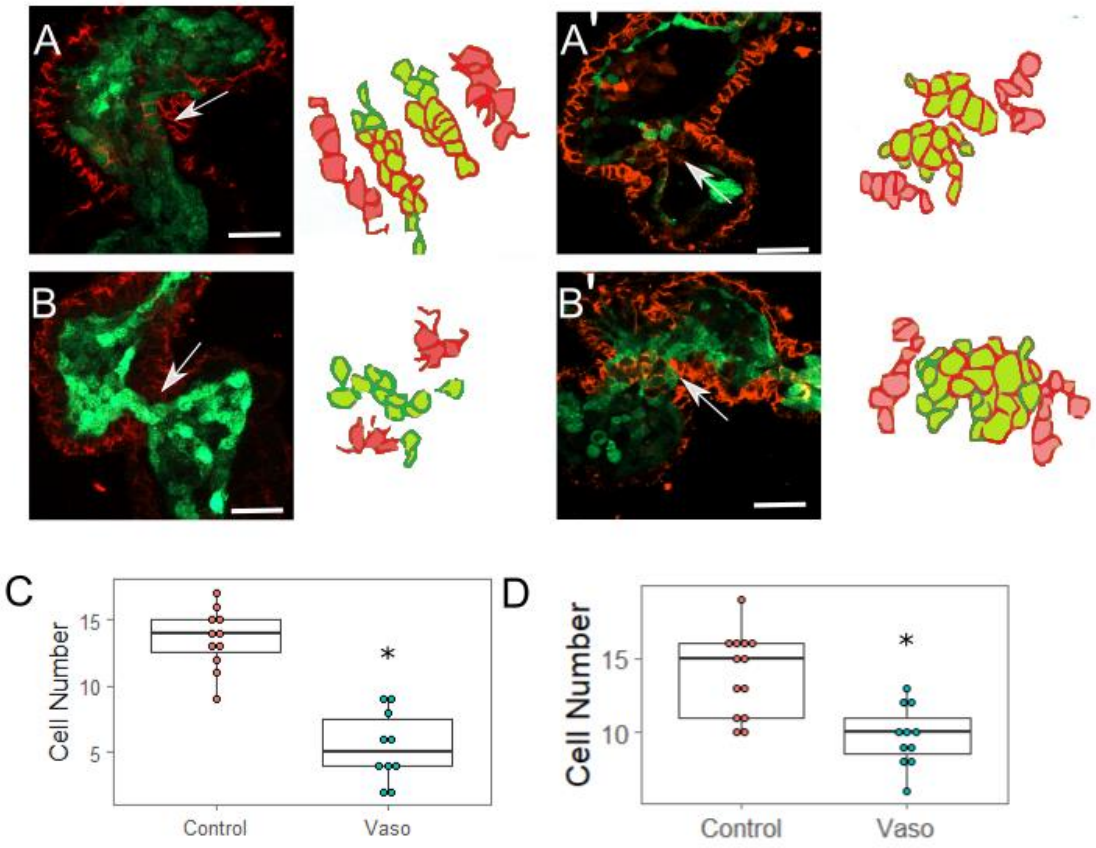

Figure 2.6: Increased Myocardial Afterload Causes Aberrant AVJ Cell Specification. A) Control hearts stained with ALCAM at 56 hpf. A') Control hearts stained with ALCAM at 72 hpf. Scale bar represents 20 µm. B-B') Representative image of vaso-treated heart at B) 56 hpf and at B') 72 hpf. C) Number of ALCAM expressing endocardial cells. N = 11 wildtype hearts, 10 vasopressin treated hearts at 56 hpf. Statistical significance was determined using t-test; * indicates $p < 0.05$. D) C) Number of ALCAM expressing endocardial cells. N = 11 wildtype hearts, 10 vasopressin-treated hearts at 72 hpf. 5 cells were analyzed per location per heart, area was measured for each cell and averaged. AVJ myocardial cells were defined as myocardial cells located in the constriction between the atrium and ventricle.

whether or not zebrafish experience hyperplasia in response to increases in afterload, we exposed Tg(myl:dsred-nuc) embryos, which express dsRED in the nucleus of cardiomyocytes to 10 µM vasopressin from 24 to 56 hpf and evaluated ventricular cell number. We found no change in the number of ventricular cardiomyocytes between control and vaso-treated embryos (control average = 82, vaso average = 87, p=0.48, n=4 control and 5 vaso-treated embryos, Supplementary Figure 12).To evaluate ventricle size in zebrafish, Tg(myl7:eGFP) embryos, which express GFP in cardiomyocytes,(Huang, Tu, Hsiao, Hsieh, & Tsai, 2003) were treated with 10 µM vasopressin from 24-56 hpf. Vaso-treated hearts showed a significant increase in overall ventricular volume (Supplemental Figure 13). To further determine if increases in loading increased myocardial cell size or shape, we evaluated cardiomyocytes using rhodamine-labeled phalloidin, which binds actin fibers located predominantly near the cell periphery. By 52 hpf, myocardial cells in the mid-ventricle were 17% larger in vaso-treated hearts relative to controls (p=0.04), but retained a similar degree of circularity (Supplemental Figure 14; p=0.23). Thus, application of vasopressin to zebrafish embryos recapitulates the hypertrophic effects of afterload observed in other vertebrate animal models.

Because embryos exposed to the 10 µM dose of vasopressin experienced an increase in stroke volume, we hypothesized that they may increase their myofibril content on a per cell basis. Following the approach of Lin et al (2012), we used the Tg(myl7:cypher-eGFP) transgenic line to visualize z-bands in the heart, and quantify their size and number per cell.(Lin, Swinburne, & Yelon, 2012) The summed length of all z-bands represents the total z-band size (TZB) per cell (Supplemental Figure 15). The TZB is normalized to the planar cross-sectional area of the cell to assess the total myofibril content per cell while accounting for differences in cell size.

To determine whether increased myofibril content could account for the increase in stroke volume observed in embryos treated with the 10 µM dose of vasopressin at 56 hpf, we

measured myofibril content of individual cardiomyocytes using the Tg(myl7:cypher-eGFP) line, in which cypher (a z-disc protein) has been tagged with eGFP. We performed immunohistochemistry using the ALCAM (activated leukocyte cell adhesion molecule; also called DmGrasp) antibody, which marks myocardial cell borders to measure the cross-sectional area of each ALCAM-labeled cell. We observed that cells exposed to 10 µM vasopressin were approximately 10% larger than their untreated counterparts ($p=0.04$), consistent with the rhodamine-phallodin data above. After being normalized to the individual cell area, the data indicated an approximately 5% average increase in TZB in vasopressin-treated cardiomyocytes beyond what was expected by the cells' larger size ($p=0.03$). Further experiments to determine whether the z band number (a rubric for the number of sarcomeres present) or average z band size (reflecting the thickness of the sarcomere) accounted for the increased TZB. We found the number of z bands per cell was significantly increased from 25.3 z bands/cell in control embryos to 32.4 z bands/cell in vasopressin-treated embryos ($p < 0.001$), suggesting treated cells increased their myofibril content. However, the average length of individual z bands was not significantly affected ($p=0.24$)(data not shown), suggesting that myofibril thickness was not changed. This pattern of increased number of sarcomeres is consistent with pathological concentric hypertrophy.

Increased Afterload Induces Retrograde Flow and Alters AVJ Mechanics

To evaluate valve formation and function, we measured how the diameter of the AVJ varied across the cardiac cycle in hearts of live embryos. Hearts of vasopressin-treated embryos were scored initially as either 'mild' or 'severe' based on their appearance at 40 hpf, and then videoed at 56 hpf. We noted that the dynamics of AVJ behavior during the cardiac cycle were significantly altered under conditions of increased loading (Figure 4). The AVJ of control embryos displayed uniform behavior, opening with an average maximal diameter of 34.7 µm (Figure 4A,D). Vasopressin-treated embryos initially scored as 'mild' showed significantly

increased average maximal diameter of 44.5 µm by 56 hpf (p=0.015 by t-test) (Figure 4B,D). Vasopressin-treated embryos initially scored as 'severe' at 40 hpf displayed reduced average maximal diameters of 27.7 µm by 56 hpf (p=0.10 by t-test)(Figure 4C,D). Moreover, AVJs in vasopressin-treated hearts open significantly earlier than control counterparts (controls at 40% all vasopressin-exposed embryos at 11%, p=0.04). Both groups of vasopressin-treated embryos displayed an increased retrograde flow fraction (RFF), quantified as: $\int_0^T |Q_{reverse}|dt$ / $\int_0^T |Q_{total}|dt$, where *Q* is the flow rate and *T* is the cardiac cycle period.(Bulk et al., 2016) In vasopressin-treated embryos, RFF increased approximately 3-fold over controls by 56 hpf (Figure 4E, p=0.01). Together, these data demonstrate that despite the ability of 10 µM vaso-treated hearts to maintain cardiac output, the alterations in loading nevertheless substantially impacted other aspects of heart development, including blood flow patterns and AVJ closing dynamics.

Increased Afterload Alters Myocardial AVJ Cell Specification

Given that AVJ functional dynamics were altered in conditions of increased afterload, we next explored whether differentiation of AVJ myocardial, and/or endocardial cells, was affected in conditions of high afterload. Focusing first on myocardial differentiation specifically at the AVJ, we evaluated the cellular morphology based on ALCAM immunostaining. By 48 hpf, wildtype AVJ myocytes have acquired a distinct trapezoidal cell morphology, express Tbx2b, and direct endocardial cell specification via Bmp signaling.(Chi, Shaw, De Val, et al., 2008; Dietrich et al., 2014) In vasopressin-treated embryos at 56 hpf, AVJ myocytes were on average more circular than their control counterparts (Supplemental Figure 16A, p=0.03), suggesting that AVJ myocytes had not fully differentiated. In contrast to ventricular outer curvature myocytes, which enlarge (Figure 3), AVJ myocytes spanned approximately the same area in vasopressin-treated hearts as in controls, suggesting that AVJ myocytes do not become hypertrophic (Supplemental Figure 16B, p=0.62). Upon assessing total myofibril content, we

observed a 22% decrease in normalized TZB in vasopressin-treated AVJ myocytes (Figure 5C, n=11 control, 10 vasopressin-treated hearts, p=0.003).

Next, we assessed the specification of AVJ myocytes via *in situ* hybridization using *bmp4* and *tbx2b* probes.(Patra et al., 2011) In normal hearts, myocardial *bmp4* and *tbx2b* are broadly expressed in the ventricle at 33-36 hpf. During the second day of development, wildtype hearts gradually down-regulate expression of these markers in the chambers while enriching them at the AVJ, such that AVJ-specific enrichment is evident by 52 hpf.(Chen et al., 1997) Failure of these markers to retract to the AVJ is observed in mutant or pharmacological conditions associated with abnormal valve development.(Patra et al., 2011) In approximately 68% of vasopressin-treated hearts at 56 hpf, *bmp4* expression failed to retract to the AVJ and instead remained broadly expressed in the ventricle or diffusely expressed throughout the heart (Figure 5G). In contrast, *tbx2b* expression was not notably altered by vasopressin-treatment (fold change = 1.10, p=0.42 by qPCR on dissected hearts). Taken together, these data demonstrate that cardiac afterload produces a biomechanical stress that precludes normal cell differentiation of myocardial cells in the AVJ.

Increased Afterload Alters Endocardial AVJ Cell Specification

During valve development in mammals, endocardial cells undergo EMT, invade the endocardial cushions and become specified valve cells.(Combs & Yutzey, 2009) Although controversy exists regarding whether true EMT occurs in the AVJ of zebrafish, (Scherz et al., 2008; Emily Steed et al., 2016) AVJ endocardial cells transition to a more cuboidal shape by 48 hpf, and endocardial cells from the superior valve leaflet fold into the cardiac jelly around 60 hpf. ALCAM is a well-characterized marker that appears at the cell periphery from 52 hpf onward only in AVJ endocardial cells that have become specified to a valve cell fate.(Beis, 2005) (In contrast, myocardial cells express ALCAM throughout development). To evaluate endocardial AVJ development, we performed immunohistochemistry on dissected wildtype and vasopressin-

treated hearts at 56 hpf to detect ALCAM. Since these hearts were derived from Tg(fli1:eGFP) embryos, this method labels myocardial cells (red), chamber endocardial cells (green), and nascent valve endocardial cells in the AVJ (double-labeled red and green)(Figure 6A-B'). Results indicated a 45% reduction in the number of double-labeled ALCAM-positive valve-forming endocardial cells in vasopressin-treated embryos (Figure 6C, p=0.000019). To test whether AVJ formation was simply delayed in vasopressin-treated embryos, we repeated the same experiment at 72 hpf. We again noted a significant reduction (approximately 30% fewer) in the number of ALCAM positive endocardial cells in vasopressin-treated embryos (n=12 control, 11 vaso; p=0.004). These data strongly suggest that aberrant loading perturbs AVJ development by limiting the number of endocardial AVJ cells that achieve a specified state.

Discussion

Here we present vasopressin-treated zebrafish as a novel *in vivo* model suitable for study of the impact of increased myocardial afterload upon the forming heart. Vasopressin treatment in embryonic zebrafish induces blood vessel constriction, leading to an altered biomechanical condition consistent with increased afterload. We find that high afterload produced a pathological cardiac phenotype, and that hearts subjected to different vasopressin doses appeared to adapt in different ways. Specifically, embryos treated with moderate doses of vasopressin (corresponding to moderate increases in afterload) responded by increasing cardiac output at 40 hpf, a change which allowed them to continue function adequately at 56 hpf. Embryos treated with a high dose of vasopressin (corresponding to a higher increase in afterload) could not increase cardiac output, but were able to maintain it, initially by increasing heart rate (at 40 hpf) and later by increasing stroke volume (at 56 hpf). Hearts in roughly one-third of these high-dose embryos were clearly compromised at 40 hpf and failing at 56 hpf. However, hearts in two-thirds of the high-dose embryos produced adaptive responses that augmented their ability to continue to function with a normal cardiac output at 56 hpf. In these

hearts, cardiac pathology is indicated by weaker contractility, slower contractile wave speeds, and increased variability in cardiac output. Evidence of putative adaptive responses include an expanded length of endothelial closure within individual heartbeats, induction of hypertrophy via increased cell size and myofibril content, and increased cardiac output by altering heart rate or stroke volume. Within the AVJ, the negative impact of high afterload is evident by the disrupted AVJ differentiation and the increased fraction of retrograde flow. Given that the embryonic heart does not express vasopressin receptors itself, we conclude that vasopressin indirectly produces a high afterload, by altering the biomechanical environment, and that these changes are pathological for normal cardiac development.

Prior studies using out-flow tract ligation to alter afterload in the chick embryos provided initial evidence to suggest that biomechanical signals derived from afterload impact function in the embryonic heart.(Francesco Boselli et al., 2015) Limitations of this model include the requirement for time-consuming surgical manipulations and the limited amenability to genetic manipulation. The zebrafish vasopressin model complements and extends the chick ligation approach. The ease of vasopressin application enables high-throughput analysis of phenotypes, and enables investigation the timing and severity of responses to different doses. The existence of numerous characterized mutant lines in zebrafish offers the further potential to assess the impact of afterload under various genetic backgrounds. To thoroughly understand the molecular circuitry underlying the afterload-response, it will be necessary to couple manipulations in loading with manipulations in genetics.

This report provides the first detailed investigation of the functional, cellular, and molecular consequences of increasing afterload in the embryonic zebrafish heart. The zebrafish embryonic heart does not express vasopressin receptors, making it unlikely that vasopressin exerts any direct effects on cardiac contractility. Upon vasopressin treatment, vasoconstriction is detected in multiple vessels after as little as 4 hours of exposure. The degree of constriction produced by 10 µM is calculated to generate at least a 124% increase in vascular resistance of

the dorsal aorta, thus generating a robust increase in cardiac afterload. Increasing the load on the embryonic heart during early development (linear heart tube stage and beyond) dramatically altered cardiac function. In zebrafish, the heart rate of 10 µM vasopressin-treated embryos increased initially at 40 hpf, but the increase was not maintained at 56 hpf. In contrast, stroke volume initially matched controls at 40 hpf, but by 56 hpf had significantly increased. Concomitantly, all embryos exposed to 10 µM vasopressin showed a significant increase in myofibril content by 56 hpf. These data suggest that upon exposure to high afterload, embryos initially respond by increasing heart rate, perhaps as a temporary compensatory measure. However, upon chronic exposure to high afterload, embryonic hearts remodel to meet physiological demands.

More specifically, high afterload produced hypertrophy of the ventricular OC cardiomyocytes by 56 hpf by mechanisms that increased ventricular cell size and increased myofibril content. This finding is consistent with studies of cultured human embryonic myocardial stem cells that displayed hypertrophy as well as increased proliferation when grown in conditions of high afterload.(Tulloch et al., 2011) Of note, high afterload in human adults can also lead to myocardial hypertrophy, reflecting increased ventricular cell size and increased myofibril content.(Machackova, Barta, & Dhalla, 2006; Tarazi & Levy, 1982) In contrast, chick embryos did not display cardiomyocyte hypertrophy under conditions of high load, but instead showed evidence of cardiomyocyte hyperplasia.(Clark et al., 1989) Which mechanotransductive mechanisms facilitate these changes remains an open question, but may include disrupted endocardial-ECM-myocardial signaling, pressure-sensitive receptors, or flow-triggered endocardial responses then communicated to the myocardium. This finding suggests that high afterload either perturbs communication between the endocardium and myocardium or generates biomechanical signals other than RFF and shear stress that impact cardiac hypertrophy.

Strikingly, retrograde flow was significantly increased by 56 hpf in vasopressin-treated embryos. Retrograde flow normally occurs in embryonic hearts aged ~36-72 hpf for a limited period of each heartbeat.(Bulk et al., 2016), (Johnson et al., 2013) Movement of blood cells or plasma against the endocardial cells within the AVJ generates wall shear stress. Imaging studies have uncovered a required contribution of shear-stress related biomechanical forces for regulating normal cardiac valve development.(Hove et al., 2003; Emily Steed et al., 2016; Vermot et al., 2009) Vermot and colleagues established that retrograde flow (i.e., "reversing flows") constitute a unique physical stimulus for valve development, and showed that loss of RFF produced defects in endocardial cushion formation.(Vermot et al., 2009) Moreover, the complex oscillatory flow patterns present in the AVJ prior to valve formation create shear stress patterns that trigger endocardial cells to converge into the endocardial cushions.(F. Boselli, Steed, Freund, & Vermot, 2017) In our case, increased RFF did not alter the number of EC converged at the AVJ by 56 hpf (Supplemental Figure 17), but we did observe that fewer of those ECs expressed the valve-specification marker, ALCAM (Figure 6). It is intriguing to speculate that distinct mechanosensitive mechanisms may regulate endocardial convergence in the AVJ and valve-cell differentiation. Of note, high afterload has the potential to impact the heart prior to the onset of detectable RFF (~36 hpf), and therefore may elicit defects independently of complex flow patterns.(Bulk et al., 2016; Vermot et al., 2009)

The cellular mechanisms leading to reduced specification of endocardial AVJ cells remain unresolved. Myocardial cells at the AVJ secrete paracrine factors that promote endocardial valve cell specification. We speculate that an increase in loading during the vulnerable valve-formation period may interfere with the appropriate targeted secretion of key signaling factors by AV myocardial cells. Alternatively, inadequate reception of these signals by endocardial receptors may lead to fewer specified endocardial valve cells. Indeed, expression of the myocardial marker *bmp4* failed to become restricted to the AVJ by 56 hpf in vasopressin-treated embryos, suggesting that myocardial AVJ cell specification is compromised in

vasopressin-treated embryos. In the myocardium, Bmp induces transcription factors critical for continued myocardial AVJ development,[65] whereas in the endocardium, the BMP-Wnt signaling axis promotes AVJ endocardial specification(Hurlstone et al., 2003; Verhoeven et al., 2011) Thus disruptions in Bmp signaling may be expected to perturb development in both myocardium and endocardium.

Taken together, our AVJ data show that under conditions of high afterload, the AVJ myocardial cells fail to develop the myofibillar content expected for their developmental stage, fail to appropriately transition to the trapezoidal shape expected for differentiating AVJ myocardial cells, and fail to display the AVJ enriched pattern of myocardial markers indicative of maturing AVJ. We postulate that these defects in AVJ myocardial cell differentiation interferes with normal communication between the endocardium and the myocardium, and contributes to a valve defect.

Many open questions remain regarding the mechanobiological means by which afterload elicits the pathological effects shown in this study. First, are some of the high afterload-associated phenotypes mediated via alterations in shear stress or oscillatory flows, whereas others are mediated via mechonotransductive cues related to pressure? Second, how are afterload-mediated mechanical signals transduced into genetic signals? One intriguing hypothesis relates to the cell-stress response. Increased afterload increases ventricular wall stress. In vivo experiments using coronary artery ligation in adult rat models show that increasing wall stress causes remodeling of the t-tubule network and disrupts calcium homeostasis.(Frisk et al., 2016) Interestingly, calcium transients have to been shown to regulate to Bmp signaling during *Drosophila melanogaster* neural development.(Swapna & Borodinsky, 2012) It is possible that increasing afterload alters calcium homeostasis during cardiac development, leading to altered Bmp signaling. More work needs to be done to investigate this hypothesis, as well as other potential cellular mechanisms for sensing and responding to afterload.

Chapter 3 – Retrograde flow regulates valve development through klf2a[1]

Summary

Aims: As the heart develops, the hemodynamic stresses on the heart rapidly increase. Changes in hemodynamic cues result in altered gene expression that ultimately serves to regulate valve development. Retrograde flow (RF) is defined as the portion of blood that flows backwards from the ventricle to the atrium each cardiac cycle. In adults, the presence of RF is an indication of cardiac valve dysfunction, but in embryos, retrograde flow acts as a normal cue to turn on gene expression in the developing valve. Decreases in RF abrogate expression of the transcription factor *klf2a,* which is required for valve development in zebrafish. While the relationship between RF and *klf2a* is well established, much remains to be learned about how RF and Klf2a work together to direct cell behavior and differentiation is. The overarching goal of this project is to better elucidate how retrograde flow and *klf2a* direct valve morphogenesis.

Methods: We first defined the developmental period in which RF occurs using high-speed videography. We then used a pharmaceutical approach to abnormally increase RF at critical developmental time periods and determined the effects upon valve cell differentiation and leaflet morphology. Finally, we overexpressed *klf2a* to determine whether valve phenotypes matched those produced by increased RF.

Results: We find that retrograde flow is most prevalent between 32-40 hpf. Increases in RF resulted in elongated, malformed valve leaflets, increased expression of *klf2a* and increased

[1] This manucscipt is currently in preparation for Frontiers in Cell and Developmental Biology

ECM production. Overexpression of *klf2a* resulted in similar alterations in valve leaflet morhplogy and ECM production. Together, our results suggest that increases in RF serve to increase *klf2a* and causes remodeling of the ECM, leading to valve pathology.

Introduction

Valve development is regulated by a series of genetic and biomechanical inputs. As the heart develops, it transitions from a linear tube with peristaltic-like contractions to a multiple chambered heart that functions as an impedance pump.(Johnson et al., 2013) As the heart undergoes this transition, blood flow in the cardiac chambers begins to exert hemodynamic stresses on the walls of the endothelium, which then trigger the expression of a variety of genes. Because hemodynamic stresses exert influence in a spatiotemporally-regulated manner, they are able to trigger a response in gene-expression in highly localized manner. Endocardial cells (ECs) located at the atrioventricular junction experience a unique set of hemodynamic stresses which serve to facilitate valve development (Hove et al., 2003).

In order to correctly build a valve, endothelial cells undergo a series of rearrangements that are tightly regulated. In zebrafish embryos, the first evidence of valve formation occurs at approximately 32 hpf. At this stage, a constriction develops at the atrioventricular junction (AVJ) and AVJ ECs begin to proliferate. By 40 hpf, the AVJ displays a visible cluster of endocardial cells present at the AVJ. At this stage, cardiac cushions – consisting of an accumulation of extracellular matrix (ECM) at the AVJ – begin to form. At 48 hpf, a portion of the zebrafish endocardial cells in the atrial and ventricular chambers but near the AVJ begin folding ito form a multilayered valve leaflet. At 56 hpf, AVJ endocardial cells extend basal profusions into the ECM and decrease expression of cell adhesion proteins such as cadherin-5. By 80 hpf, the developing valve leaflet consists of three cell layers that extend into the ECM between the myo- and endocardial cell layers (Emily Steed et al., 2016).

Retrograde flow (RF) and shear stress have large roles in coordinating cellular rearrangements during valve morphogenesis. Retrograde flow is defined as the portion of blood flow that travels backwards from the ventricle to the atrium each cardiac cycle and occurs specifically at the valvular region. Shear stress is created by frictional stress applied to the endothelial cells by blood flow and can be mathematicllay described as $\tau = \frac{\mu 8v}{d}$, where T is shear stress, μ is the viscosity of blood, v is the velocity of blood, and d is the diameter of the vessel.(F. Boselli et al., 2017) Because the entire volume of blood flow must past through the narrow diameter of the AVJ, the shear stress at the AVJ is significantly higher than in the chamber endocardium. Because shear stress and RF are localized to the AVJ, they stand out as attractive candidates for flow-mediated cues that regulate valve development.

Indeed, RF is required for atrioventricular valve development. Insight from zebrafish embryos demonstrated RF at the AVJ triggered expression of mechanosensitive transcription factor *Kruppel-like factor 2a* (*klf2a)* at 48 hpf. Knockdown of either the *gata1* or the *gata2* gene decreased the production of blood cells in the body, and consequently decreased blood viscosity. Interestingly, knockdown of these two hematopoietic genes differentially affected hemodynamic patterns: decreases in *gata1* expression increased RF while knockdown of *gata2* expression decreased RF. Decreases in RF abolished the expected *klf2a* expression at the AVJ and resulted in dysmorphic valve structures.(Vermot et al., 2009) Later work demonstrated that RF activates the mechanosensitive calcium ion channels Trpv and Trpv4, producing an increased intracellular calcium content that activated *klf2a* expression.(Heckel et al., 2015)

While the relationship between *klf2a* and RF has been well understood, several open questions remain regarding how *klf2a* works to direct valve morphogenesis. Morpholino knockdown of *klf2a* led to the failure of valve cells to adopt stereotypical valve morphology and ultimately led to poorly functional valves.(Vermot et al., 2009) However, the morpholino knockdown phenotype was not recapitulated in *klf2a* mutants, potentially due to the off-target

effects associated with morpholino technology. A different zebrafish *klf2a* mutant was found to lack fibronectin synthesis in the developing valve and displayed dysmorphic valve structures.(Emily Steed et al., 2016) In mouse embryos, knockout of *KLF2* prevented endothelial EMT and eventually produced enlarged, hypoplastic valves, a phenotype recapitulated by *Wnt9*b knockout. (Goddard et al., 2017) Together, these data highlight the diversity of roles that *klf2a* plays in valve development.

To better elucidate the precise role of *klf2a* in valve development, we first identified the developmental stage in which *klf2a* expression was initiated at the valve. We then utilized vasopressin, a vasoconstrictive drug that results in an increase in afterload. We find that increase in afterload result in an increase retrograde flow at 56 hpf and a dose-dependent increase in valve leaflet length at 72 hpf. In addition, we find that increases in RF result in dramatic remodeling of the developing ECM. These phenotypes can be recapitulated through overexpression of *klf2a* in the absence of any abnormalities in RF. Our results suggest that Klf2a activity is particularly important between 32-40 hpf in the AVJ endocardium, where it directs remodeling of the ECM to create a permissive environment for valve morphogenesis.

Methods

Zebrafish Husbandry and Vasopressin Application

Zebrafish were raised as per Colorado State University Animal Care and Use Protocols. Zebrafish embryos were raised at 28.5°C until 24 hpf in E3 medium, and dechorionated. Arginine-Vasopressin Acetate Salt (Sigma, catalog number V9879) was diluted in E3 embryo media to a final concentration of 10 µmol/L, unless otherwise specified.

Live Imaging

For vessel and whole heart live imaging, samples were immobilized in agarose and treated with MESAB to temporarily stop heartbeats. Quantification of vessel diameter was performed in Image J.(Rueden et al., 2017) Quantification of cardiac chamber volume and looping angle was performed as previously described.(J Yang et al., 2014),(Berndt et al., 2014)

For live imaging of the valves, confocal microscopy was used. Embryos were treated with MESAB until cardiac contraction stopped, and then mounted in low-melt agarose in a depression slide in the same orientation, such the heart was roughly parallel to the coverslip.

Quantification of Cardiac Parameters

Quantification of cardiac parameters was performed as previously described.(Johnson et al., 2013) Briefly, embryos were raised at 28.5°C until 55 hpf. Fish were mounted in low melt agarose, with no MESAB. Videos were taken with a Photon SA3 camera at 1000 frames per second, across at least 3 cardiac cycles. Videos were analyzed as previously described using a line scan and spatiotemporal kymographs to quantify cell movement along the line scan.(Johnson et al., 2013)

Immunohistochemistry

Immunohistochemistry was performed on dissected zebrafish hearts as previously described.(Jingchun Yang & Xu, 2012) Briefly, hearts were dissected in an L15-10%FBS solution and then placed on a polylysine-coated slide. Hearts were fixed for 40 minutes in 4% PFA and permeabilized with a 1% solution of Triton-X. For phalloidin labelling, hearts were placed in 1:100 dilution of Alexa-546 conjugated-phalloidin. For ALCAM labelling, zn5 antibody was used at 1:10 dilution. Embryos were washed 3X with PBST solution and then incubated with Alexa-546 anti-goat IgG secondary antibody at a 1:200 dilution. 50% glycerol was then added to the slides, and coverslips were added. Images were taken on the Zeiss LSM800 and analyzed blind.

Klf2a-Overexpression

For *klf2a* overexpression experiments, full-length *klf2a* cDNA was first cloned into the pCRII vector using a Dual-Promotor Cloning Kit (Invitrogen) according to manufacturer's protocol. The plasmid was then sequenced to verify orientation and sequence fidelity. Using the T7 promoter located in the pCRII vector, capped *klf2a* mRNA was synthesized using a mMesage mMachine kit (Ambion). This mRNA was then injected into zebrafish embryos at 4ng of mRNA per embryo. Embryos were incubated at 28.5°C.

In Situ Hybridization Probe Synthesis

In Situ probe synthesis was carried out as previously described.(Thisse & Thisse, 2008) In brief, *versican a* plasmids were obtained and previously validated.(Parrie, Renfrew, Wal, Mueller, & Garrity, 2013) Plasmids were in linearized with the appropriate restriction enzyme, and linearized plasmids were then purified via ethanol precipitation. Linearized DNA was then used in an in vitro transcription reaction to synthesize the anti-sense RNA strand labeled with Digoxigenin (DIG). In brief, linearlized DNA was placed with T7 polymerase and reaction buffer (Ambion Maxiscript Kit). Reaction was supplemented with 2 µL of DIG-UTP (Roche) and incubated according to manufacturer's directions. Resulting RNA probes were then purified via ethanol precipitation.

In Situ Hybridization

In situ hybridization was carried out as previously described.(Thisse & Thisse, 2008) In brief, zebrafish embryos at the appropriate stage were fixed in 4% paraformaldehyde at 4°C overnight. Embryos were then placed in 100% methanol, and placed in -20°C for at least 2 hours. Embryos were then gradually rehydrated from methanol to phosphate buffered saline with 1% Tween-20. Embryos were then permeabilized with proteinase K for 20 minutes at room temperature. Embryos were then placed in 4% paraformaldehyde for 20 minutes at room temperature, and washed 5 times with phosphate buffered saline. Embryos were then incubated

with DIG-labeled probe of interest in hybridization mixture (50% formamide, 5x saline sodium-citrate solution, 1% Tween-20) overnight at 60°C. Embryos were then washed with sodium citrate solution and PBT to remove all unbound probe. Embryos were then incubated with secondary antibody (Anti-Digoxigenin-AP Fab fragments, Roche) at a concentration of 1:5000 overnight in 4°C. Embryos were then washed with PBT several times to remove unbound secondary antibody. Embryos were then placed in a staining solution consisting of 1% 4-Nitro blue tetrazolium chloride (Roche) and 0.7% 5-Bromo-4-chloro-3-indoyl-phosphate (Roche). Embryos were kept in the dark and monitored for signal development. After the controls developed adequate signal, reactions were stopped by placing embryos in 4% paraformaldehyde.

Quantitative Polymerase Chain Reaction

Hearts were dissected in L15-10% FBS. 10-20 hearts per treatment were pooled, and RNA was extracted using TRIzol (Invitrogen) according to the manufacturer's protocol. Nucleotide concentration was determined by absorbance at 260 nm and 2 µg of RNA was used for 20-µl cDNA synthesis reaction. cDNA synthesis was performed using AMV reverse transcriptase (Fisher Scientific) and Oligo(dT)$_{12–18}$ primer (Invitrogen). Resulting cDNA was treated with RNase H (New England Biolabs, Ipswich, MA). 1 µL of CDNA was used in each 10µL qPCR reaction. Roche LightCycler 480 SyberGreen mastermix was used for all reactions according to manufacturer's protocols. Standards curves were performed in triplicate for every gene. Reactions were run on Roche LC480 qPCR machine. Accompanying software (Roche LightCycler 480 software, version 1.2) was used to calculate Ct values. Pfaffl analysis was used to determine relative expression

For all qPCR experiments, the Pfaffl method was used.(Pfaffl, 2001) In brief, standard curves for each gene were created and efficiencies were calculated for both the genes of interest and the reference in gene. In all experiments, the reference gene used was *Elongation Factor α (EF α)*,

a well validated housekeeping gene.(McCurley & Callard, 2008) These efficiencies were then used in the Pfaffl equation, to calculate fold change of the gene of interest compared to the control. 3 biological replicates were analyzed per gene. Each biological replicate was ran as three technical replicates, whose C_t values were then averaged. These averaged C_t values were checked for normality, log transformed and then used to determine statistical significance.

Detailed Statistical Analysis

All data was analyzed in R (version 3.4.2), and graphs were made using the ggplot2 package. Data was first checked for normality using Shapiro-Wilk function built into base R. If the Shapiro-Wilk test returned a p-value greater than 0.05, then a two tailed t-test was used to analyze the data. If the Shapiro-Wilk test returned a value less than 0.05 and the number of replicates were less than 40, than the Kruskal-wallis test was used to determine statistical significance. For multiple comparisons, Tukey's test was used for parametric data and Dunnet's many-against-one test was used for nonparametric data.

Results

Onset of Klf2a expression at the atrioventricular junction accords with the period of high retrograde flow

As the heart develops, it transforms from a linear tube with peristaltic-like contraction to a two-chambered heart that functions more as a impedance pump.(Johnson et al., 2013) Consequently, the hemodynamic stresses on the AV valve also change through developmental time. To evaluate how cardiac function changes throughout development, we acquired high-

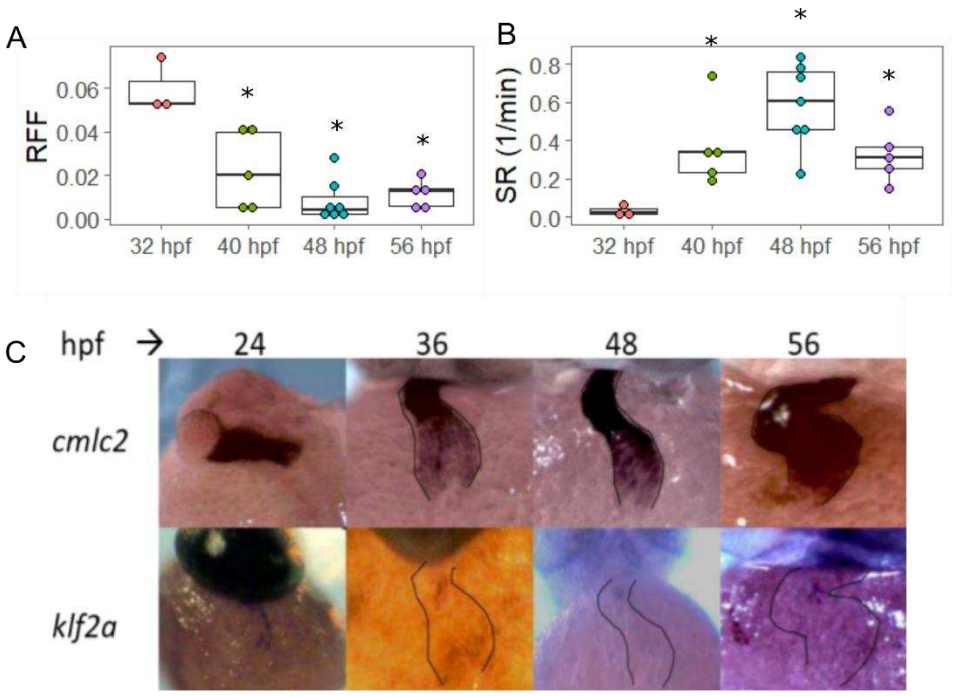

Figure 3.1: *Klf2a* becomes restricted to the atrioventricular junction by 36 hpf, a time period experiencing high retrograde flow. A) Retrograde flow is highest at 32 hours, and significantly decreases by 40 hpf. Retrograde flow is almost zero by 56 hpf.n =3 embryos at 32, 5 embryos at 40, 7 embryos at 48 hpf, and 5 embryos at 56 hpf; p-value for 32hpf vs 40 hpf = 0.0019, p-value for 32hpf vs 48 hpf < 0.0001, 32hpf vs 56 hpf = 0.0002 by Dunnett's test. B) Shear stress increases throughout development. B) Shear rate increases throughout development. $p < 0.01$ for 32 vs 40 hpf, 0.02 for 32 vs 48 hpf, and 0.04 for 32 vs 56 hpf. C) In situ hybridization of control gene, cmlc2, and klf2a throughout development.

speed videos of the beating zebrafish heart at four different timepoints from 32 to 56 hpf. 32 hpf corresponds to a stage where the constriction at the atrioventricular junction has developed, but heart contraction is not yet robust. At 40 hpf, the chambers are clearly developed, and cardiac contraction is robust. At 48 hpf, the endocardial cushions initiate development and begin functioning as a primitive valve. At 56 hpf, endocardial cushion development is robust. As expected, cardiac output increased approximately five-fold between 32 and 40 hpf (Supplementary Figure 1A, n=3 at 32 hpf, n=5 at 40 hpf, p = 0.02 by Dunnett's test), then remained at approximately the same level throughout the remaining time points measured. To determine how this increase in cardiac output was achieved, we assessed both stroke volume and cardiac output. While no significant difference in stroke volume was detected (p =0.10 by Anova), there was a trend of increasing stroke volume between 32 and 40 hpf (Supplementary Figure 1B; stroke volume = 0.19 at 32 hpf, 0.60 at 40 hpf, n=3 embryos at 32 hpf, and 5 embryos at 40 hpf). Heart rate, in contrast, increased linearly throughout development (Supplementary Figure 1C, heart rate = 59.4 bpm at 32 hpf, 98.7 bpm at 40 hpf, 104.0 bpm at 48 hpf, and 134 bpm at 56 hpf; n =3 embryos at 32, 5 embryos at 40, 7 embryos at 48 hpf, and 5 embryos at 56 hpf; p-value for 32hpf vs 40 hpf = 0.0005, p-value for 32hpf vs 48 hpf = 0.0001, 32hpf vs 56 hpf < 0.0001 by Dunnett's test). These data suggest that increases in heart rate mediate increases in cardiac output after 32 hpf.

To assess how hemodynamic stresses at the atrioventricular junction changed over time, we measured the retrograde flow fraction (RFF) and the average shear rate impacting endothelial cells at the AVJ at several time points in early heart development. RFF is defined as the fraction of blood cells that moved from the ventricle to the atrium each cardiac cycle.(Bulk et al., 2016) RFF was highest at 32 hpf, with an average RFF of 0.06. By 40 hpf, RFF significantly decreased to an average of 0.01, although some embryos displayed higher RFF values. Embryos at 48 and 56 hpf displayed very little retrograde flow, with RFF values less than 0.01 (Figure 1A, n =3 embryos at 32, 5 embryos at 40, 7 embryos at 48 hpf, and 5 embryos at 56

hpf; p-value for 32 hpf vs 40 hpf = 0.0019, p-value for 32 hpf vs 48 hpf < 0.0001, 32 hpf vs 56 hpf = 0.0002 by Dunnett's test). To assess shear stress, we quantified shear rate. Shear stress is equivalent to the shear rate multiplied by the blood viscosity. Because the viscosity of embryonic blood is in zebrafish is controversial, we simply measured shear rate to assess how fluid forces may change during embryogenesis. Shear rates displayed the opposite trend as the RFF, with shear rate steadily increasing throughout cardiac development.(Ercan & Koksal, 2003) Shear rate increased approximately four fold from 32 to 40 hpf ($p < 0.001$) and continued to increase up to 48 hpf. Together this data indicates that RF is most prevalent at earlier stages of development of the AV valve, whereas later stages are exposed to more shear stress.

Several reports have established that the mechanosensitive transcription factor *klf2a* responds to changes in blood flow by modulating its level of transcription, although there is some debate over whether it responds to shear stress or to oscillatory flow.(Dietrich et al., 2014; Goddard et al., 2017; Heckel et al., 2015; Emily Steed et al., 2016; Vermot et al., 2009) To more precisely assess when *klf2a* expression initiates in the AVJ, we performed *in situ* hybridization at several stages of development.. We did not find discernable *klf2a* expression at 24 hpf; however, *klf2a* did appear in the AVJ by 36 hpf. *klf2a* then maintained it's restricted expression at the AVJ through at least 72 hpf (Figure 1C). Because 36 hpf is corresponds to a time when RF is high, but shear rate is low, this data suggests that RF may trigger the onset of *klf2a* expression.

Increases in RF and shear stress cause an elongation of the valve leaflet

To manipulate hemodynamic stresses in the developing embryo, we applied vasopressin, a vasoconstrictive drug. We previously showed that vasopressin receptors are not expressed in embryonic cardiac tissue of zebrafish, indicating that vasopressin application produce an increase in afterload by increasing vasoconstriction rather than via direct effects on

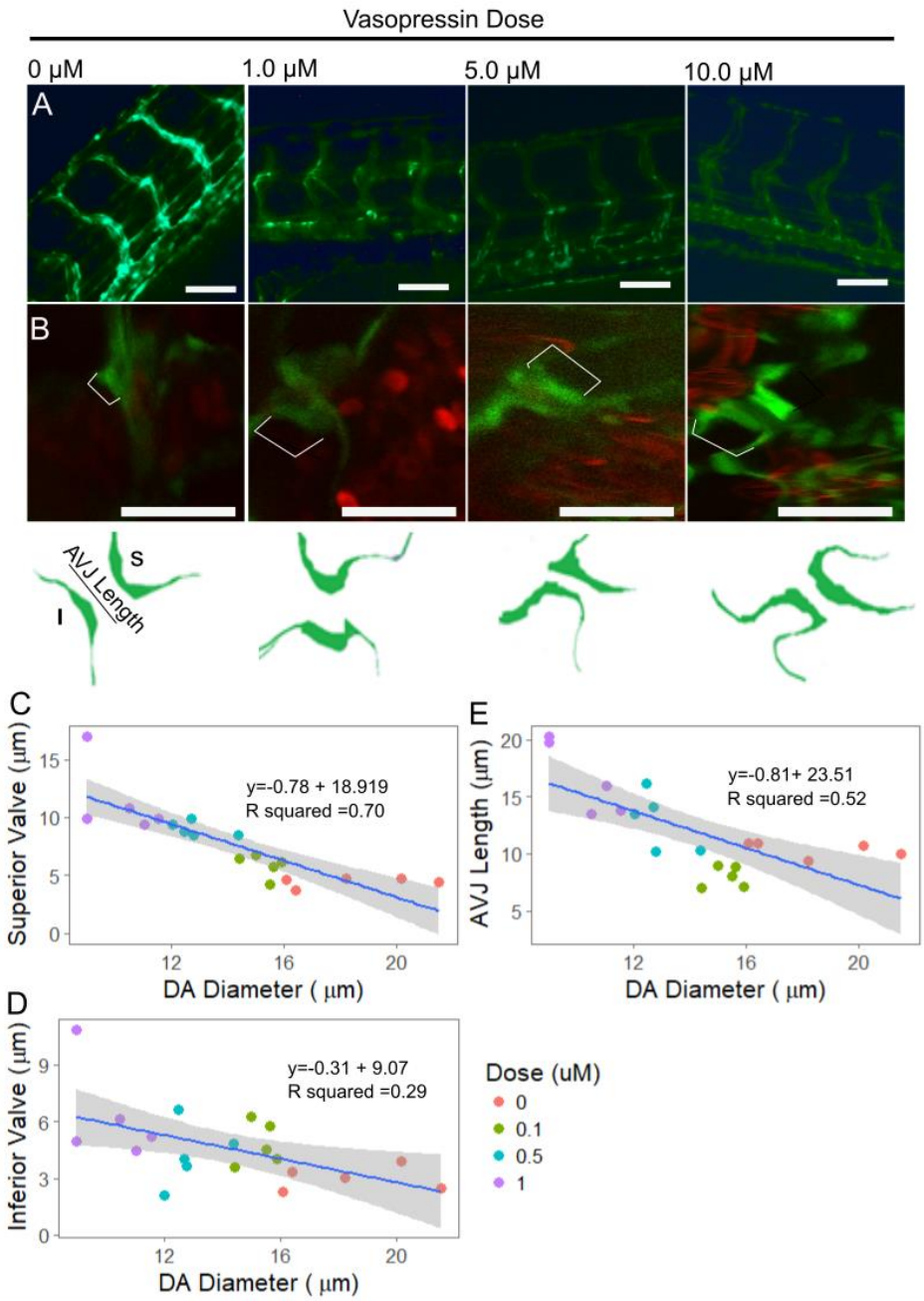

Figure 3.2: Increasing Afterload Produces a Dose-Dependent Valve Defect. A) Dorsal aorta and B) valve leaflet under varying concentrations of vasopressin at 72 hpf. Scale bar represents 20µm. Arrows indicate AVJ. Green diagrams underneath represent tracings of the developing valve leaflets. For C-E: Each dot represents measurements for one fish. Best fit line and trendline equation were developed in R. Gray area represents 95% confidence levels. C)Scatter plot of superior valve width plotted again dorsal aorta diameter. R^2 value = 0.70. D) Scatter plot of inferior valve width plotted again dorsal aorta diameter. R^2 value = 0.29. E) Scatter plot of AVJ length plotted again dorsal aorta diameter. R^2 value = 0.52.

cardiac tissue (Ahuja 2020, in review). To determine how high afterload impacts intracardiac flow patterns, we measured RF and shear rate in embryos treated with increasing doses of vasopressin. Application of 2.5 µM vasopressin at 24 hpf was sufficient to produce a 4-fold increase in RF by 56 hpf (Supplementary Figure 2A , n =5 embryos at each dose, p = 0.02 for control vs 2.5, 0.01 for control vs 5, 0.03 for control vs 7.5, 0.04 for control vs 10). Further increases in vasopressin dosage did not produce greater increases in RF. Interestingly, the average shear rate at the AVJ was not significantly affected at vasopressin dose (Supplementary Figure 2B, p = 0.72 by anova). Consequently, vasopressin application maybe used to probe how retrograde flow impacts valve development, independent of changes in average shear stress.

To determine how increasing RF affected valve development, we evaluated the structure of the valve leaflet using Tg(Fli1:eGFP) embryos in response to increasing doses of vasopressin. Expression of GFP in endothelial and endocardial cells allowed simultaneous tracking of endocardial cushions in the heart and vasculature diameter. The diameter of the dorsal aorta decreased with increasing concentrations of vasopressin, constricting from 21 µm at 0 µmol/L vasopressin to 12 µm under 10 µmol/L vasopressin. Thus, vasopressin produced a dose-dependent constrictive effect (Supplementary Figure 3, R^2 =0.77). The diameter of the dorsal aorta showed a strong inverse correlation with the length of the superior valve leaflet (Figure 2C, R^2 = 0.70), implying that morphology in this leaflet was highly sensitive to biomechanical cues. In contrast, the inferior valve leaflet diameter was not affected by vasopressin application (Figure 2D, R^2 = 0.29).The overall length of the AVJ (defined here as the region of AV constriction) correlated moderately with the dorsal aorta diameter (Figure 2E, R^2 = 0.52). Together, these data demonstrate that valve morphology is impacted by retrograde flow, and that certain regions of nascent valve tissue are particularly sensitive to disturbance.

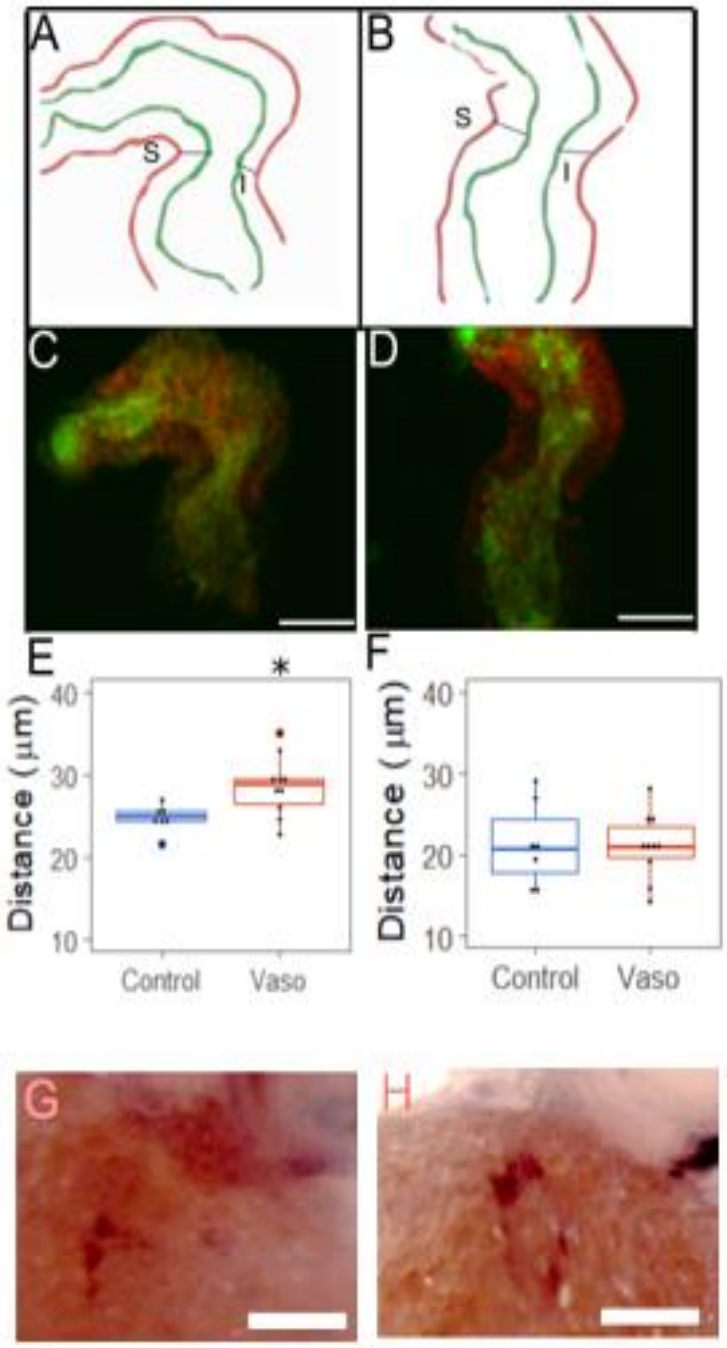

Figure 3.3: Increased Afterload Causes an Increase in ECM production. A-B) Tracing of the myocardial and endocardial layers of wildtype and vaso-treated heart, respectively. Line indicates site of measurement. S and I indicate superior versus inferior cushion, respectively. C-D) Phalloidin (red) stained transgenic wildtype and vaso treated hearts. E-F) Distance between endocardial and myocardial layer at the superior and inferior cushions. G) In suit of versican at 56 hpf.

Disturbed Hemodynamic Cues Lead to Increased ECM Production in Endocardial Cushions

We next investigated the molecular basis for the observed valve phenotypes. Alteration of ECM composition can lead to valve defects, raising the possibility that aberrancies in endocardial cushion formation or cardiac jelly may account the extended valve morphology observed at 72 hpf. To test this hypothesis, we examined the thickness of the endocardial cushions at the AVJ and cardiac jelly in the ventricle. We dissected Tg(Fli1:eGFP) zebrafish hearts at 52 hpf and subjected them to rhodamine-phalloidin to label the myocardium. We quantified the distance between the endocardial and myocardial layers at the AVJ. Vasopressin-treated hearts displayed a significant 82% increase in the size of the superior endocardial cushion compared to hearts from buffer-treated embryos, whereas the inferior endocardial cushions were not significantly affected (Figure 3, n=7 control, 10 vaso-treated, $p = 0.02$ for superior cushion, $p = 0.88$ for inferior cushion). Within the ventricular chamber, the distance between the myocardial and endocardial layers increased significantly in the outer curvature, suggesting that cardiac jelly may be more extensive in this region, while endo/myocardial separation remained unaffected in the inner curvature (Supplementary Figure 4, $p = 0.002$). This observation suggests that sub-regions of the heart may differentially respond to hemodynamic perturbations, and that changes in amount or distribution of cardiac jelly are a component of this response.

The enlarged endocardial cushions may be due to increases in extra-cellular matrix (ECM) production. To test this hypothesis, we performed qRT-PCR on dissected hearts at 52 hpf to evaluate expression levels of *has2*. Hyaluronan synthase, encoded by *has2*, is the enzyme primarily responsible for producing hyaluronan (HA), a principle component of ECM in endocardial cushions.(Patra et al., 2011)·(Camenisch, Biesterfeldt, Brehm-Gibson, Bradley, & McDonald, 2001) Thus, *has2* mRNA levels are likely to be indicative of HA production. qRT-PCR experiments indicated that *has2* expression increased 1.4-fold in vasopressin-treated

embryos at 53 hpf (Supplementary Figure 5, p =0.03). *Versican a* synthesizes versican, which is an ECM proteoglycan and a principal component of the cardiac jelly. *Versican a* expression was enhanced, predominantly at the superior cushion (Figure 3G-H). Combined, these data strongly suggest that afterload-mediated changes in hemodynamics increased ECM production in the endocardial cushions, which may contribute to the elongated valve phenotype.

Klf2a overexpression partially phenocopies vasopressin application

The *Kruppel-like factor 2a (klf2a)* transcription factor is expressed in endocardial cells in the AVJ during zebrafish endocardial cushion formation, and mediates mechanosensitive signaling.(Vermot et al., 2009) Prior work by Vermot and colleagues identified a decrease in expression of the RF-responsive transcription factor *klf2a* when RF was decreased.(Vermot et al., 2009) When embryos were treated with lidocaine to slow heart rate, RFF was decreased, and a corresponding decrease in *klf2a* expression could be detected in ~46 hpf hearts as little as 6-10 hours after lidocaine application. Under all treatments that inhibit RF, later valve morphogenesis was impaired.

In vasopressin-treated embryos, RFF is increased, leading us to wonder whether hearts are capable of detecting greater than normal oscillatory flows, and whether increases in *klf2a* underlie the observed ECM and valve morphology phenotypes. Therefore, we investigated whether vasopressin-treated hearts demonstrating increased RF showed increased *klf2a* expression. Indeed, qRT-PCR experiments indicated that relative to wildtype levels, *klf2a* expression in vasopressin-treated hearts was ~2-fold greater by 48 hpf. Well after RF was eliminated by development of valve leaflets, *klf2a* expression remained dramatically increased (>6-fold by 72 hpf) (Supplementary figure 3).

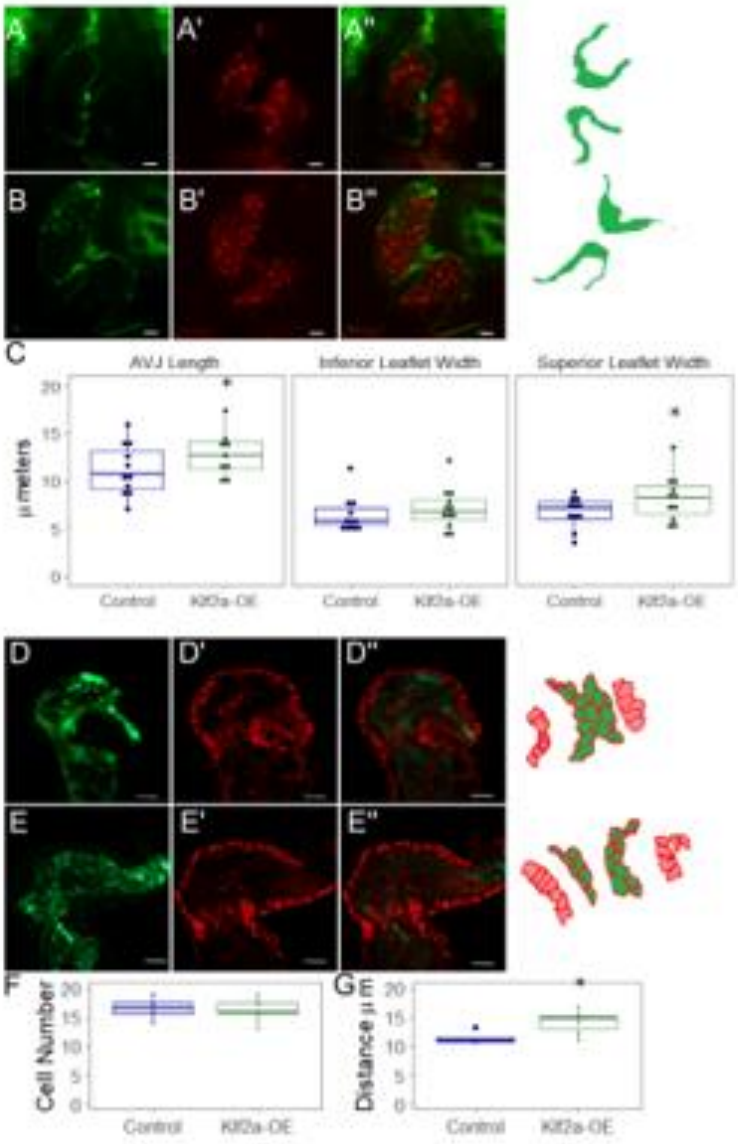

Figure 3.4: Klf2a-Overexpression Recapitulates the Afterload-Phenotype Through Increasing Cardiac Jelly Production. A-A'') Tg(Fli1:eGFP) and Tg(Gata:dsRed) of control hearts at 72 hpf. B-V'') Klf2a-OE hearts at 72 hpf. C) Superior leaflet width at 72 hpf. D) AVJ length at 72 hpf. For A-D: n= 11 control and 11 klf2a-OE hearts. D and F) Endocardial layer of noninjected and Klf2a-OW hearts. D' and E') Alcam immunohistochemistry. D'' and E'') Merge. F) Number of Alcam positive endocardial cells. G) Disrance between two cell layers at superior valve. For A-d') n = 4 control and 8- klf2a-OW hearts. Students T-test was used to determine statistical significane. * indicates $p < 0.05$

To determine whether Klf2a functioned upstream and is potentially causative of the observed AVJ defects, we overexpressed *klf2a* via mRNA injection into newly fertilized embryos. In embryos overexpressing *klf2a* (*klf2a*-OE embryos), we measured the diameter of the dorsal aorta in by confocal microscopy of Tg(Fli1:eGFP) embryos (see Figure 1). As expected, the dorsal aorta diameter did not detectably change, indicating that Klf2a does not cause vasoconstriction (Supplementary Figure 4). Remarkably, *klf2a* overexpression also elicited the elongated superior, but not inferior, valve leaflets (Figure 8A-C, $p = 0.05$ for superior leaflet and $p = 0.81$ for inferior leaflet), as observed in vasopressin-treated hearts. These data suggest that in response to increased afterload, the increased Klf2a levels mediate the defects in endocardial cushion and leaflet formation.

Finally, we assessed the effect of *klf2a* overexpression on valve cell specification. In wildtype hearts, specification of the AV canal occurs over a period of about 22-48 hpf.(Chi, Shaw, De Val, et al., 2008; Walsh & Stainier, 2001) ALCAM is broadly expressed in the myocardium by 36 hpf, but turns on in the AVJ endocardial cells by 55 hpf, concordant with their transition from a squamous to cuboidal shape at the onset of endocardial leaflet morphogenesis.(Beis, 2005) In these experiments, we used ALCAM immunohistochemistry to assay valve cell specification and assay the distance between the endocardial and myocardial layers at 56 hpf. We find that high afterload hearts showed no differences from controls in the number of endocardial cells initiating ALCAM expression, suggesting that valve cell specification was not significantly affected by *klf2a* overexpression (Figure 4D-EC, $p=0.40$). However, as in vasopressin-treated embryos, the distance between the endocardial and myocardial layers at the superior cushion was 32% larger in the *klf2a*-OE embryos (Figure 4F, $p=0.04$), suggesting that *klf2a* overexpression leads to an increase in the production of cardiac jelly. This data is consistent with previous reports suggesting that *klf2a* regulates production of ECM components, including fibronectin.(Steed, Boselli, & Vermot, 2016) In sum, our data suggest that *klf2a*

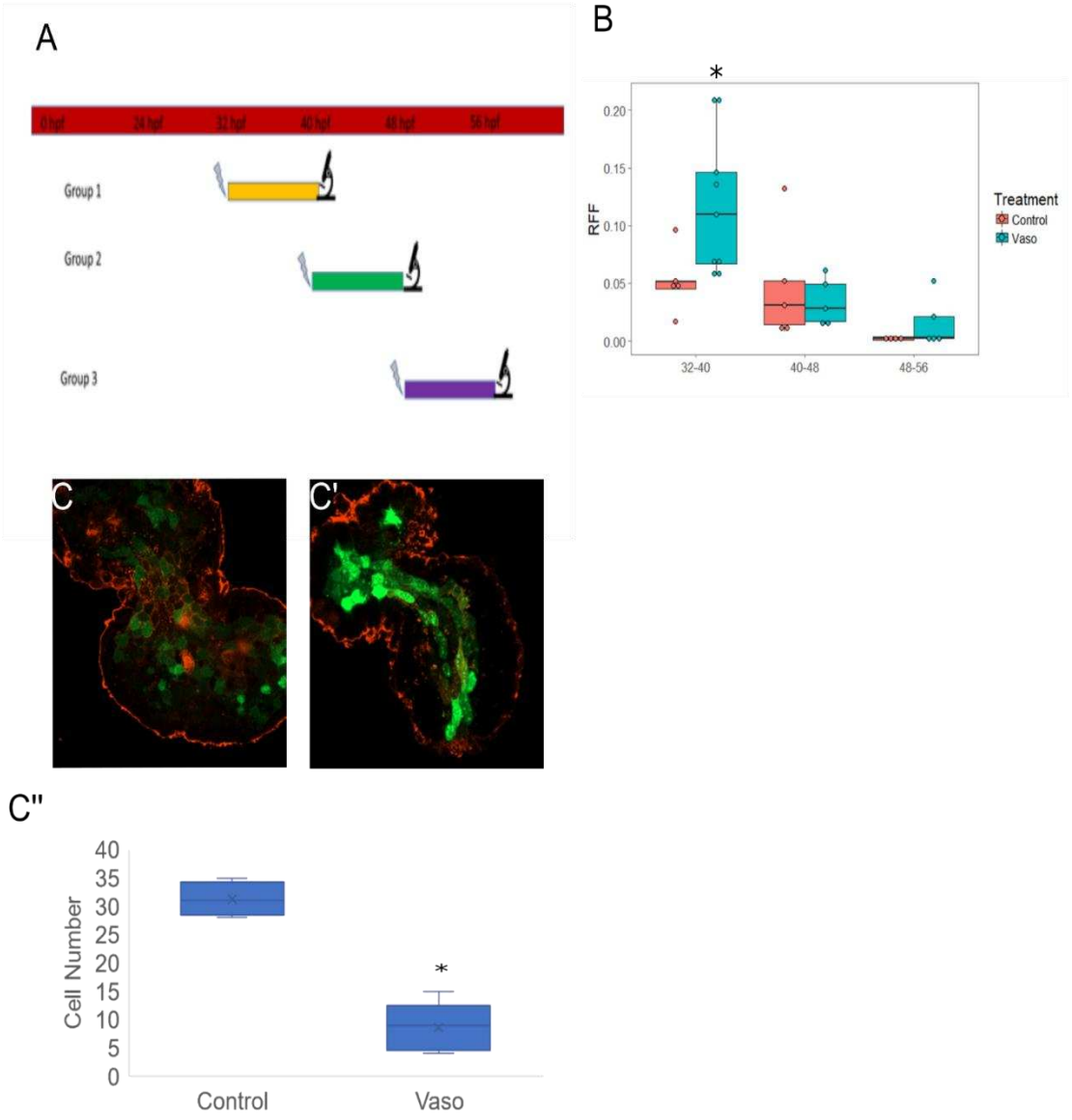

Figure 3.5. A) Embryos were incubated for 8-hour intervals between 32 and 56 hpf. After their incubation period, hearts were immediately recorded, and retrograde flow was analyzed. B) Retrograde flow significantly increased only in the 32-40 hpf window of vasopressin application. C) Alcam staining of control and C') Vasopressin-treated embryos between 32-40 hpf. Vaso-treated embryos have no ALCAM specified valve cells at the AVJ.

upregulation was not sufficient for altering valve cell specification, but may play a role in increasing cardiac jelly within the endocardial cushions.

Increasing retrograde flow between 32-40 hpf is sufficient to increase ECM production and cause valve defects

To determine what developmental time period is most susceptible to changes in retrograde grade flow, we incubated embryos in 10 µM vasopressin for 8 hour intervals, and then measured cardiac function using our previously described high-speed video techniques.(Bulk et al., 2016; Johnson et al., 2013) We found that incubation of vasopressin between 32 and 40 hpf was sufficient to increase RF over 3-fold (Figure 5A, n = 5 embryos for both control and vasopressin-treated hearts, p =0.03) at 40 hpf. Embryos treated between 40-48 hpf, and between 48-56 hpf did not appear to have significantly affected retrograde flow (p = 0.54 for embryos treated between 40-48 hpf, and 0.24 for embryos treated between 48-56 hpf).

During each cardiac cycle, there exists a period during which the endothelial layers lining either side of the AVJ come into brief physical contact to act as a primitive valve. Our group previously showed that increases in the length of endothelial closure can function as an adaptive mechanism that hearts use to limit backflow as pressure increases in the cardiac cycle.(Bulk et al., 2016) To investigate why embryos treated with vasopressin between 40-48 hpf and between 48-56 hpf did not increases in RF, we measured the length of endothelial closure in control and vasopressin-treated embryos at the end of each treatment period. In embryos treated with vasopressin between 32-40hpf, there is no change in the length of endothelial closure at 40hpf. Embryos treated between 40-48hpf experienced a 1.5 fold increase in endothelial closure at 48hpf, though this result was not significant (Figure 5B, n=5 control and vasopressin-treated embryos, p = 0.15). Embryos treated between 48-56 hpf experienced a approximately 3-fold significant increase in endothelial closure (n=5 control and vasopressin-treated embryos, p = 0.03). Together this data demonstrates that embryos treated

with vasopressin after 40hpf able to adapt by increasing the length of endothelial closure to prevent increased RF.

To test how changes in RF between 32 and 40 hpf impacts later valve development, we performed immunohistochemistry. As mentioned earlier, the expression of ALCAM in AVJ endothelium marks valve-specified cells. Application of vasopressin between 32 and 40 hpf abrogated endocardial ALCAM expression at 56 hpf, suggesting that endocardial cells do not properly undergo specification (Figure 5C). Together, this data highlights that endocardial cells are particularly sensitive to changes in afterload and flow between 32 and 40 hpf. Moreover, a negative impact during this window can have long-lasting changes that impede later steps in valve maturation.

Discussion

RF and Shear Stress display opposite temporal patterns in embryonic zebrafish valve development.

Several studies have focused on elucidating the role that RF and shear stress play in the regulation of valve development. Here, we characterize the developmental time periods in which RF and shear stress are present. We find that RF is robust at 32 hpf, but declines by 40 hpf. At 56 hpf, the RFF is almost zero (Figure 1). Conversely, shear stress is during the initial stages of cardiac development is relatively low, but increases as development progresses. This intuitively suggests a model wherein RF might dictate the developmental events early in valvulogenesis, and shear stress regulates later remodeling events.

Vasopressin application produces a dose-dependent elongation of the developing valve leaflet that is likely mediated by increases in RF

To perturb hemodynamic patterns in the developing zebrafish embryo, we chose to use vasopressin, a vasoconstrictive drug. We have previously shown that increases in vasopressin result in an increase in afterload, which then goes on to regulate both myocardial and endocardial valve cell differentiation (Ahuja et al., 2020, in review) Here, we show that

increases in afterload result in an increase in retrograde flow, but not shear stress. Increases in afterload result in a dose-dependent elongation of the developing valve leaflet, likely through increases in ECM and an increase in *klf2a.* Because *klf2a* has been previously associated with regulation by retrograde flow, we are reasonably confidant that phenotypes seen in both *klf2a*-OE and vasopressin-treated embryos are caused by increases in RF. However, because vasopressin directly alters afterload, and increases afterload may result in other secondary alterations in flow, it is possible that vasopressin-phenotypes are mediated by an alternate flow-related mechanism. Future studies should work on teasing apart changes in flow from changes in afterload.

Strikingly, we find that RF was significantly increased by 52 hpf in vasopressin-treated embryos. Retrograde flow normally occurs in embryonic hearts aged ~36-72 hpf for a limited period of each heartbeat.(Bulk et al., 2016), (Johnson et al., 2013) Movement of blood cells or plasma against the endocardial cells within the AVJ generates wall shear stress. Imaging studies have uncovered a contribution of biomechanical forces for regulating normal cardiac valve development.(Hove et al., 2003; Emily Steed et al., 2016; Vermot et al., 2009) In a detailed study that identified and perturbed retrograde flow, Vermot and colleagues examined mutant or pharmacological interventions that decreased preload in embryonic zebrafish.(Vermot et al., 2009) They established that retrograde flow (i.e., “reversing flows”) constitute a unique physical stimulus for valve development, and showed that loss of RF produced consistent defects in endocardial cushion formation. In our study it was therefore intriguing to note that *increases* in RF likewise perturbed valve morphogenesis, but generate a distinct set of cellular and molecular phenotypes.

Increases in RF Causes Defects in Endocardial Cushion Formation but Differentially Impact Valve Leaflet formation

The developing endocardial cushions were initially assessed in our study by measurement of endo-myocardial separation at the AVJ. Vasopressin-treated embryos

generated a significantly larger superior endocardial cushion, suggesting that ECM production was increased in this cushion. Supporting this idea, vasopressin-treated embryos showed upregulation of two genes involved in making principle components of the ECM, *has2* and *versican a* . HA and Versican are both abundant components of endocardial cushions, and others have shown that loss-of-function mutations that impact these components aberrantly affect valve development.(Mjaatvedt, Yamamura, Capehart, Turner, & Markwald, 1998; Patra et al., 2011; Yamamura, Zhang, Markwald, & Mjaatvedt, 1997) Our findings align with an cell culture study utilizing neonatal rat cardiomyocytes that suggested increases in afterload stimulate ECM production.(Hirt et al., 2012)

By 72 hpf, it was evident that increased RF had produced differential effects upon the nascent valve leaflets. Specifically, the width of the superior valve leaflet developed to be significantly thicker than control embryos, whereas the inferior valve leaflet was not detectably affected. The differential response of each valve leaflet may reflect differences in hemodynamic perturbations experienced by the endocardial cushions, given their non-equivalent positions in the looping heart, as morphogenesis proceeds. Future studies should investigate more closely the basis for the differential response in the superior and inferior valve.

Kfl2a overexpression resulted in elongated valve leaflets, similar to vasopressin-treatment

The Kruppel-like Factor2 is among the best studied transcription factors known to respond to shear stress by a change in transcription levels.(Dietrich et al., 2014; Heckel et al., 2015; Emily Steed et al., 2016; Vermot et al., 2009) Retrograde flow in particular appears to be a potent regulator of *klf2a* transcription. Most studies to date document that loss of RF leads to decreased *klf2a* expression in the AVJ. We now show that the converse is also true: endocardial cells appear capable of sensing levels of RF that exceed normal values, and they respond by increasing levels of *klf2a* transcription. The relevancy of *klf2a* for transducing the abnormal biomechanical cues induced by high afterload is demonstrated here by *klf2a*

overproduction experiments. In alignment with phenotypes observed in vasopressin-treated hearts, Klf2a-OE hearts developed enlarged endocardial cushions, and later generated superior valve leaflets of abnormal size and morphology, while inferior valve leaflet remained normal. Conversely, increased Klf2a did not recapitulate all the defects promulgated by high afterload in AVJ myocardial specification, suggesting these cellular responses may be mediated via a Klf2a-independent mechanism.

Chapter 4: Identification of Regulators of AVJ myocyte development

Summary

Congenital valve defects are one of the most common birth defects in the United States and occur in over 50% of all congenital heart disease. Despite clinical relevance, the etiology of valve diseases remains poorly understood; currently, we can only ascribe genetic causes to approximately 35% of congenital disease. As cardiomyocytes mature, they undergo regionally-confined morphological and functional changes that are required for proper physiological function. Myocytes at the developing atrioventricular junction (AVJ) are especially specialized; these myocytes have a distinct trapezoidal shape and must secrete signaling molecules such as Bone Morphogenetic Protein 4 (bmp4) to initiate valve formation. How these functional and morphological differences arise is not well understood. Here, we take an RNA-sequencing approach to identify regulators of atrioventricular myocyte maturation in a zebrafish model. We find that the transcriptional changes that underlie atrioventricular and chamber myocytes maturation processes are vastly different. We have identified different signaling pathways and transcription factors utilized in their respective development. Our results highlight nuclear porin *nup155* as putatively being a key regulator of cardiomyocyte differentiation and maturation. Together, these results identify a novel cohort of genes that are involved in the maturation of valve myocytes and chamber myocytes.

Introduction

In the United States, it is estimated that 8 out of every 1000 newborns will be born with a congenital heart defect, and approximately 38% of them will require cardiac intervention (Hoffman & Kaplan, 2002). With current treatments, the expected mortality rate for patients

afflicted with CHD ranges from 10 to 35% in the first year of life (Hinton & Ware, 2017). The current deficiency in scientific understanding of the genetic basis for how valves form represents a significant barrier to improving patient outcomes. Of congenitally-driven defects, the gene responsible is known in only 35% of cases (Simmons & Brueckner, 2017). Identification of additional genetic factors required for proper valve development and their underlying interactions is required to overcome this knowledge gap.

The valve-forming AVJ myocytes are morphologically and functionally distinct from both atrial and ventricular myocytes. At the onset of cardiac development (linear tube stage), all cardiac myocytes are physiologically indistinguishable. These *immature myocytes* are "slow-conducting," that is to say, the electrical impulses that drive the heartbeat travel slowly through the single layer of myocytes that comprise the heart tube. As heart cells continue to differentiate, the atrial and ventricular myocytes (the *chamber myocytes*) become "fast-conducting", while the *AVJ myocytes* retain their slow-conducting phenotype (Bressan et al., 2014). By 48 hpf, AVJ myocytes take on a distinct trapezoidal shape, whereas ventricular myocytes are cuboidal and atrial myocytes are large and flat (Auman et al., 2007; Chi, Shaw, Jungblut, et al., 2008). AVJ myocytes secrete a protein called Bone Morphogenetic Protein 4 (bmp4), which enters the extracellular space and serves as a cue to the nearby endocardial cells to start valve development (Combs & Yutzey, 2009). How differences between AVJ myocytes and chamber myocytes arise is poorly understood, in part because researchers have identified only a subset of active genes in differentiating valve cells.

The overall phenotype of a cell is determined both by autonomous internal signals (such as transcription factors) and by external signals (such as secreted molecules or physical forces from the local environment). To date, few internal signaling pathways have been identified as regulators of AVJ myocyte differentiation. Moreover, the scientific understanding of how internal and external signaling pathways interact has many gaps. To address these gaps, we utilized two transgenic lines: a bmp4 reporter (Tg[bmp4:egfp)], which specifically labels valve

myocardial cells, and cmlc2 reporter [Tg(cmlc2:egfp)], which labels all cardiac myocytes. We isolated each of these developing cell populations using flow cytometry on 48 hpf embryos, and subjected the isolated cell populations to RNA-sequencing. To gain information regarding molecular changes involved in development, we also isolated and sequenced undifferentiated cardiomyocytes from 24 hpf (Figure 1). We provide a comprehensive list of genes specifically expressed in the developing AVJ myocytes which provides novel insight into pathways and processes that could drive differentiation. Increased understanding of these genes is necessary to unravel regulatory mechanisms that govern normal valve development, and to assess the congenital defects associated with loss of their function.

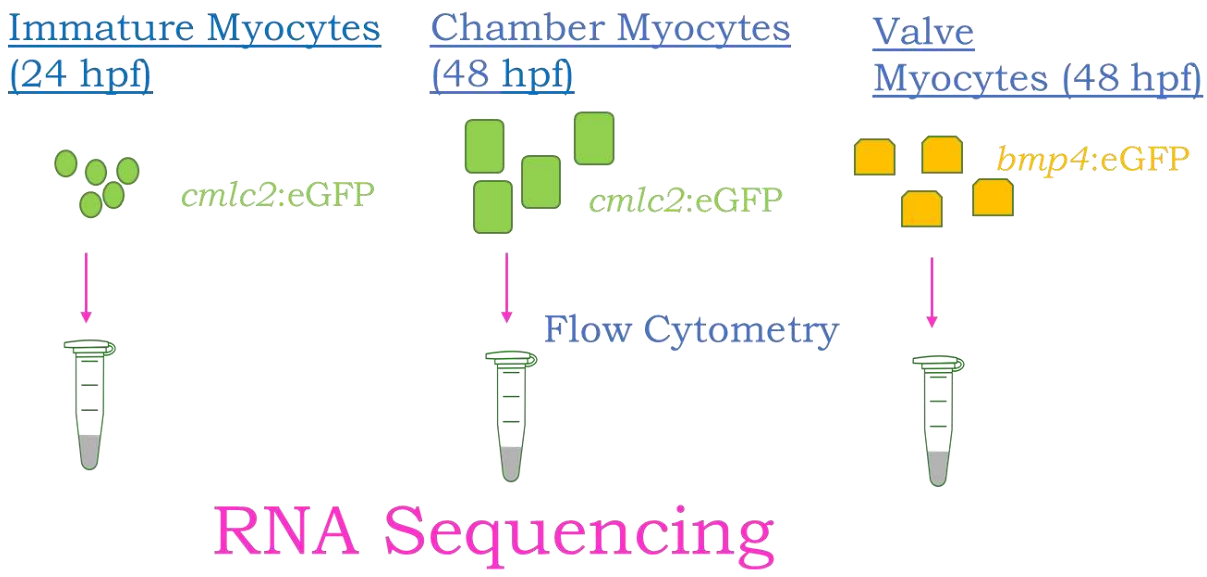

Figure 4.1: Experimental workflow. Cells were gathered from two temporal stages and isolated using flow cytometry. Cells were then utilized for RNA-seq.

Methods

Cell Isolation and Flow Cytometry

We isolated subsets of myocytes by using Fluorescent Activated Cell Sorting (FACS) on embryonic tissue from two transgenic lines that express fluorescent proteins in a spatially restricted manner. The first transgenic line contains coding sequences for eGFP (a fluorescent protein that emits red light under the appropriate conditions) driven by heart-specific regulatory sequences (*cardiac myosin light chain*). The *cardiac myosin light chain* regulatory sequences drive eGFP expression in both chamber myocytes and AVJ myocytes (Auman et al., 2007). The second transgenic line contains coding sequences for GFP (a fluorescent protein that emits green light) inserted into its genome under the control of the regulatory elements for bmp4 (Shentu et al., 2003). The bmp4 regulatory sequences cause GFP expression only in AVJ myocytes. We utilized flow cytometry to separate AVJ and chamber myocytes present in hearts (Samsa, Fleming, Magness, Qian, & Liu, 2016) [Figure 2]. AVJ myocyte (48 hpf) samples (at the stage of nascent endocardial cushions) were compared with immature myocytes (24 hpf) isolated from younger embryos (linear heart tube stage), as well as chamber myocytes (48 hpf) from atrium or ventricle. For each genotype, we isolated 3 biological replicates. Each biological replicate was collected from a different clutch of embryos. To avoid batch effects, only one sample of each genotype was processed at a time.

Cell isolation was performed according to standard protocols. In brief, approximately 100 zebrafish embryos of the appropriate age and genotype were dechlorinated, and then deyolked by placing the embryos in a bicarbonate buffer. Embryos were then placed in cell dissociation buffer, consisting of trypsin, 1 mM EDTA, phosphate buffered saline, and DNase. Cells were placed in 30-degree Celsius water bath for 30-second intervals and homogenized via pipetting until embryos were no longer intact. Cells were then placed in stop buffer, consisting of L-15/10% FBS and 1 mM EDTA and strained through a 70 µM nylon mesh. To assess for viability

we utilized Ghost Dye (Tonbo Biosciences), which stains dead cells. After being strained through the nylon mesh, cells were washed three times with PBS. Ghost dye was added according to manufacturer's protocol, and cells were incubated in the dark at room temperature for one hour. Cells were then placed in L15/10 FBS to remove unreacted dye. Because both FBS and EDTA can interfere with downstream library preparation, cells were then washed five times with EDTA-free PBS.

Cell isolation was done with the help of Dr. Allen at CSU's Flow cytometry core. In brief, cells were loaded into the FACS Aria III and sorted for GFP+ positive cells. Gates were set to exclude any cellular aggregates and debris, as well as any Ghost dye positive (dead) cells. GFP-positive cells from this sort were then resorted using the same sorting parameters – each sample was sorted twice to increase sorting purity. Post-sort purity checks revealed that final samples consisted of >85% GFP positive cells (Figure 2). Between 50 and 200 cells were isolated per sample. Cells were sorted directly into lysis buffer (Clontech Smartseq v4 Reaction buffer) containing 1uL of RNAase inhibitor (Clontech Smartseq v4 RNase Inhibitor). Samples were stored at -80 degrees until library preparation.

RNA Sequencing

Library preparation and RNA sequencing was performed by Omega Bioservices. In brief, RNA extraction and library preparation was performed by using Clontech Ultralow Input RNA library prep kit. Indexing was performed according to manufacturers protocol, resulting in dual in-line Illumina adapters (Bio). Samples were run on an Illumina HiSeq 2500 to generate ~40 million 150-bp paired-end reads for each.

Analysis

Analysis was performed according to standard protocols (Pertea, Kim, Pertea, Leek, & Salzberg, 2016). Adapter removal and read filtering was performed using Trimmomatic Version 0.39 (Bolger, Lohse, & Usadel, 2014). Quality of all samples was fairly good, with phred scores greater than 30 across the entire read (Supplemental Figure 1). Alignment to the genome

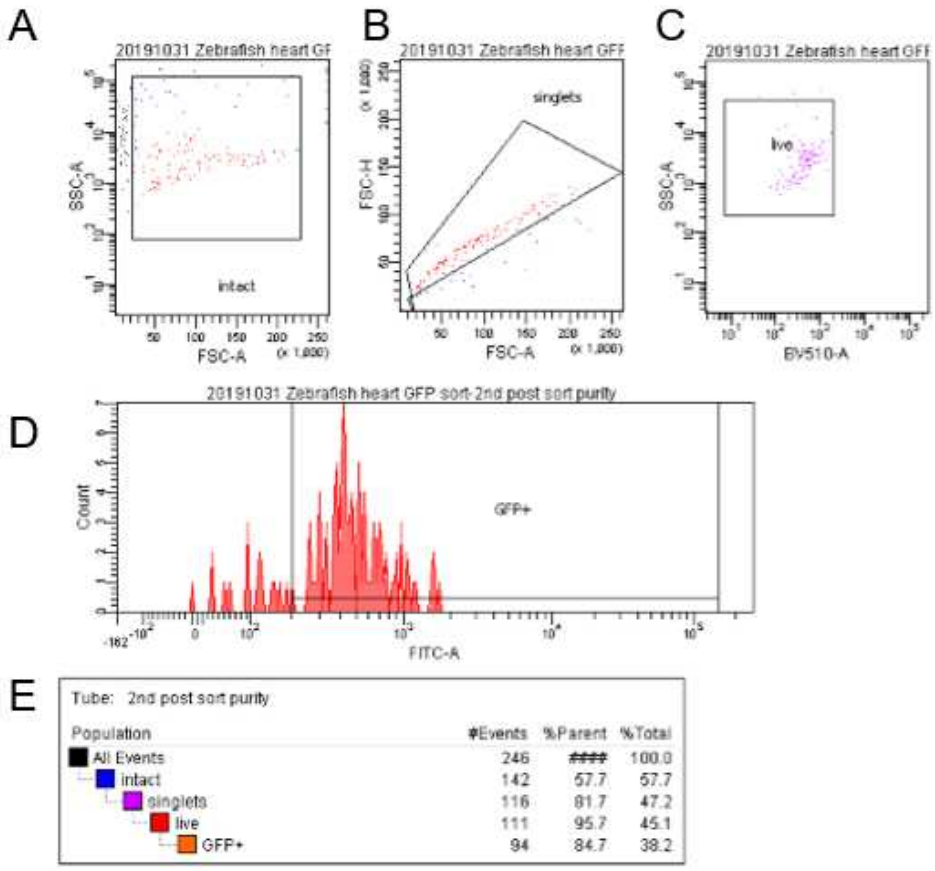

Figure 4.2: Representative flow cytometry result from the second iterative sort. A) Selection of cells based on forward and side scatter. B) Selection of single cells. C) Selection of alive cells based on ghost dye labeling. D) Selection of GFP positive cells based on fluorescence. E) ~85% of alive single cells expressed GFP. These cells were then sorted directly into Clontech Reaction Buffer with RNAse inhibitor.

(zebrafish v11) was performed using HISAT2 version 2.2.0, and transcriptome assembly was performed using Stringtie v2.1.1 (Pertea et al., 2016). Differential expression analysis was performed using Ballgown (Pertea et al., 2016). Gene ontology analysis was performed using The Gene Ontology Resource. The Venn diagram was created using BioVenn.

Results

Differential Expression Analysis Reveals Significant Transcriptional Differences between Immature, Chamber, and AVJ myocytes

At 24 hpf in zebrafish, cardiomyocytes throughout the entire heart tube are physiologically indistinguishable; they are all relatively small**,** slow-conducting, and express *bmp4*. By 48 hpf, chamber myocytes and AVJ myocytes have distinct characteristics. Chamber myocytes are large, cuboidal, fast-conducting cells, while AVJ myocytes are smaller, and retain a slow-conducting phenotype (Chi, Shaw, De Val, et al., 2008). How these distinct characteristics arise is not well understood. To evaluate how transcription changes between immature, AVJ, and chamber, we performed RNA-sequencing on flow-isolated cells from 24 hpf eGFP-labeled cardiomyocytes], and 48 hpf AVJ myocytes isolated using the Tg(bmp4:eGFP) line. We then performed pairwise differential-expression analysis between the following pairs: AVJ myocytes vs chamber myocytes, AVJ myocytes vs immature myocytes, and chamber myocytes vs immature myocytes. We identified significantly (p-value < 0.05) differentially expressed genes (DEGS) in all three comparisons; we found 361 DEGs between chamber and AVJ myocytes, 661 DEGS between immature and AVJ myocytes, and 612 DEGs between immature and chamber myocytes (Figure 3).

To gain a better understanding of how AVJ and chamber myocytes mature over time, we compared genes that were significantly upregulated in both AVJ and chamber myocytes, as compared to immature myocytes. We specifically compared genes that had a greater than two-fold increase and an adjusted p-value < 0.05. Surprisingly, genes that were upregulated in the

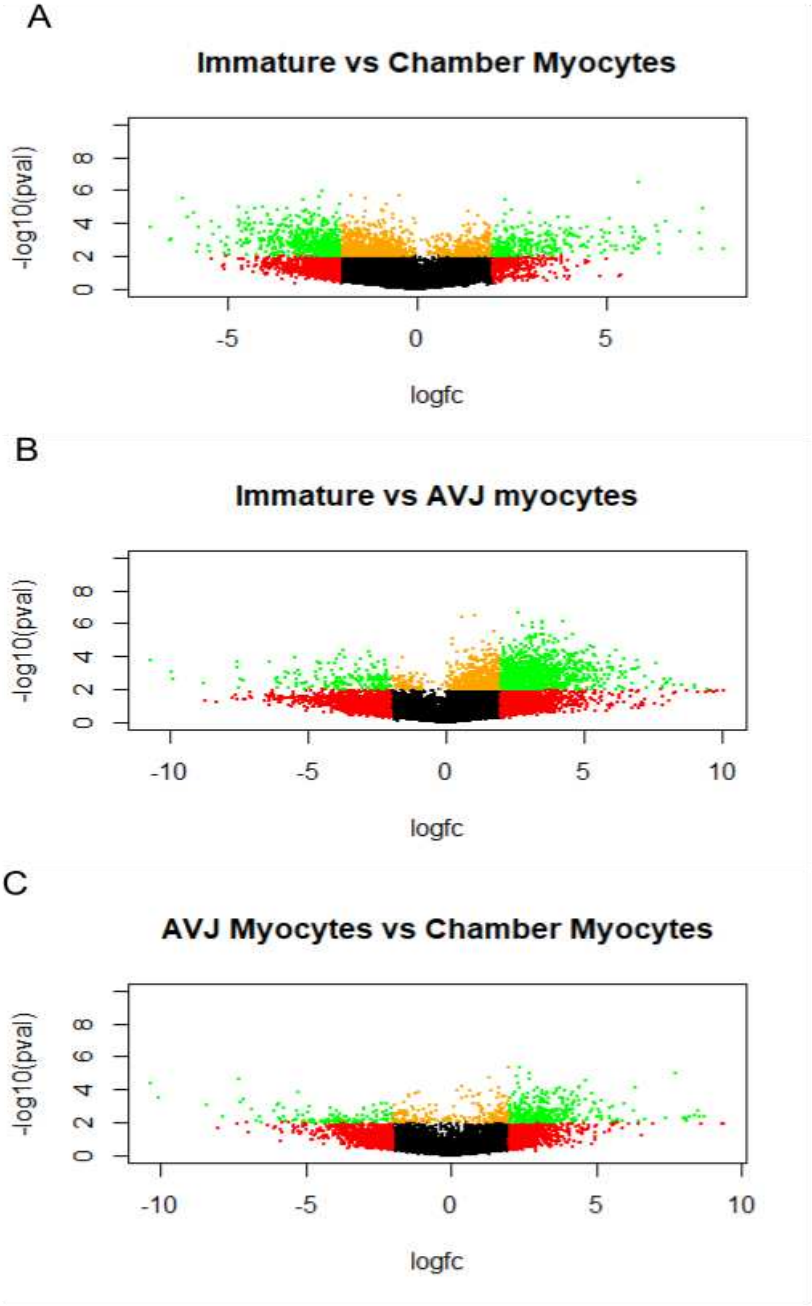

Figure 4.3: Differential expression of immature, chamber, and AVJ myocytes. Each dot represents a single gene. Black dots represent no significant change. Red dots represent genes with at least a log(2) fold change. Orange dots represent genes significantly changed genes with q-value < 0.05. Green dots represent genes with that have undergone at least a log(2) fold change and have a q-value <0.05.

AVJ myocytes shared little overlap with genes that were upregulated in chamber r myocytes (Figure 4A). That is to say, there were only four genes that shared increased expression in both the 48 hpf AVJ myocytes and 48 hpf chamber myocytes, relative to the 24 hpf immature myocytes. These genes were involved in ATP synthesis or were novel genes (Supplemental Table 1). To characterize transcriptional changes that occur during the development of AVJ myocytes, we performed gene ontology analysis on the 37 genes that were specifically upregulated in AVJ myocytes relative to immature myocytes. We found enrichment in several GO terms, including cell signaling, biosynthesis, and metabolism (Figure 4B). No significant GO enrichment was detected for genes that were upregulated in chamber myocytes relative to immature myocytes.

There were 85 genes that were co-downregulated in AVJ and chamber myocytes relative to immature myocytes (Figure 4C). These genes consisted of DNA replication machinery, transcription factors, and several novel genes (Supplemental Table 2). Genes that were downregulated exclusively in AVJ myocytes seemed to be involved in metabolism and oxidative phosphorylation, while genes that were downregulated in chamber myocytes were more involved in macromolecule assembly and cell cycle (Figure 4D, Supplemental Figure 2). Together, these results highlight the vast difference in the maturation of AVJ myocytes as compared to chamber myocytes.

To identify regulators of cardiomyocyte differentiation, we chose to prioritize genes that were differentially expressed in multiple conditions (Figure 5). We identified one gene, *nup155*, that was differentially expressed in all three pairwise comparisons. We identified 12 genes that were differentially expressed in both AVJ and chamber myocytes as compared to immature myocytes (Supplementary Table 3). We identified 38 genes that were differentially expressed in both AVJ anad immature myocytes, as compared to chamber myocytes (Supplementary Table

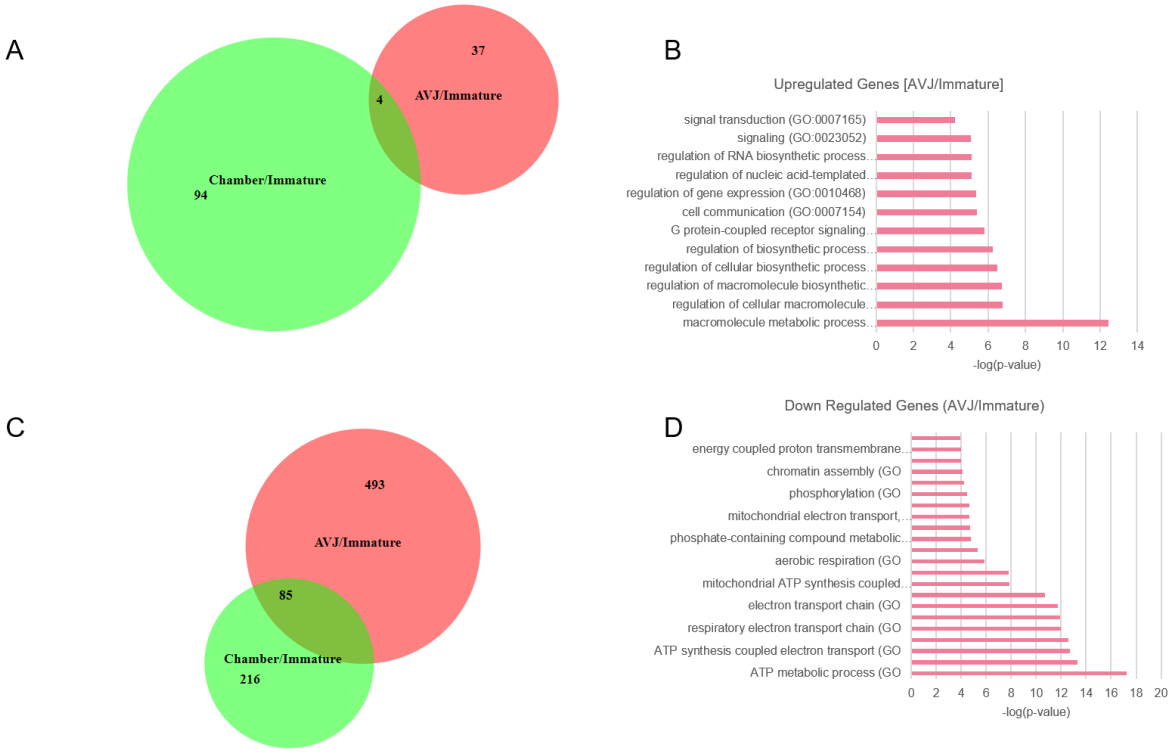

Figure 4.4: AVJ and Chamber myocytes undergo distinct transcriptional changes. A) 4 genes are co-upregulated in chamber and AVJ myocytes as compared to immature myocytes. Only genes that returned an adjusted p-value < 0.05 and had greater than a 2-fold change were included. B) Genes that were exclusively upregulated in AVJ myocytes were involved in cell communication and macromolecule synthesis. C) 85 genes were co-downregulated in both AVJ and chamber myocytes relative to immature myocytes. D) Genes that were downregulated exclusively in AVJ myocytes were involved in ATP synthesis and respiration.

4). There were 331 genes that were differentially expressed in both chamber and AVJ myocytes, as compared to immature myocytes (Figure 5).

We next decided to characterize the 331 genes that were differentially regulated in both Chamber/Immature myocytes and in AVJ/Immature myocytes. Because genes in this category were differentially expressed in both later stages (AVJ and chamber myocytes) as compared to immature myocytes, we reasoned that changes the expression of these genes may represent 2transcriptional changes required for myocyte maturation. To characterize this large set of genes, we performed gene ontology analysis on these co-differentially expressed genes. We found significant enrichment in processes such macromolecule synthesis, chromatin modification, and metabolic processes (Supplementary Figure 3).

Nup155 regulates maturation of cardiomyocytes

In every pairwise comparison performed, *nup155* was differentially expressed. *Nup155* was most highly expressed in immature myocytes. Nup155 expression decreased 6-fold in chamber myocytes and was completely abolished in AVJ myocytes (Figure 5A, adjusted p =0.01 between immature and AVJ myocytes, adjusted p=0.03 between immature and AVJ myocytes). Chamber myocytes had a 10-fold increase in expression as compared to AVJ myocytes (adjusted p-value=0.03). Because *nup155* was differentially expressed in all three conditions, we hypothesized that *nup155* may be involved in the differentiation of chamber cardiomyocytes. *Nup155* encodes a nucleporin involved in the transport of macromolecules across the nuclear membrane. *Nup155* missense mutations were identified of families with histories of atrial fibrillation and sudden onset pediatric cardiac death syndrome (X. Zhang et al., 2008). Homozygous knockout *nup155* -/- mice die by E8.5, while heterozygous mice show an atrial fibrillation phenotype (X. Zhang et al., 2008). Transcriptome analysis of *nup155* +/- embryonic stem cells revealed differential expression in 326 genes relative to wildtype embryos,

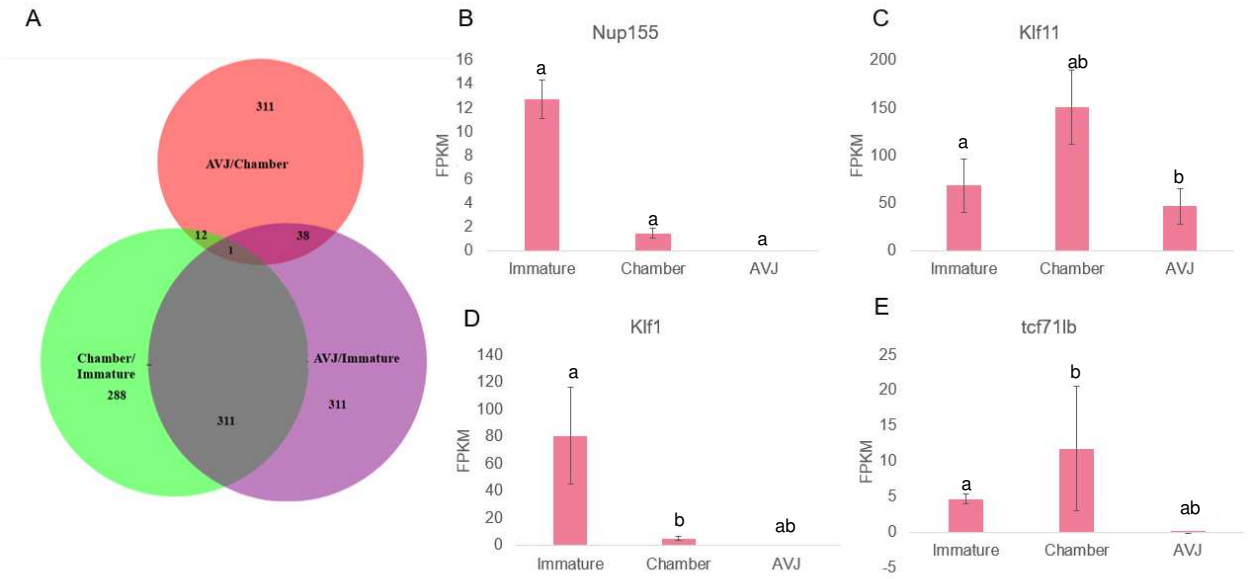

Figure 4.5: A) Venn diagram comparing all genes that were differentially expressed between immature, chamber, and AVJ myocytes. B) *Nup155* expression is highest in immature myocytes, decreases in chamber myocytes and is abolished in AVJ myocytes. P=0.03 between immature and chamber myocytes, 0.01 between immature and AVJ myocytes, and 0.03 between chamber and AVJ myocytes C) Adjusted p-value = 0.04 between AVJ and chamber cardiomyocytes, p =0.88 between immature and AVJ myocytes, p=0.02 between immature and chamber myocytes. D) Adjusted p-value = 0.002 between chamber and AVJ cardiomyocytes, p=0.01 between immature and AVJ cardiomyocytes, p=0.07 between chamber and immature myocytes. E) Adjusted p-value = 0.02 between chamber and AVJ cardiomyocytes, 0.03 between immature and AVJ cardiomyocytes, p=0.79 between chamber and immature myocytes. Letters indicates significant, same letter denotes significant different in the pairwise comparison performed for a given gene.

including several signaling pathways such as Rho/Rac, integrin, and tryrosine kinase(Preston et al., 2018). Further analysis of the same transcriptome revealed differential expression in 96 noncoding RNAs, including several microRNAs. (Preston et al., 2019) Together, these data strongly support a role for *nup155* in cardiac development and cardiomyocyte differentiation.

Transcription factors *klf11b, klf1,* and tcf7lb are involved in differentiation of cardiomyocytes

To identify more putative regulators of AVJ myocyte development, we next examined the co-differentially regulated genes between AVJ/chamber myocytes and Chamber/Immature myocytes. There were 12 genes total in this category, largely involved in cell signaling and extracellular matrix remodeling (Supplementary table 2). One of these genes, *Kruppel-like factor 11b*, is a zinc-finger transcription factor in the Kruppel family. *Klf11b* is expressed in immature myocytes and undergoes an approximate 2-fold increase in expression in chamber myocytes (Figure 4C, p=0.02). AVJ myocytes displayed a 30% reduction in *klf11b* expression as compared with chamber myocytes and was not significantly different from immature myocytes (Figure 4C, p=0.04 between AVJ and chamber myocytes, p=0.88 between AVJ and immature myocytes). Because of this expression pattern, it seems likely that *klf11b* is involved in the differentiation of chamber myocytes. Expression of KLF11 is reduced in failing adult murine hearts, and overexpression of KLF11 protects against pathological hypertrophy and fibrosis (Zheng, Kong, & Li, 2014). These data warrant further investigation into the role *klf11* plays in cardiac development.

We further evaluated genes that were co-differentially expressed between AVJ/immature myocyte and AVJ/Chamber myocytes. There are 38 of these genes in total, with functions in extracellular matrix remodeling, ion-channels, and chromatin modification. We identified 2 transcription factors, *klf1* and *tcfl7*, to be co-differentially regulated in this group.

Klf1 is another member of the Kruppel-like transcription factor family. *Klf1* expression was highest in immature myocytes. As development progressed, it underwent an approximate

12-fold reduction in chamber myocytes, though this difference was not significantly different. (Figure 5D, p=0.01 between immature and AVJ cardiomyocytes, p=0.07 between chamber and immature myocytes). Expression in chamber myocytes increased 5-fold as compared to AVJ myocytes (Figure 5D, Adjusted p-value = 0.002 between chamber and AVJ cardiomyocytes). *Klf1* is perhaps best known for its role in erythropoiesis; in mice, KLF1 is expressed specifically in red blood cells, and knockout of KLF1 abrogates red blood cell formation (Perkins, Sharpe, & Orkin, 1995). In zebrafish, the function of *klf1* is not well understood, and its dynamic expression pattern warrant further follow-up (Oates et al., 2001).

Tcfl71b is a zebrafish homolog of Tcfl7 (T-cell factor/lymphoid enhancer like 7), transcription factor that is activated by *Wnt* signaling. In our analysis, expression increased approximately 3-fold between immature and chamber myocytes. AVJ myocytes had significantly reduced expression compared to both chamber and immature myocytes. Because expression of *tcfl71b* is specifically upregulated in chamber myocytes, it seems likely that it is involved in the differentiation of chamber myocytes. Knockout mice displayed embryonic lethality and severe cardiac defects, including missing hearts (Merrill et al., 2004). Knockout of Tcfl71 in embryonic stem cells prevented cardiomyocyte differentiation(Liang & Liu, 2018). In zebrafish, knockdown of *tcf7l1b* using morpholinos caused cardiomyocyte proliferation, and facilitated restriction of cardiomyocyte markers (Sorrell, Dohn, D'Aniello, & Waxman, 2013). Together, this data suggests *tcfl71b* functions to facilitate cardiomyocyte differentiation. While the role of *tcfl71b* in the initial differentiation of cardiomyocytes is becoming increasingly understood, how *tcf7l1b* functions in later stages of development is not well elucidated. Because *tcfl71b* expression is specifically repressed in AVJ myocytes, it seems likely that *tcf7l1b* plays a role in directing cardiomyocyte maturation. We have therefore prioritized it as a target for follow-up studies.

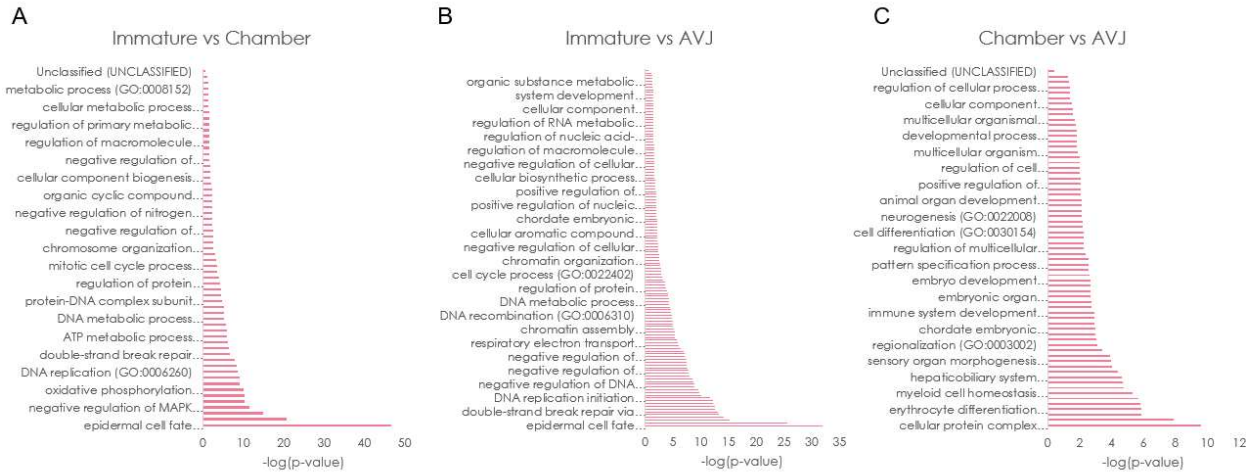

Figure 4.6: Gene ontology analysis. A) Chamber myocytes undergo significant alterations in genes involved in MAPK, epidermal cell fate, and cell cycle. B) AVJ myocytes undergo significant changes in chromatin modification, macromolecule synthesis, and epidermal cell fate. C) Chamber and AVJ myocytes differ predominantly in cellular signaling and genes involved in differentiation.

Gene Ontology Analysis reveals roles for mapK inhibition, chromatin remodeling in cardiomyocyte differentiation

To determine how the transcriptional profile of AVJ cells differs from immature myocytes and chamber myocytes, we used GO to classify sets of RNAseq genes based on known functions of similar genes in NCBI databases. Atrioventricular myocytes and chamber differ in developmental signaling pathways, extracellular matrix factors, and calcium handling proteins (Figure 6). Between 24 hpf and 48 hpf, chamber myocytes undergo many changes in many pathways, and MapK inhibition. AVJ myocytes demonstrate several changes in chromatin modification, highlighting the role of epigenetics in valve development. Factors involved in epidermal cell fate decisions seem to involve in the maturation of cardiomyocytes, as they were enriched in both AVJ/immature and chamber/immature data sets. AVJ and chamber myocytes primarily differ in cellular processes and signaling, consistent with AVJs role in communication with the overlying endocardial cells. Together this data highlights different transcriptional processes involved in making chamber and AVJ myocytes.

Conclusions

While AVJ myocytes and chamber myocytes arise from the same population of cells, AVJ myocytes have distinct functional and morphological phenotypes. Here, we have identified a unique set of genes that govern the development of AVJ and chamber myocytes from their progenitors. Surprisingly, transcriptional changes that occur between AVJ-immature and chamber-AVJ myocytes share little overlap, suggesting that different signaling processes regulate the maturation of these cell types. Our results highlight 4 genes (*nup155, klf1, klf11b, tcf7l1b*) for further investigation. Altogether, our results provide invaluable insights into the development of the valve.

References

Amstrup Funder, J., Christian Danielsen, C., Baandrup, U., Martin Bibby, B., Carl Andelius, T., Toft Brøndum, E., . . . Michael Hasenkam, J. (2017). How Heart Valves Evolve to Adapt to an Extreme-Pressure System: Morphologic and Biomechanical Properties of Giraffe Heart Valves. *J Heart Valve Dis, 26*(1), 63-71.

Ando, K., Fukuhara, S., Nanae, I., Nakajima, H., Fukui, H., Kelsh, R. N., & Mochizuki, N. (2016). Clarification of mural cell coverage of vascular endothelial cells by live imaging of zebrafish. *Development, 143*(8), 1328–1339.

Astrof, S., Crowley, D., & Hynes, R. O. (2007). Multiple cardiovascular defects caused by the absence of alternatively spliced segments of fibronectin. *Dev Biol, 311*(1), 11-24. doi:10.1016/j.ydbio.2007.07.005

Auman, H. J., Coleman, H., Riley, H. E., Olale, F., Tsai, H. J., & Yelon, D. (2007). Functional modulation of cardiac form through regionally confined cell shape changes. *PLoS Biol, 5*(3), e53. doi:10.1371/journal.pbio.0050053

Bakkers, J. (2011). Zebrafish as a model to study cardiac development and human cardiac disease. *Cardiovasc Res, 91*(2), 279-288. doi:10.1093/cvr/cvr098

Balachandran, K., Konduri, S., Sucosky, P., Jo, H., & Yoganathan, A. P. (2006). An ex vivo study of the biological properties of porcine aortic valves in response to circumferential cyclic stretch. *Ann Biomed Eng, 34*(11), 1655-1665. doi:10.1007/s10439-006-9167-8

Balachandran, K., Sucosky, P., Jo, H., & Yoganathan, A. P. (2010). Elevated cyclic stretch induces aortic valve calcification in a bone morphogenic protein-dependent manner. *Am J Pathol, 177*(1), 49-57. doi:10.2353/ajpath.2010.090631

Banjo, T., Grajcarek, J., Yoshino, D., Osada, H., Miyasaka, K. Y., Kida, Y. S., . . . Ogura, T. (2013). Haemodynamically dependent valvulogenesis of zebrafish heart is mediated by flow-dependent expression of miR-21. *Nat Commun, 4*, 1978. doi:10.1038/ncomms2978

Bark, D. L., Johnson, B., Garrity, D., & Dasi, L. P. (2017). Valveless pumping mechanics of the embryonic heart during cardiac looping: Pressure and flow through micro-PIV. *J Biomech, 50*, 50-55. doi:10.1016/j.jbiomech.2016.11.036

Barnette, D. N., VandeKopple, M., Wu, Y., Willoughby, D. A., & Lincoln, J. (2014). RNA-seq analysis to identify novel roles of scleraxis during embryonic mouse heart valve remodeling. *PLoS One, 9*(7), e101425. doi:10.1371/journal.pone.0101425

Beekman, R. H., Rocchini, A. P., Dick II, M., Crowley, D. C., & Rosenthal, A. (1984). Vasodilator Therapy in Children: Acute and Chronic Effects in Children with Left Ventricular Dysfunction or Mitral Regurgitation. *Pediatrics, 73*(1).

Beis, D. (2005). Genetic and Cellular Analyses of Zebrafish Atrioventricular Cushion and Valve Development. *Development, 132*(18), 4193-4204.

Bernardo, B. C., Weeks, K. L., Pretorius, L., & McMullen, J. R. (2010). Molecular distinction between physiological and pathological cardiac hypertrophy: experimental findings and therapeutic strategies. *Pharmacol Ther, 128*(1), 191-227. doi:10.1016/j.pharmthera.2010.04.005

Berndt, C., Poschmann, G., Stühler, K., Holmgren, A., & Bräutigam, L. (2014). Zebrafish heart development is regulated via glutaredoxin 2 dependent migration and survival of neural crest cells. *Redox Biol, 2*, 673-678. doi:10.1016/j.redox.2014.04.012

Bio, T. SMART-Seq® v4 3′ DE

Kit User Manual. In.

Bloomekatz, J., Singh, R., Prall, O. W., Dunn, A. C., Vaughan, M., Loo, C. S., . . . Yelon, D. (2017). Platelet-derived growth factor (PDGF) signaling directs cardiomyocyte movement toward the midline during heart tube assembly. *Elife, 6*. doi:10.7554/eLife.21172

Blue, G. M., Kirk, E. P., Sholler, G. F., Harvey, R. P., & Winlaw, D. S. (2012). Congenital heart disease: current knowledge about causes and inheritance. *Med J Aust, 197*(3), 155-159.

Bolger, A. M., Lohse, M., & Usadel, B. (2014). Trimmomatic: a flexible trimmer for Illumina sequence data. *Bioinformatics, 30*(15), 2114-2120. doi:10.1093/bioinformatics/btu170

Boselli, F., Freund, J. B., & Vermot, J. (2015). Blood flow mechanics in cardiovascular development. *Cell Mol Life Sci, 72*(13), 2545–2559.

Boselli, F., Steed, E., Freund, J. B., & Vermot, J. (2017). Anisotropic shear stress patterns predict the orientation of convergent tissue movements in the embryonic heart. *Development, 144*(23), 4322-4327. doi:10.1242/dev.152124

Bowen, C. J., Zhou, J., Sung, D. C., & Butcher, J. T. (2015). Cadherin-11 coordinates cellular migration and extracellular matrix remodeling during aortic valve maturation. *Dev Biol, 407*(1), 145-157. doi:10.1016/j.ydbio.2015.07.012

Breinholt, J. P., & John, S. (2019). Management of the Adult with Arterial Switch. *Methodist Debakey Cardiovasc J, 15*(2), 133-137. doi:10.14797/mdcj-15-2-133

Bressan, M., Yang, P. B., Louie, J. D., Navetta, A. M., Garriock, R. J., & Mikawa, T. (2014). Reciprocal myocardial-endocardial interactions pattern the delay in atrioventricular junction conduction. *Development, 141*(21), 4149-4157. doi:10.1242/dev.110007

Buja, L. M., & Butany, J. (2015). *Cardiovascular Pathology*: Academic Press.

Bulk, A., Bark, D., Johnson, B., Garrity, D., & Dasi, L. (2016). Mechanisms influencing retrograde flow in the atrioventricular canal during early embryonic cardiogenesis. *Journal of Biomechanics.*

Burridge, K. (2017). Focal adhesions: a personal perspective on a half century of progress. *FEBS J, 284*(20), 3355-3361. doi:10.1111/febs.14195

Bustelo, X. R., Sauzeau, V., & Berenjeno, I. M. (2007). GTP-binding proteins of the Rho/Rac family: regulation, effectors and functions in vivo. *Bioessays, 29*(4), 356-370. doi:10.1002/bies.20558

Camenisch, T. D., Biesterfeldt, J., Brehm-Gibson, T., Bradley, J., & McDonald, J. A. (2001). Regulation of cardiac cushion development by hyaluronan. *Exp Clin Cardiol, 6*(1), 4-10.

Chang, C. P., Neilson, J. R., Bayle, J. H., Gestwicki, J. E., Kuo, A., Stankunas, K., . . . Crabtree, G. R. (2004). A field of myocardial-endocardial NFAT signaling underlies heart valve morphogenesis. *Cell, 118*(5), 649-663. doi:10.1016/j.cell.2004.08.010

Chen, J. N., van Eeden, F. J., Warren, K. S., Chin, A., Nusslein-Volhard, C., Haffter, P., & Fishman, M. C. (1997). Left-right pattern of cardiac BMP4 may drive asymmetry of the heart in zebrafish. *Development*, 4373-4382.

Chi, N. C., Shaw, R. M., De Val, S., Kang, G., Jan, L. Y., Black, B. L., & Stainier, D. Y. (2008). Foxn4 directly regulates tbx2b expression and atrioventricular canal formation. *Genes Dev, 22*(6), 734-739. doi:10.1101/gad.1629408

Chi, N. C., Shaw, R. M., Jungblut, B., Huisken, J., Ferrer, T., Arnaout, R., . . . Stainier, D. Y. (2008). Genetic and physiologic dissection of the vertebrate cardiac conduction system. *PLoS Biol, 6*(5), e109. doi:10.1371/journal.pbio.0060109

Choi, B. S., Kwon, B. S., Kim, G. B., Bae, E. J., Noh, C. I., Choi, J. Y., . . . Kim, Y. J. (2010). Long-term outcomes after an arterial switch operation for simple complete transposition of the great arteries. *Korean Circ J, 40*(1), 23-30. doi:10.4070/kcj.2010.40.1.23

Clark, E. B., Hu, N., Frommelt, P. K. V., G. K., Dummett, J. L., & Tomanek, R. J. (1989). Effect of increased pressure on ventricular growth in stage 21 chick embryos. *American Journal of Physiology - Heart and Circulatory Physiology, 257*(1).

Combs, M. D., & Yutzey, K. E. (2009). Heart valve development: regulatory networks in development and disease. *Circ Res, 105*(5), 408-421. doi:10.1161/CIRCRESAHA.109.201566

Congenital Heart Defects. (2017, October 26). *Centers for Disease Control and Prevention*. Retrieved from https://www.cdc.gov/ncbddd/heartdefects/data.html

Cui, X., Zhang, X., Bu, H., Liu, N., Li, H., Guan, X., . . . Cheng, M. (2017). Shear stress-mediated changes in the expression of complement regulatory protein CD59 on human endothelial progenitor cells by ECM-integrinα. *Biochem Biophys Res Commun, 494*(1-2), 416-421. doi:10.1016/j.bbrc.2017.09.019

Cui, Y., Zheng, Y., Liu, X., Yan, L., Fan, X., Yong, J., . . . Tang, F. (2019). Single-Cell Transcriptome Analysis Maps the Developmental Track of the Human Heart. *Cell Rep, 26*(7), 1934-1950.e1935. doi:10.1016/j.celrep.2019.01.079

Cześniewicz, P. J., & Kusa, J. (2017). Approaching the 50. *Kardiochir Torakochirurgia Pol, 14*(3), 186-191. doi:10.5114/kitp.2017.70533

d'Udekem, Y., Xu, M. Y., Galati, J. C., Lu, S., Iyengar, A. J., Konstantinov, I. E., . . . Brizard, C. P. (2012). Predictors of survival after single-ventricle palliation: the impact of right ventricular dominance. *J Am Coll Cardiol, 59*(13), 1178-1185. doi:10.1016/j.jacc.2011.11.049

Davey, B., Szwast, A., & Rychik, J. (2012). Diagnosis and management of heart failure in the fetus. *Minerva Pediatr, 64*(5), 471-492.

Davila, C. D., & Forfia, P. R. (2015). Management of Severe Pulmonary Hypertension in Patients Undergoing Mitral Valve Surgery. *Current Treatment Options in Cardiovascular Medicine, 17*(6).

Daza, D. O., Lewicka, M., & Larhammar, D. (2012). The Oxytocin/vasopressin Receptor Family Has at Least Five Members in the Gnathostome Lineage, Inclucing Two Distinct V2 Subtypes. *General and Comparative Endocrinology*, 135-143.

Dekker, R. J., Boon, R. A., Rondaij, M. G., Kragt, A., Volger, O. L., Elderkamp, Y. W., . . . Horrevoets, A. J. (2006). KLF2 provokes a gene expression pattern that establishes functional quiescent differentiation of the endothelium. *Blood, 107*(11), 4354-4363. doi:10.1182/blood-2005-08-3465

Dietrich, A. C., Lombardo, V. A., Veerkamp, J., Priller, F., & Abdelilah-Seyfried, S. (2014). Blood flow and Bmp signaling control endocardial chamber morphogenesis. *Dev Cell, 30*(4), 367-377. doi:10.1016/j.devcel.2014.06.020

Dirkx, E., da Costa Martins, P. A., & De Windt, L. J. (2013). Regulation of fetal gene expression in heart failure. *Biochim Biophys Acta, 1832*(12), 2414-2424. doi:10.1016/j.bbadis.2013.07.023

Donat, S., Lourenço, M., Paolini, A., Otten, C., Renz, M., & Abdelilah-Seyfried, S. (2018). Heg1 and Ccm1/2 proteins control endocardial mechanosensitivity during zebrafish valvulogenesis. *Elife, 7*. doi:10.7554/eLife.28939

Endo, H., Shiraishi, H., & Yanagisawa, M. (1994). Afterload reduction by hydralazine in children with a ventricular septal defect as determined by aortic input impedance. *Cardiovascular Drugs and Therapy, 8*(1), 161-166.

Ercan, M., & Koksal, C. (2003). The relationship between shear rate and vessel diameter. *Anesth Analg, 96*(1), 307; author reply 307-308. doi:10.1097/00000539-200301000-00073

Fahed, A. C., Gelb, B. D., Seidman, J. G., & Seidman, C. E. (2014). Genetics of Congenital Heart Disease: The Glass Half Empty. *Circ Res, 112*(4).

Fish, J. E., Wythe, J. D., Xiao, T., Bruneau, B. G., Stainier, D. Y., Srivastava, D., & Woo, S. (2011). A Slit/miR-218/Robo regulatory loop is required during heart tube formation in zebrafish. *Development, 138*(7), 1409-1419. doi:10.1242/dev.060046

Flanagan, T. C., & Pandit, A. (2003). Living artificial heart valve alternatives: a review. *Eur Cell Mater, 6*, 28-45; discussion 45. doi:10.22203/ecm.v006a04

Forouhar, A. S., Liebling, M., Hickerson, A., Nasiraei-Moghaddam, A., Tsai, H. J., Hove, J. R., . . . Gharib, M. (2006). The embryonic vertebrate heart tube is a dynamic suction pump. *Science, 312*(5774), 751-753. doi:10.1126/science.1123775

Frank, D., & Frey, N. (2011). Cardiac Z-disc signaling network. *J Biol Chem, 286*(12), 9897-9904. doi:10.1074/jbc.R110.174268

Freud, L. R., McElhinney, D. B., Marshall, A. C., Marx, G. R., Friedman, K. G., del Nido, P. J., . . . Tworetzky, W. (2014). Fetal aortic valvuloplasty for evolving hypoplastic left heart syndrome: postnatal outcomes of the first 100 patients. *Circulation, 130*(8), 638-645. doi:10.1161/CIRCULATIONAHA.114.009032

Frisk, M., Ruud, M., Espe, E. K., Aronsen, J. M., Røe, Å., Zhang, L., . . . Louch, W. E. (2016). Elevated ventricular wall stress disrupts cardiomyocyte t-tubule structure and calcium homeostasis. *Cardiovasc Res, 112*(1), 443-451. doi:10.1093/cvr/cvw111

Fulmer, D., Toomer, K., Guo, L., Moore, K., Glover, J., Moore, R., . . . Lipschutz, J. H. (2019). Defects in the Exocyst-Cilia Machinery Cause Bicuspid Aortic Valve Disease and Aortic Stenosis. *Circulation, 140*(16), 1331-1341. doi:10.1161/CIRCULATIONAHA.119.038376

Gallina, D., & Lincoln, J. (2019). Dynamic Expression Profiles of Sox9 in Embryonic, Post Natal, and Adult Heart Valve Cell Populations. *Anat Rec (Hoboken), 302*(1), 108-116. doi:10.1002/ar.23913

Galvin, K. M., Donovan, M. J., Lynch, C. A., Meyer, R. I., Paul, R. J., Lorenz, J. N., . . . Huszar, D. (2000). A role for smad6 in development and homeostasis of the cardiovascular system. *Nat Genet, 24*(2), 171-174. doi:10.1038/72835

George, E. L., Baldwin, H. S., & Hynes, R. O. (1997). Fibronectins are essential for heart and blood vessel morphogenesis but are dispensable for initial specification of precursor cells. *Blood, 90*(8), 3073-3081.

Ghodke, B., Kalkekar, S., & Radke, M. (2014). Long-term survival in tricuspid atresia after palliative surgery. In (Vol. 1, pp. 101-104). MGM J Med Sci.

Gilboa, S. M., Salemi, J. L., Nembhard, W. N., Fixler, D. E., & Correa, A. (2010). Mortality resulting from congenital heart disease among children and adults in the United States, 1999 to 2006. *Circulation, 122*(22), 2254-2263. doi:10.1161/CIRCULATIONAHA.110.947002

Goddard, L. M., Duchemin, A. L., Ramalingan, H., Wu, B., Chen, M., Bamezai, S., . . . Kahn, M. L. (2017). Hemodynamic Forces Sculpt Developing Heart Valves through a KLF2-WNT9B Paracrine Signaling Axis. *Dev Cell, 43*(3), 274-289.e275. doi:10.1016/j.devcel.2017.09.023

Gould, R. A., Yalcin, H. C., MacKay, J. L., Sauls, K., Norris, R., Kumar, S., & Butcher, J. T. (2016). Cyclic Mechanical Loading Is Essential for Rac1-Mediated Elongation and Remodeling of the Embryonic Mitral Valve. *Curr Biol, 26*(1), 27-37. doi:10.1016/j.cub.2015.11.033

Greutmann, M., Tobler, D., Kovacs, A. H., Greutmann-Yantiri, M., Haile, S. R., Held, L., . . . Colman, J. M. (2015). Increasing mortality burden among adults with complex congenital heart disease. *Congenit Heart Dis, 10*(2), 117-127. doi:10.1111/chd.12201

Groenendijk, B. C., Van der Heiden, K., Hierck, B. P., & Poelmann, R. E. (2007). The role of shear stress on ET-1, KLF2, and NOS-3 expression in the developing cardiovascular system of chicken embryos in a venous ligation model. *Physiology (Bethesda), 22*, 380-389. doi:10.1152/physiol.00023.2007

Gu, X., & Masters, K. S. (2011). Role of the Rho pathway in regulating valvular interstitial cell phenotype and nodule formation. *Am J Physiol Heart Circ Physiol, 300*(2), H448-458. doi:10.1152/ajpheart.01178.2009

Guilluy, C., Swaminathan, V., Garcia-Mata, R., O'Brien, E. T., Superfine, R., & Burridge, K. (2011). The Rho GEFs LARG and GEF-H1 regulate the mechanical response to force on integrins. *Nat Cell Biol, 13*(6), 722-727. doi:10.1038/ncb2254

Gunawan, F., Gentile, A., Gauvrit, S., Stainier, D., & Bensimon-Brito, A. (2020). Nfatc1 Promotes Interstitial Cell Formation During Cardiac Valve Development in Zebrafish. *Circ Res*. doi:10.1161/CIRCRESAHA.119.315992

Gutgesell, H. P., Garson, A., & McNamara, D. G. (1979). Prognosis for the newborn with transposition of the great arteries. *Am J Cardiol, 44*(1), 96-100. doi:10.1016/0002-9149(79)90256-x

Haack, T., & Abdelilah-Seyfried, S. (2016). The force within: endocardial development, mechanotransduction and signalling during cardiac morphogenesis. *Development, 143*, 373-386.

Heckel, E., Boselli, F., Roth, S., Krudewig, A., Belting, H.-G., Charvin, G., & Vermot, J. (2015). Oscillatory Flow Modulates Mechanosensitive klf2a Expression through trpv4 and trpp2 during Heart Valve Development. *Current Biology, 25*(10), 1354-1361.

Heineke, J., Ruetten, H., Willenbockel, C., Gross, S. C., Naguib, M., Schaefer, A., . . . Wollert, K. C. (2005). Attenuation of cardiac remodeling after myocardial infarction by muscle LIM protein-calcineurin signaling at the sarcomeric Z-disc. *Proc Natl Acad Sci U S A, 102*(5), 1655-1660. doi:10.1073/pnas.0405488102

Hinton, R. B., & Ware, S. M. (2017). Heart Failure in Pediatric Patients With Congenital Heart Disease. *Circ Res, 120*(6), 978-994. doi:10.1161/CIRCRESAHA.116.308996

Hirt, M. N., Sörensen, N. A., Bartholdt, L. M., Boeddinghaus, J., Schaaf, S., Eder, A., & … Eschenhagen, T. (2012). Increased afterload induces pathological cardiac hypertrophy: a new in vitro model. *Basic Research in Cardiology, 107*(6), 307.

Hofferberth, S. C., Nathan, M., Marx, G. R., Lu, M., Sleeper, L. A., Marshall, A. C., . . . Emani, S. M. (2018). Valve-sparing repair with intraoperative balloon dilation in tetralogy of Fallot: Midterm results and therapeutic implications. *J Thorac Cardiovasc Surg, 155*(3), 1163-1173.e1164. doi:10.1016/j.jtcvs.2017.08.147

Hoffman, J., & Kaplan, S. (2002). The Incidence of congential heart disease. *Jounral of the American College of Cardiology, 39*, 1890-1900.

Holmes, C. L., Landry, D. W., & Granton, J. T. (2004). Science Review: Vasopressin and the cardiovascular system part 2 – clinical physiology. *Critical Care, 8*(1), 15-23.

Holtzman, N. G., Schoenebeck, J. J., Tsai, H. J., & Yelon, D. (2007). Endocardium is necessary for cardiomyocyte movement during heart tube assembly. *Development, 134*(12), 2379-2386. doi:10.1242/dev.02857

Hove, J. R., Köster, R. W., Forouhar, A. S., Acevedo-Bolton, G., Fraser, S. E., & Gharib, M. (2003). Intracardiac fluid forces are an essential epigenetic factor for embryonic cardiogenesis. *Nature, 421*(6919), 172-177. doi:10.1038/nature01282

Huang, C. J., Tu, C. T., Hsiao, C. D., Hsieh, F. J., & Tsai, H. J. (2003). Germ-line transmission of a myocardium-specific GFP transgene reveals critical regulatory elements in the cardiac myosin light chain 2 promoter of zebrafish. *Dev Dyn, 228*(1), 30-40. doi:10.1002/dvdy.10356

Hulin, A., Hortells, L., Gomez-Stallons, M. V., O'Donnell, A., Chetal, K., Adam, M., . . . Yutzey, K. E. (2019). Maturation of heart valve cell populations during postnatal remodeling. *Development, 146*(12). doi:10.1242/dev.173047

Hurlstone, A. F., Haramis, A. P., Wienholds, E., Begthel, H., Korving, J., Van Eeden, F., . . . Clevers, H. (2003). The Wnt/beta-catenin pathway regulates cardiac valve formation. *Nature, 425*(6958), 633-637. doi:10.1038/nature02028

Israeli-Rosenberg, S., Manso, A. M., Okada, H., & Ross, R. S. (2014). Integrins and integrin-associated proteins in the cardiac myocyte. *Circ Res, 114*(3), 572-586. doi:10.1161/CIRCRESAHA.114.301275

Iwasaki, & Kenichi. (2013). Expression of Arginine Vasotocin Receptors in the Developing Zebrafish CNS. *Gene expression patterns : GEP, 13*(8).

Jain, R., Engleka, K. A., Rentschler, S. L., Manderfield, L. J., Li, L., Yuan, L., & Epstein, J. A. (2011). Cardiac neural crest orchestrates remodeling and functional maturation of mouse semilunar valves. *J Clin Invest, 121*(1), 422-430. doi:10.1172/JCI44244

Jarrell, D. K., Lennon, M. L., & Jacot, J. G. (2019). Epigenetics and Mechanobiology in Heart Development and Congenital Heart Disease. *Diseases, 7*(3). doi:10.3390/diseases7030052

Jeong, D., Kim, J. M., Cha, H., Oh, J. G., Park, J., Yun, S. H., . . . Park, W. J. (2008). PICOT attenuates cardiac hypertrophy by disrupting calcineurin-NFAT signaling. *Circ Res, 102*(6), 711-719. doi:10.1161/CIRCRESAHA.107.165985

Johnson, B., Garrity, D., & Dasi, P. (2013). The transitional cardiac pumping mechanics in the embryonic heart. *Cardiovascular Engineering and Technology, 4*(3), 246-255.

Jost, Attenhofer, C. H., Connolly, , H. M., Dearani, A., J., . . . K., G. (2007). Ebstein's Anomaly. In (Vol. 115, pp. 277-285). Circulation Research.

Keyte, A., & Hutson, M. R. (2012). The neural crest in cardiac congenital anomalies. *Differentiation, 84*(1), 25-40. doi:10.1016/j.diff.2012.04.005

Kim, T. H., Yang, H. K., Jang, H. J., Yoo, S. J., Khalili, K., & Kim, T. K. (2018). Abdominal imaging findings in adult patients with Fontan circulation. *Insights Imaging, 9*(3), 357-367. doi:10.1007/s13244-018-0609-2

Koenig, S. N., Bosse, K., Majumdar, U., Bonachea, E. M., Radtke, F., & Garg, V. (2016). Endothelial Notch1 Is Required for Proper Development of the Semilunar Valves and Cardiac Outflow Tract. *J Am Heart Assoc, 5*(4). doi:10.1161/JAHA.115.003075

Krüger, M., & Kötter, S. (2016). Titin, a Central Mediator for Hypertrophic Signaling, Exercise-Induced Mechanosignaling and Skeletal Muscle Remodeling. *Front Physiol, 7*, 76. doi:10.3389/fphys.2016.00076

Kumar, S., Kim, C. W., Simmons, R. D., & Jo, H. (2014). Role of flow-sensitive microRNAs in endothelial dysfunction and atherosclerosis: mechanosensitive athero-miRs. *Arterioscler Thromb Vasc Biol, 34*(10), 2206-2216. doi:10.1161/ATVBAHA.114.303425

Kumar, S., Williams, D., Sur, S., Wang, J. Y., & Jo, H. (2019). Role of flow-sensitive microRNAs and long noncoding RNAs in vascular dysfunction and atherosclerosis. *Vascul Pharmacol, 114*, 76-92. doi:10.1016/j.vph.2018.10.001

Kuo, C. F., Lin, Y. S., Chang, S. H., Chou, I. J., Luo, S. F., See, L. C., . . . Chu, P. H. (2017). Familial Aggregation and Heritability of Congenital Heart Defects. *Circ J, 82*(1), 232-238. doi:10.1253/circj.CJ-17-0250

LaCombe, P., & Lappin, S. (2019). *Physiology, Afterload Reduction*. In. Retrieved from https://www.ncbi.nlm.nih.gov/books/NBK493174

Lessey, E. C., Guilluy, C., & Burridge, K. (2012). From mechanical force to RhoA activation. *Biochemistry, 51*(38), 7420-7432. doi:10.1021/bi300758e

Levy, D., Larson, M. G., Vasan, R. S., Kannel, W. B., & Ho, K. K. (1996). The progression from hypertension to congestive heart failure. *JAMA, 275*(20), 1557-1562.

Liang, R., & Liu, Y. (2018). Tcf7l1 directly regulates cardiomyocyte differentiation in embryonic stem cells. *Stem Cell Res Ther, 9*(1), 267. doi:10.1186/s13287-018-1015-x

Liew, W. C., & Orbán, L. (2014). Zebrafish sex: a complicated affair. *Brief Funct Genomics, 13*(2), 172-187. doi:10.1093/bfgp/elt041

Lin, Y. F., Swinburne, I., & Yelon, D. (2012). Multiple influences of blood flow on cardiomyocyte hypertrophy in the embryonic zebrafish heart. *Dev Biol, 362*(2), 242-253. doi:10.1016/j.ydbio.2011.12.005

Lincoln, J., Alfieri, C. M., & Yutzey, K. E. (2004). Development of heart valve leaflets and supporting apparatus in chicken and mouse embryos. *Dev Dyn, 230*(2), 239-250. doi:10.1002/dvdy.20051

Lincoln, J., & Garg, V. (2014). Etiology of valvular heart disease-genetic and developmental origins. *Circ J, 78*(8), 1801-1807. doi:10.1253/circj.cj-14-0510

Lincoln, J., Kist, R., Scherer, G., & Yutzey, K. E. (2007). Sox9 is required for precursor cell expansion and extracellular matrix organization during mouse heart valve development. *Dev Biol, 305*(1), 120-132. doi:10.1016/j.ydbio.2007.02.002

Lindsey, S. E., Butcher, J. T., & Yalcin, H. C. (2014). Mechanical regulation of cardiac development. *Front Physiol, 5*, 318. doi:10.3389/fphys.2014.00318

Ma, L., Lu, M. F., Schwartz, R. J., & Martin, J. F. (2005). Bmp2 is essential for cardiac cushion epithelial-mesenchymal transition and myocardial patterning. *Development, 132*(24), 5601-5611. doi:10.1242/dev.02156

Ma, P., Gu, S., Karunamuni, G. H., Jenkins, M. W., Watanabe, M., & Rollins, A. M. (2016). Cardiac neural crest ablation results in early endocardial cushion and hemodynamic flow abnormalities. *Am J Physiol Heart Circ Physiol, 311*(5), H1150-H1159. doi:10.1152/ajpheart.00188.2016

Maarman, G. e. a. (2013). A Comprehensive Review: The Evolution of Animal Models in Pulmonary Hypertension Research; 3.4, Are We There Yet? *Pulmonary Circulation, 3*(4), 739–756.

Machackova, J., Barta, J., & Dhalla, N. S. (2006). Myofibrillar remodeling in cardiac hypertrophy, heart failure and cardiomyopathies. *Can J Cardiol, 22*(11), 953-968. doi:10.1016/s0828-282x(06)70315-4

Manderfield, L. J., Aghajanian, H., Engleka, K. A., Lim, L. Y., Liu, F., Jain, R., . . . Epstein, J. A. (2015). Hippo signaling is required for Notch-dependent smooth muscle differentiation of neural crest. *Development, 142*(17), 2962-2971. doi:10.1242/dev.125807

Marshall, W. F., & Nonaka, S. (2006). Cilia: tuning in to the cell's antenna. *Curr Biol, 16*(15), R604-614. doi:10.1016/j.cub.2006.07.012

Mason, C. A., Kirby, R. S., Sever, L. E., & Langlois, P. H. (2005). Prevalence is the preferred measure of frequency of birth defects. *Birth Defects Res A Clin Mol Teratol, 73*(10), 690-692. doi:10.1002/bdra.20211

McCain, M. L., & Parker, K. K. (2011). Mechanotransduction: the role of mechanical stress, myocyte shape, and cytoskeletal architecture on cardiac function. *Eur J Physiol, 462*, 89–104.

McCurley, A. T., & Callard, G. V. (2008). Characterization of housekeeping genes in zebrafish: male-female differences and effects of tissue type, developmental stage and chemical treatment. *BMC Mol Biol, 9*, 102. doi:10.1186/1471-2199-9-102

Menon, V., Eberth, J. F., Goodwin, R. L., & Potts, J. D. (2015). Altered Hemodynamics in the Embryonic Heart Affects Outflow Valve Development. *J Cardiovasc Dev Dis, 2*(2), 108-124. doi:10.3390/jcdd2020108

Merrill, B. J., Pasolli, H. A., Polak, L., Rendl, M., García-García, M. J., Anderson, K. V., & Fuchs, E. (2004). Tcf3: a transcriptional regulator of axis induction in the early embryo. *Development, 131*(2), 263-274. doi:10.1242/dev.00935

Midgett, M., López, C. S., David, L., Maloyan, A., & Rugonyi, S. (2017). Increased Hemodynamic Load in Early Embryonic Stages Alters Endocardial to Mesenchymal Transition. *Front Physiol, 8*, 56. doi:10.3389/fphys.2017.00056

Midgett, M., & Rugonyi, S. (2014). Congenital heart malformations induced by hemodynamic altering surgical interventions. *Frontiers in Physiology, 5*(287).

Mjaatvedt, C. H., Yamamura, H., Capehart, A. A., Turner, D., & Markwald, R. R. (1998). The Cspg2 gene, disrupted in the hdf mutant, is required for right cardiac chamber and endocardial cushion formation. *Dev Biol, 202*(1), 56-66. doi:10.1006/dbio.1998.9001

Mongkoldhumrongkul, N., Latif, N., Yacoub, M. H., & Chester, A. H. (2016). Effect of Side-Specific Valvular Shear Stress on the Content of Extracellular Matrix in Aortic Valves. *Cardiovascular Engineering and Technology*, 1-7.

Nonaka, S., Tanaka, Y., Okada, Y., Takeda, S., Harada, A., Kanai, Y., . . . Hirokawa, N. (1998). Randomization of left-right asymmetry due to loss of nodal cilia generating leftward flow of extraembryonic fluid in mice lacking KIF3B motor protein. *Cell, 95*(6), 829-837. doi:10.1016/s0092-8674(00)81705-5

O'Leary, P. (2002). Prevalence, clinical presentation and natural history of patients with single ventricle. In (Vol. 16, pp. 31-38). Progress in Pediatric Cardiology.

Oates, A. C., Pratt, S. J., Vail, B., Yan Yl, Ho, R. K., Johnson, S. L., . . . Zon, L. I. (2001). The zebrafish klf gene family. *Blood, 98*(6), 1792-1801. doi:10.1182/blood.v98.6.1792

Odelin, G., Faure, E., Coulpier, F., Di Bonito, M., Bajolle, F., Studer, M., . . . Zaffran, S. (2018). Krox20 defines a subpopulation of cardiac neural crest cells contributing to arterial valves and bicuspid aortic valve. *Development, 145*(1). doi:10.1242/dev.151944

Oomen, P. J. A., Holland, M. A., Bouten, C. V. C., Kuhl, E., & Loerakker, S. (2018). Growth and remodeling play opposing roles during postnatal human heart valve development. *Sci Rep, 8*(1), 1235. doi:10.1038/s41598-018-19777-1

Pagnozzi, L. A., & Butcher, J. T. (2017). Mechanotransduction Mechanisms in Mitral Valve Physiology and Disease Pathogenesis. *Front Cardiovasc Med, 4*, 83. doi:10.3389/fcvm.2017.00083

Pala, R., Jamal, M., Alshammari, Q., & Nauli, S. M. (2018). The Roles of Primary Cilia in Cardiovascular Diseases. *Cells, 7*(12). doi:10.3390/cells7120233

Palencia-Desai, S., Rost, M. S., Schumacher, J. A., Ton, Q. V., Craig, M. P., Baltrunaite, K., . . . Sumanas, S. (2015). Myocardium and BMP signaling are required for endocardial differentiation. *Development, 142*(13), 2304-2315. doi:10.1242/dev.118687

Pang, K. L., Parnall, M., & Loughna, S. (2017). Effect of altered haemodynamics on the developing mitral valve in chick embryonic heart. *Journal of Molecular and Cellular Cardiology, 108*, 114-126.

Pant, A. D., Thomas, V. S., Black, A. L., Verba, T., Lesicko, J. G., & Amini, R. (2018). Pressure-induced microstructural changes in porcine tricuspid valve leaflets. *Acta Biomater, 67*, 248-258. doi:10.1016/j.actbio.2017.11.040

Pappano, A. J., & Wier, W. G. (2013). 10 – Control of Cardiac Output: Coupling of Heart and Blood Vessels. In *Cardiovascular Physiology (Tenth Edition)* (pp. 195-222). Philadelphia: Elsevier.

Parra, V., & Rothermel, B. A. (2017). Calcineurin signaling in the heart: The importance of time and place. *J Mol Cell Cardiol, 103*, 121-136. doi:10.1016/j.yjmcc.2016.12.006

Parri, M., & Chiarugi, P. (2010). Rac and Rho GTPases in cancer cell motility control. *Cell Commun Signal, 8*, 23. doi:10.1186/1478-811X-8-23

Parrie, L. E., Renfrew, E. M., Wal, A. V., Mueller, R. L., & Garrity, D. M. (2013). Zebrafish tbx5 paralogs demonstrate independent essential requirements in cardiac and pectoral fin development. *Dev Dyn, 242*(5), 485-502. doi:10.1002/dvdy.23953

Patra, C., Diehl, F., Ferrazzi, F., van Amerongen, M. J., Novoyatleva, T., Schaefer, L., . . . Engel, F. B. (2011). Nephronectin regulates atrioventricular canal differentiation via Bmp4-Has2 signaling in zebrafish. *Development*.

Perkins, A. C., Sharpe, A. H., & Orkin, S. H. (1995). Lethal beta-thalassaemia in mice lacking the erythroid CACCC-transcription factor EKLF. *Nature, 375*(6529), 318-322. doi:10.1038/375318a0

Pertea, M., Kim, D., Pertea, G. M., Leek, J. T., & Salzberg, S. L. (2016). Transcript-level expression analysis of RNA-seq experiments with HISAT, StringTie and Ballgown. *Nat Protoc, 11*(9), 1650-1667. doi:10.1038/nprot.2016.095

Pesevski, Z., Kvasilova, A., Stopkova, T., Nanka, O., Drobna Krejci, E., Buffinton, C., . . . Sedmera, D. (2018). Endocardial Fibroelastosis is Secondary to Hemodynamic Alterations in the Chick Embryonic Model of Hypoplastic Left Heart Syndrome. *Dev Dyn, 247*(3), 509-520. doi:10.1002/dvdy.24521

Pestel, J., Ramadass, R., Gauvrit, S., Helker, C., Herzog, W., & Stainier, D. Y. R. (2016). Real-time 3D Visualization of Cellular Rearrangements during Cardiac Valve Formation. *Development, 143*(12), 2217-2227.

Pettersen, M. D. (2019). Pediatric Complete Atrioventricular Septal Defects.

Peyronnet, R., Nerbonne, J. M., & Kohl, P. (2016). Cardiac Mechano-Gated Ion Channels and Arrhythmias. *Circ Res, 118*(2), 311-329. doi:10.1161/CIRCRESAHA.115.305043

Pfaffl, M. W. (2001). A new mathematical model for relative quantification in real-time RT–PCR. *Nucleic Acids Research, 29*(9), e45.

Phillips, H. M., Mahendran, P., Singh, E., Anderson, R. H., Chaudhry, B., & Henderson, D. J. (2013). Neural crest cells are required for correct positioning of the developing outflow cushions and pattern the arterial valve leaflets. *Cardiovasc Res, 99*(3), 452-460. doi:10.1093/cvr/cvt132

Phoon, C. K. (2001). Circulatory physiology in the developing embryo. *Curr Opin Pediatr, 13*(5), 456-464. doi:10.1097/00008480-200110000-00013

Pillutla, P., Shetty, K. D., & Foster, E. (2009). Mortality associated with adult congenital heart disease: Trends in the US population from 1979 to 2005. *Am Heart J, 158*(5), 874-879. doi:10.1016/j.ahj.2009.08.014

Plein, A., Fantin, A., & Ruhrberg, C. (2015). Neural crest cells in cardiovascular development. *Curr Top Dev Biol, 111*, 183-200. doi:10.1016/bs.ctdb.2014.11.006

Pozzoli, A., Zuber, M., Reisman, M., Maisano, F., & Taramasso, M. (2018). Comparative Anatomy of Mitral and Tricuspid Valve: What Can the Interventionlist Learn From the Surgeon. *Front Cardiovasc Med, 5*, 80. doi:10.3389/fcvm.2018.00080

Preston, C. C., Storm, E. C., Burdine, R. D., Bradley, T. A., Uttecht, A. D., & Faustino, R. S. (2019). Nucleoporin insufficiency disrupts a pluripotent regulatory circuit in a pro-arrhythmogenic stem cell line. *Sci Rep, 9*(1), 12691. doi:10.1038/s41598-019-49147-4

Preston, C. C., Wyles, S. P., Reyes, S., Storm, E. C., Eckloff, B. W., & Faustino, R. S. (2018). NUP155 insufficiency recalibrates a pluripotent transcriptome with network remodeling of a cardiogenic signaling module. *BMC Syst Biol, 12*(1), 62. doi:10.1186/s12918-018-0590-x

Rahimi, K., Mohseni, H., Kiran, A., Tran, J., Nazarzadeh, M., Rahimian, F., . . . Otto, C. M. (2018). Elevated blood pressure and risk of aortic valve disease: a cohort analysis of 5.4 million UK adults. *Eur Heart J, 39*(39), 3596-3603. doi:10.1093/eurheartj/ehy486

Rahimi, K., Mohseni, H., Otto, C. M., Conrad, N., Tran, J., Nazarzadeh, M., . . . MacMahon, S. (2017). Elevated blood pressure and risk of mitral regurgitation: A longitudinal cohort study of 5.5 million United Kingdom adults. *PLoS Med, 14*(10), e1002404. doi:10.1371/journal.pmed.1002404

Rathan, S., Ankeny, C. J., Arjunon, S., Ferdous, Z., Kumar, S., Fernandez Esmerats, J., . . . Jo, H. (2016). Identification of side- and shear-dependent microRNAs regulating porcine aortic valve pathogenesis. *Sci Rep, 6*, 25397. doi:10.1038/srep25397

Rauch, G.-J., Granato, M., & Haffter, P. (1997). A polymorphic zebrafish line for genetic mapping using SSLPs on high-percentage agarose gels.

Remenyi, B., & Gentles, T. L. (2012). Congenital mitral valve lesions : Correlation between morphology and imaging. *Ann Pediatr Cardiol, 5*(1), 3-12. doi:10.4103/0974-2069.93703

Rueden, C. T., Schindelin, J., Hiner, M. C., DeZonia, B. E., Walter, A. E., Arena, E. T., & Eliceiri, K. W. (2017). ImageJ2: ImageJ for the next generation of scientific image data. *BMC Bioinformatics, 18*(1), 529. doi:10.1186/s12859-017-1934-z

Sabatino, J., Wicik, Z., De Rosa, S., Eyileten, C., Jakubik, D., Spaccarotella, C., . . . Indolfi, C. (2019). MicroRNAs fingerprint of bicuspid aortic valve. *J Mol Cell Cardiol, 134*, 98-106. doi:10.1016/j.yjmcc.2019.07.001

Samsa, L. A., Fleming, N., Magness, S., Qian, L., & Liu, J. (2016). Isolation and Characterization of Single Cells from Zebrafish Embryos. *J Vis Exp*(109). doi:10.3791/53877

Samsa, L. A., Givens, C., Tzima, E., Stainier, D. Y., Qian, L., & Liu, J. (2015). Cardiac contraction activates endocardial Notch signaling to modulate chamber maturation in zebrafish. *Development, 142*(23), 4080-4091. doi:10.1242/dev.125724

Sathanoori, R., Rosi, F., Gu, B. J., Wiley, J. S., Müller, C. E., Olde, B., & Erlinge, D. (2015). Shear stress modulates endothelial KLF2 through activation of P2X4. *Purinergic Signal, 11*(1), 139-153. doi:10.1007/s11302-014-9442-3

Scherz, P. J., Huisken, J., Sahai-Hernandez, P., & and Stainier, D. Y. (2008). High-speed imaging of developing heart valves reveals interplay of morphogenesis and function. *Development, 135*(6), 1179-1187.

Schoen, F. J. (2008). Evolving concepts of cardiac valve dynamics: the continuum of development, functional structure, pathobiology, and tissue engineering. *Circulation, 118*(18), 1864-1880. doi:10.1161/CIRCULATIONAHA.108.805911

Sedmera, D., Pexieder, T., Rychterova, V., Hu, N., & Clark, E. B. (1999). Remodeling of chick embryonic ventricular myoarchitecture under experimentally changed loading conditions. *Anat Rec, 254*(2), 238-252. doi:10.1002/(SICI)1097-0185(19990201)254:2<238::AID-AR10>3.0.CO;2-V

Shentu, H., Wen, H. J., Her, G. M., Huang, C. J., Wu, J. L., & Hwang, S. P. (2003). Proximal upstream region of zebrafish bone morphogenetic protein 4 promoter directs heart expression of green fluorescent protein. *Genesis, 37*(3), 103-112. doi:10.1002/gene.10240

Simmons, M. A., & Brueckner, M. (2017). The genetics of congenital heart disease… understanding and improving long-term outcomes in congenital heart disease: a review for the general cardiologist and primary care physician. *Curr Opin Pediatr, 29*(5), 520-528. doi:10.1097/MOP.0000000000000538

Sittiwangkul, R., Azakie, A., Van Arsdell, G. S., Williams, W. G., & McCrindle, B. W. (2004). Outcomes of tricuspid atresia in the Fontan era. *Ann Thorac Surg, 77*(3), 889-894. doi:10.1016/j.athoracsur.2003.09.027

Siu, S. C., & Silversides, C. K. (2010). Bicuspid aortic valve disease. *J Am Coll Cardiol, 55*(25), 2789-2800. doi:10.1016/j.jacc.2009.12.068

Slough, J., Cooney, L., & Brueckner, M. (2008). Monocilia in the embryonic mouse heart imply a direct role for cilia in cardiac morphogenesis. *Developmental Dynamics, 237*(9), 2304-2314.

Sorrell, M. R., Dohn, T. E., D'Aniello, E., & Waxman, J. S. (2013). Tcf7l1 proteins cell autonomously restrict cardiomyocyte and promote endothelial specification in zebrafish. *Dev Biol, 380*(2), 199-210. doi:10.1016/j.ydbio.2013.05.016

Steed, E., Boselli, F., & Vermot, J. (2016). Hemodynamics driven cardiac valve morphogenesis. *Biochim Biophys Acta.*

Steed, E., Faggianelli, N., Roth, S., Ramspacher, C., Concordet, J.-P., & Vermot, J. (2016). Klf2a Couples Mechanotransduction and Zebrafish Valve Morphogenesis through Fibronectin Synthesis. *Nature Communications*.

Stellin, G., Padalino, M., Milanesi, O., Vida, V., Favaro, A., Rubino, M., . . . Casarotto, D. (2000). Repair of congenital mitral valve dysplasia in infants and children: is it always possible? *Eur J Cardiothorac Surg, 18*(1), 74-82. doi:10.1016/s1010-7940(00)00457-7

Sugi, Y., Kern, M. J., Markwald, R. R., & Burnside, J. L. (2012). Periostin Expression is Altered in Aortic Valves in Smad6 Mutant Mice. *J Neonatal Biol, 1*. doi:10.4172/2167-0897.1000101

Sugi, Y., Yamamura, H., Okagawa, H., & Markwald, R. R. (2004). Bone morphogenetic protein-2 can mediate myocardial regulation of atrioventricular cushion mesenchymal cell formation in mice. *Dev Biol, 269*(2), 505-518. doi:10.1016/j.ydbio.2004.01.045

Swapna, I., & Borodinsky, L. N. (2012). Interplay between electrical activity and bone morphogenetic protein signaling regulates spinal neuron differentiation. *Proc Natl Acad Sci U S A, 109*(40), 16336-16341. doi:10.1073/pnas.1202818109

Tan, H., Biechler, S., Junor, L., Yost, M. J., Dean, D., Li, J., . . . Goodwin, R. L. (2013). Fluid flow forces and rhoA regulate fibrous development of the atrioventricular valves. *Dev Biol, 374*(2), 345-356. doi:10.1016/j.ydbio.2012.11.023

Tarazi, R. C., & Levy, M. N. (1982). Cardiac responses to increased afterload. State-of-the-art review. *Hypertension, 4*(3 Pt 2), 8-18.

Ten Dijke, P., Egorova, A. D., Goumans, M. J., Poelmann, R. E., & Hierck, B. P. (2012). TGF-β signaling in endothelial-to-mesenchymal transition: the role of shear stress and primary cilia. *Sci Signal, 5*(212), pt2. doi:10.1126/scisignal.2002722

Thisse, C., & Thisse, B. (2008). High-resolution in situ hybridization to whole-mount zebrafish embryos. *Nat Protoc, 3*(1), 59-69. doi:10.1038/nprot.2007.514

Toshima, T., Watanabe, T., Narumi, T., Otaki, Y., Shishido, T., Aono, T., . . . Watanabe, M. (2019). Therapeutic inhibition of microRNA-34a ameliorates aortic valve calcification via modulation of Notch1-Runx2 signaling. *Cardiovasc Res*. doi:10.1093/cvr/cvz210

Totong, R., Schell, T., Lescroart, F., Ryckebüsch, L., Lin, Y. F., Zygmunt, T., . . . Yelon, D. (2011). The novel transmembrane protein Tmem2 is essential for coordination of myocardial and endocardial morphogenesis. *Development, 138*(19), 4199-4205. doi:10.1242/dev.064261

Trinh, L. A., & Stainier, D. Y. (2004). Fibronectin regulates epithelial organization during myocardial migration in zebrafish. *Dev Cell, 6*(3), 371-382. doi:10.1016/s1534-5807(04)00063-2

Tulloch, N., Muskheli, V., Razumova, M., Korte, F., Regnier, M., Hauch, K., . . . Reinecke, H. M., CE. (2011). Growth of engineered human myocardium with mechanical loading and vascular coculture. *Circulation Research*, 47-59.

Van der Bom, T., Zomer, A., Zwinderman, A., Meijboom, F., Bouma, B., & Mulder, B. (2011). The changing epidemiology of congenital heart disease. *Nat Rev Cardiol, 8*, 50-60.

van der Bom, T., Zomer, A. C., Zwinderman, A. H., Meijboom, F. J., Bouma, B. J., & Mulder, B. J. (2011). The changing epidemiology of congenital heart disease. *Nat Rev Cardiol, 8*(1), 50-60. doi:10.1038/nrcardio.2010.166

van Wijk, B., Moorman, A. F., & van den Hoff, M. J. (2007). Role of bone morphogenetic proteins in cardiac differentiation. *Cardiovasc Res, 74*(2), 244-255. doi:10.1016/j.cardiores.2006.11.022

Verburg, B. O., Jaddoe, V. W., Wladimiroff, J. W., Hofman, A., Witteman, J. C., & Steegers, E. A. (2008). Fetal hemodynamic adaptive changes related to intrauterine growth: the Generation R Study. *Circulation, 117*(5), 649-659. doi:10.1161/CIRCULATIONAHA.107.709717

Verhoeven, M. C., Haase, C., Christoffels, V. M., Weidinger, G., & Bakkers, J. (2011). Wnt signaling regulates atrioventricular canal formation upstream of BMP and Tbx2. *Birth Defects Res A Clin Mol Teratol, 91*(6), 435-440. doi:10.1002/bdra.20804

Vermot, J., Forouhar, A., Liebling, M., Wu, D., Plummer, D., & Gharib, M. (2009). Reversing Blood Flows Act through klf2a to Ensure Normal Valvulogenesis in the Developing Heart. *PLoS Biol, 7*(11).

Villafañe, J., Lantin-Hermoso, M. R., Bhatt, A. B., Tweddell, J. S., Geva, T., Nathan, M., . . . Council, A. C. o. C. s. A. C. a. P. C. (2014). D-transposition of the great arteries: the

current era of the arterial switch operation. *J Am Coll Cardiol, 64*(5), 498-511. doi:10.1016/j.jacc.2014.06.1150

Voet, A., Rega, F., de Bruaene, A. V., Troost, E., Gewillig, M., Van Damme, S., & Budts, W. (2012). Long-term outcome after treatment of isolated pulmonary valve stenosis. *Int J Cardiol, 156*(1), 11-15. doi:10.1016/j.ijcard.2010.10.038

Wagner, M., & Siddiqui, M. A. (2007). Signal transduction in early heart development (I): cardiogenic induction and heart tube formation. *Exp Biol Med (Maywood), 232*(7), 852-865.

Walker, G. A., Masters, K. S., Shah, D. N., Anseth, K. S., & Leinwand, L. A. (2004). Valvular myofibroblast activation by transforming growth factor-beta: implications for pathological extracellular matrix remodeling in heart valve disease. *Circ Res, 95*(3), 253-260. doi:10.1161/01.RES.0000136520.07995.aa

Walsh, E. C., & Stainier, D. Y. (2001). UDP-glucose dehydrogenase required for cardiac valve formation in zebrafish. *Science, 293*(5535), 1670-1673. doi:10.1126/science.293.5535.1670

Wang, Y., Wu, B., Chamberlain, A. A., Lui, W., Koirala, P., Susztak, K., . . . Zhou, B. (2013). Endocardial to myocardial notch-wnt-bmp axis regulates early heart valve development. *PLoS One, 8*(4), e60244. doi:10.1371/journal.pone.0060244

Warnes, C. A., Williams, R. G., Bashore, T. M., Child, J. S., Connolly, H. M., Dearani, J. A., . . . Webb, G. D. (2008). ACC/AHA 2008 guidelines for the management of adults with congenital heart disease: a report of the American College of Cardiology/American Heart Association Task Force on Practice Guidelines (Writing Committee to Develop Guidelines on the Management of Adults With Congenital Heart Disease). Developed in Collaboration With the American Society of Echocardiography, Heart Rhythm Society, International Society for Adult Congenital Heart Disease, Society for Cardiovascular Angiography and Interventions, and Society of Thoracic Surgeons. *J Am Coll Cardiol, 52*(23), e143-e263. doi:10.1016/j.jacc.2008.10.001

Warnock, J. N., Nanduri, B., Pregonero Gamez, C. A., Tang, J., Koback, D., Muir, W. M., & Burgess, S. C. (2011). Gene Profiling of Aortic Valve Interstitial Cells under Elevated Pressure Conditions: Modulation of Inflammatory Gene Networks. *Int J Inflam, 2011*, 176412. doi:10.4061/2011/176412

Woods, R. K., Pasquali, S. K., Jacobs, M. L., Austin, E. H., Jacobs, J. P., Krolikowski, M., . . . Tweddell, J. S. (2012). Aortic valve replacement in neonates and infants: an analysis of the Society of Thoracic Surgeons Congenital Heart Surgery Database. *J Thorac Cardiovasc Surg, 144*(5), 1084-1089. doi:10.1016/j.jtcvs.2012.07.060

Wu, W., Pang, K., Lin, Q., Zhang, A., Wang, W., Zhang, M., . . . Wang, H. (2015). Echocardiography in the diagnosis of patients with absent pulmonary valve syndrome: a review study of 12 years. *Int J Cardiovasc Imaging, 31*(7), 1353-1359. doi:10.1007/s10554-015-0693-z

Yalcin, H. C., Shekhar, A., McQuinn, T. C., & Butcher, J. T. (2011). Hemodynamic patterning of the avian atrioventricular valve. *Dev Dyn, 240*(1), 23-35. doi:10.1002/dvdy.22512

Yamamura, H., Zhang, M., Markwald, R. R., & Mjaatvedt, C. H. (1997). A heart segmental defect in the anterior-posterior axis of a transgenic mutant mouse. *Dev Biol, 186*(1), 58-72. doi:10.1006/dbio.1997.8559

Yang, J., Hartjes, K., Nelson, T., & Xu, X. (2014). Cessation of contraction induces cardiomyocyte remodeling during zebrafish cardiogenesis. *Am J Physiol Heart Circ Physiol, 306*(3), 382-395.

Yang, J., & Xu, X. (2012). Immunostaining of Dissected Zebrafish Embryonic Heart. *J. Vis. Exp.*

Yang, Q., Chen, H., Correa, A., Devine, O., Mathews, T. J., & Honein, M. A. (2006). Racial differences in infant mortality attributable to birth defects in the United States, 1989-2002. *Birth Defects Res A Clin Mol Teratol, 76*(10), 706-713. doi:10.1002/bdra.20308

Yong, M. S., Yim, D., Brizard, C. P., Robertson, T., Bullock, A., d'Udekem, Y., & Konstantinov, I. E. (2014). Long-term outcomes of patients with absent pulmonary valve syndrome: 38 years of experience. *Ann Thorac Surg, 97*(5), 1671-1677. doi:10.1016/j.athoracsur.2014.01.035

Yuasa, S., & Fukuda, K. (2008). Multiple roles for BMP signaling in cardiac development. *Drug Discovery Today: Therapeutic Strategies, 5*(4), 209-214.

Zhang, H., Liu, L., & Tian, J. (2019). Molecular mechanisms of congenital heart disease in down syndrome. *Genes Dis, 6*(4), 372-377. doi:10.1016/j.gendis.2019.06.007

Zhang, J., Chang, J. Y., Huang, Y., Lin, X., Luo, Y., Schwartz, R. J., . . . Wang, F. (2010). The FGF-BMP signaling axis regulates outflow tract valve primordium formation by promoting cushion neural crest cell differentiation. *Circ Res, 107*(10), 1209-1219. doi:10.1161/CIRCRESAHA.110.225318

Zhang, X., Chen, S., Yoo, S., Chakrabarti, S., Zhang, T., Ke, T., . . . Wang, Q. K. (2008). Mutation in nuclear pore component NUP155 leads to atrial fibrillation and early sudden cardiac death. *Cell, 135*(6), 1017-1027. doi:10.1016/j.cell.2008.10.022

Zhao, Z., & Rivkees, S. A. (2000). Programmed cell death in the developing heart: regulation by BMP4 and FGF2. *Dev Dyn, 217*(4), 388-400. doi:10.1002/(SICI)1097-0177(200004)217:4<388::AID-DVDY6>3.0.CO;2-N

Zheng, Y., Kong, Y., & Li, F. (2014). Krüppel-like transcription factor 11 (KLF11) overexpression inhibits cardiac hypertrophy and fibrosis in mice. *Biochem Biophys Res Commun, 443*(2), 683-688. doi:10.1016/j.bbrc.2013.12.024

APPENDIX 1: Supplemental Material for Chapter 2

Detailed Methods

Zebrafish Husbandry and Strains

Zebrafish were raised as per Colorado State University Animal Care and Use Protocols. Specifically, adult zebrafish are maintained in a fish facility with recirculating water, at an approximate temperature of 28°C. For all non-transgenic experiments, the WIK line was used.(Rauch, Granato, & Haffter, 1997) For transgenic experiments, Tg(Fli1:eGFP; gata1:dsRED), Tg(myl7:cypher-egfp), Tg(myl7:dsRed-nuc), and Tg(myl17:eGFP) lines were obtained from ZIRC. Embryos were kept in E3 medium supplemented with methylene blue at a density of no more than 60 embryos/20mL E3 in a petri dish.

At 24 hpf, embryos were screened and any embryos that showed gross morphological or developmental defects were discarded. Embryos were then dechorionated and randomly assigned into either the control or treatment groups. Simple randomization was used to assign embryos into either control or treatment groups. Details regarding sex of the embryos used are not provided because, at the stages of interest, the sex of zebrafish embryos has not yet been determined.(Liew & Orbán, 2014) Therefore, it is not possible to control for this variable this early on in development.

All zebrafish procedures were approved by the Institutional Animal Care and Use Committee at Colorado State University.

Quantitative Polymerase Chain Reaction

Hearts were dissected in L15-10% FBS. 10-20 hearts per treatment were pooled, and RNA was extracted using TRIzol (Invitrogen) according to the manufacturer's protocol. cDNA synthesis

was performed using AMV reverse transcriptase (Fisher Scientific) and Oligo(dT)$_{12–18}$ primer (Invitrogen). Resulting cDNA was treated with RNase H (New England Biolabs, Ipswich, MA). Standards curves were performed in triplicate for every gene. Reactions were run on Roche LC480 qPCR machine. Accompanying software (Roche LightCycler 480 software, version 1.2) was used to calculate Ct values. Pfaffl analysis was used to determine relative expression.(Pfaffl, 2001) In all experiments, the reference gene used was *Elongation Factor α (EF α)*, a well validated housekeeping gene.(McCurley & Callard, 2008)

Live Fluorescence Imaging

For vessel, samples were immobilized in agarose and treated with MESAB to temporarily stop heartbeats. Samples were visualized using an Olympus SZX12 Fluorescent stereo-dissecting microscope. Images were taken using a QI-imaging camera Quantification of vessel diameter was performed in Image J.(Rueden et al., 2017) Quantification of cardiac chamber volume and looping angle was performed as previously described.(J Yang et al., 2014),(Berndt et al., 2014)

Quantification of Cardiac Chamber Volume and Looping Angle

After being randomly assigned to either control or treatment groups, embryos were incubated until 56 hours post fertilization. Embryos were then treated with tricaine, and incubated until their hearts stopped. They were then mounted in low-melt agarose such that both chambers of their heart were in focus, ventral-side up. They were then imaged immediately under an Olympus SZX-12 stereomicroscope. Image analysis was performed in ImageJ.

To measure cardiac chamber volume, the both the length and width of the chamber were measured. Volume of the chamber volume was determined using the following formula: $V = \pi r^2 h$, where r was defined as the width of the ventricle and h was defined as the length. To measure looping angle, the angle between the line parallel to blood flow through the AVJ and bisecting the atrium was quantified in imageJ.(Johnson et al., 2013)

Quantification of Total Z-band Size

To visualize cell membranes, Tg(*myl7*:cypher-egfp) hearts underwent immunohistochemistry as described in the methods section. Z-stacks spanning the entire heart were taken on the Zeiss LSM 800 confocal microscope and processed in Image J Fiji. Briefly, 5 cells from the region of interest (either the outer curvature or AVJ) were selected and traced using the polygon tool to measure area. Each of these cells was then analyzed for total Z-band size. In each slice of the z-stack, the z-bands were traced and added to the ROI manager. The entire cell through 3-dimensions was scanned for z-bands, all z-bands were traced. The length of each z-band was measured and summed to determine total z-band size.

Quantification of the Contractile Wave

To quantify the contractile wave in each heart, videos were taken as described in the methods section. Image sequences were opened in Image J Fiji. First, total frames per cycle was determined by finding the number of frames between successive atrial inlet contractions. The point where the lumen was closest together was manually tracked at throughout the cardiac cycle, and distance between the two points was measured by manually tracing the path of contraction and noting the distance and frame number between each point. Frame number was converted to time, and speed of the contractile was quantified as distance over time. Velocity was plotted over normalized time, defined as ((current frame number – starting frame number)/ total frames per cycle)).

Quantification of Cardiomyocyte Cell Number

To quantify cardiomyocyte cell number, hearts from Tg(myl7:dsred-nuc) embryos were dissected as previously described.(Jingchun Yang & Xu, 2012) Hearts were then exposed to 4% PFA for 40 minutes, and washed 3 times with PBT. Hearts were mounted in 50% glycerol and

imaged on the LSM800. Images were made into maximum intensity projections using ImageJ and ventricular cells were manually counted.

In Situ Hybridization

In situ hybridization was carried out as previously described.(Thisse & Thisse, 2008) In brief, zebrafish embryos at the appropriate stage were fixed in 4% paraformaldehyde at 4°C overnight. Embryos were then placed in 100% methanol, and placed in -20°C for at least 2 hours. Embryos were then gradually rehydrated from methanol to phosphate buffered saline with 1% Tween-20. Embryos were then permeabilized with proteinase K for 20 minutes at room temperature. Embryos were then placed in 4% paraformaldehyde for 20 minutes at room temperature, and washed 5 times with phosphate buffered saline. Embryos were then incubated with DIG-labeled probe of interest in hybridization mixture (50% formamide, 5x saline sodium-citrate solution, 1% Tween-20) overnight at 60°C. Embryos were then washed with sodium citrate solution and PBT to remove all unbound probe. Embryos were then incubated with secondary antibody (Anti-Digoxigenin-AP Fab fragmants, Roche) at a concentration of 1:5000 overnight in 4°C. Embryos were then washed with PBT several times to remove unbound secondary antibody. Embryos were then placed in a staining solution consisting of 1% 4-Nitro blue tetrazolium chloride (Roche) and 0.7% 5-Bromo-4-chloro-3-indoyl-phosphate (Roche). Embryos were kept in the dark and monitored for signal development. After the controls developed adequate signal, reactions were stopped by placing embryos in 4% paraformaldehyde.

Detailed Statistical Analysis All data was analyzed in R (version 3.4.2), and graphs were made using the ggplot2 package. Data was first checked for normality using shapiro-wilk function built into base R. If the shapiro-wilk test returned a p-value greater than 0.05, then a two tailed t-test was used to analyze the data. If the shapiro-wilk test returned a value less than 0.05 and the number of replicates were less than 40, than the Kruskal-wallis test was used to determine

statistical significance. For multiple comparisons, Tukey''s test was used for parametric data and Dunnet's many-against-one test was used for nonparametric data.

Supplemental Figures

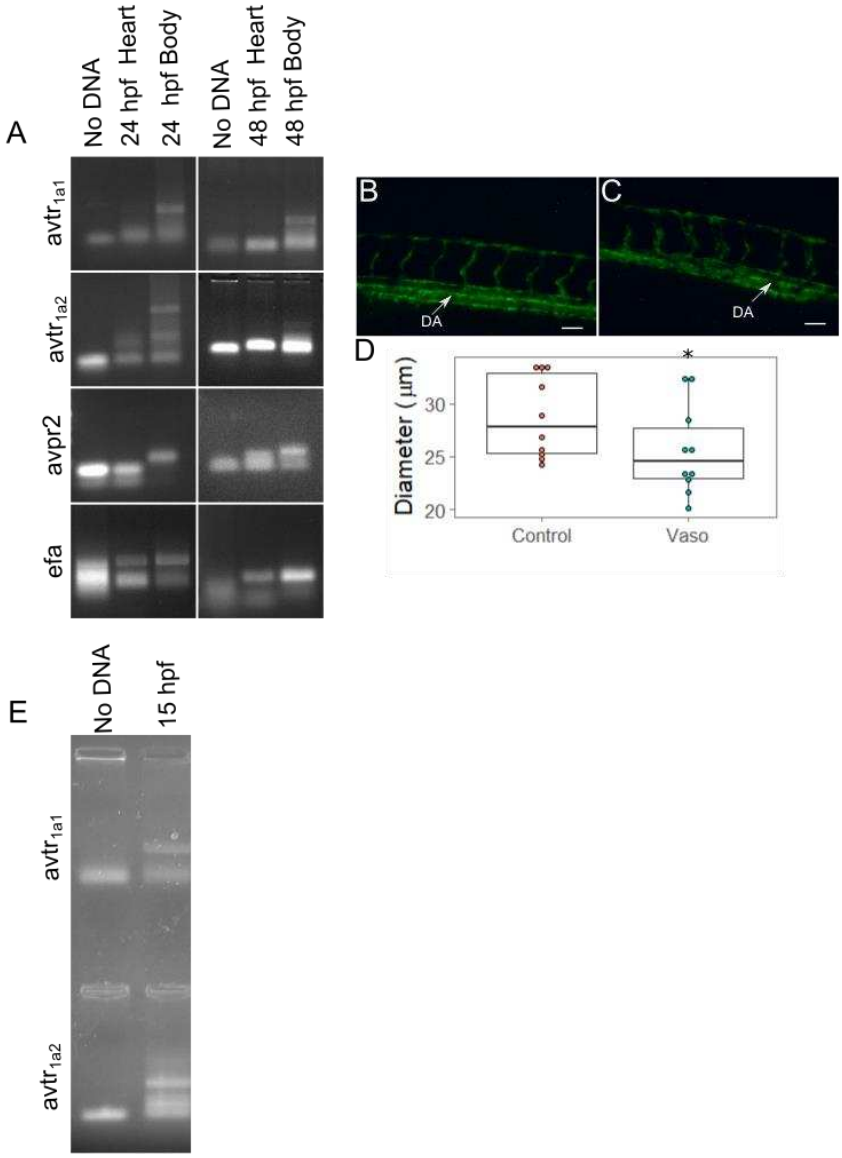

Supplemental Figure 1.1. Vasopressin application causes constriction in as little as 4 hours post application. A) Vasopressin receptors are not expressed in cardiac tissue either at 24 hpf, or at 48 hpf, in contrast to whole bodiesControl gene *efa* is robustly expressed in all DNA samples. B) Control vessels at 28 hpf. See figure 1 for expected band sizes. C) Vasopressin-treated vessels at 28 hpf. Vasopressin was applied at 24 hpf. D) Diameter of the dorsal aorta in vasopressin-treated embryos is significantly smaller than in control

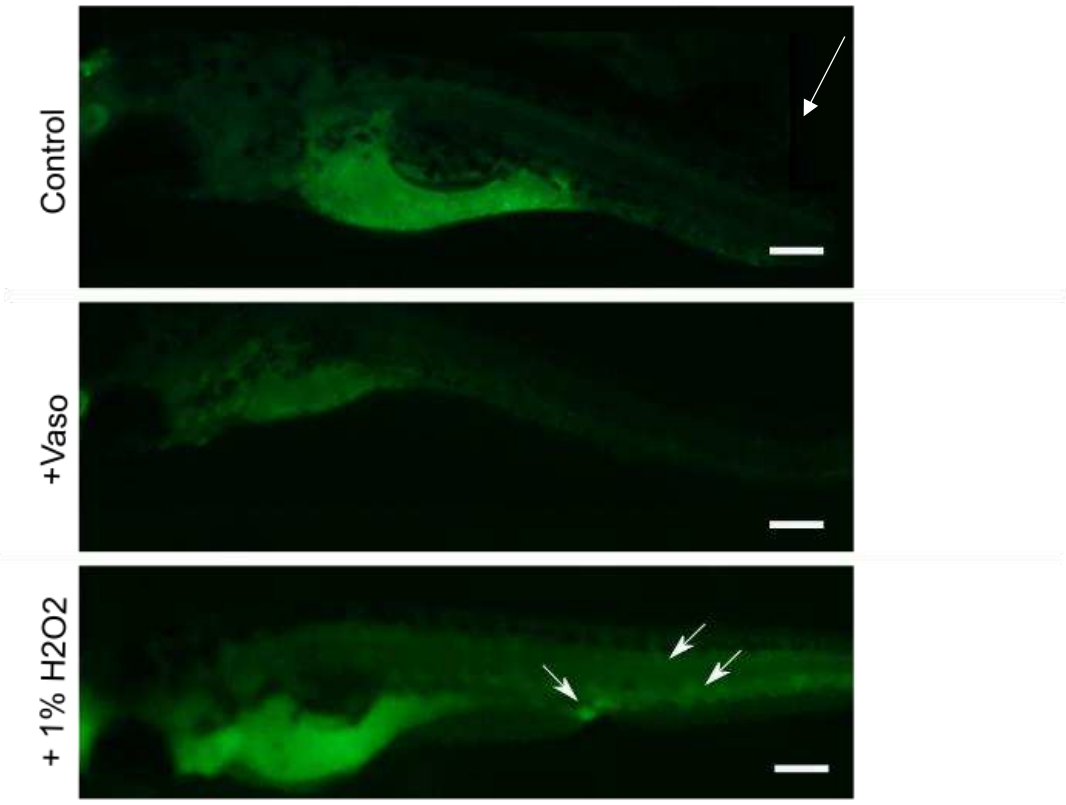

Supplemental Figure 1.2: Vasopressin application does not detectably cause cell death by 72hpf. Acridine orange stain was applied to detect cell death in embryos. Control and vasopressin-treated embryos have no significant signal other than the yolk autofluorescence, while positive control embryos treated with 1% H_2O_2 show foci throughout (indicated by the white arrows). Foci indicate cell death.

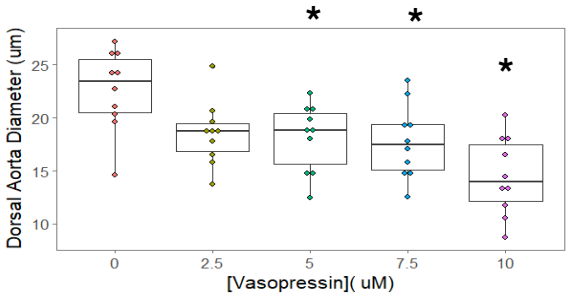

Supplemental Figure 1.3: Vasopressin application induces a dose-dependent constriction on the zebrafish dorsal aorta by 40hpf. Statistical significance was determined using Anova. N= 10 embryos were analyzed for each dose. Control vs 5 µM, p = 0.04; control vs 7.5 µM, p = 0.02; control vs 10 µM, p < 0.0001 .

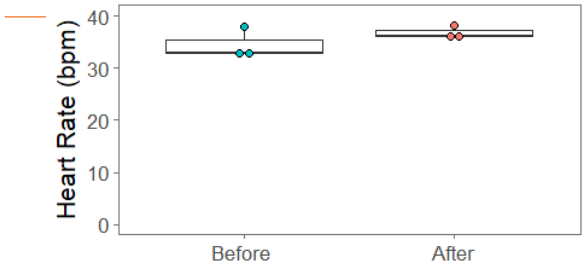

Supplemental Figure 1.4: Vasopressin exposure does not result in immediate changes in cardiac function. After 5 minutes of vasopressin-exposure, heart rates of 24hpf embryos did not change. N = 3 control, and 3 vaso-treated embryos. P = 0.29

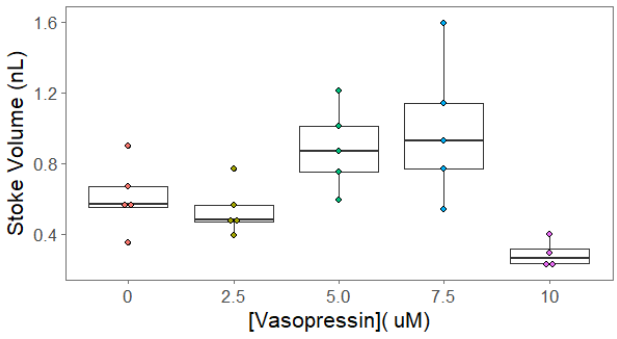

Supplemental Figure 1.5: Increased afterload does not significantly alter stroke volume; however, hearts under extremely high afterload trend toward decreased afterload. Dunnet's test was used to assess statistical significance. N=5 fish analyzed per treatment. Control vs 2.5 µM, p = 0.93; control vs 5 µM, p = 0.25; control vs 7.5 µM, p = 0.07; control vs 10 µM, p = 0.19.

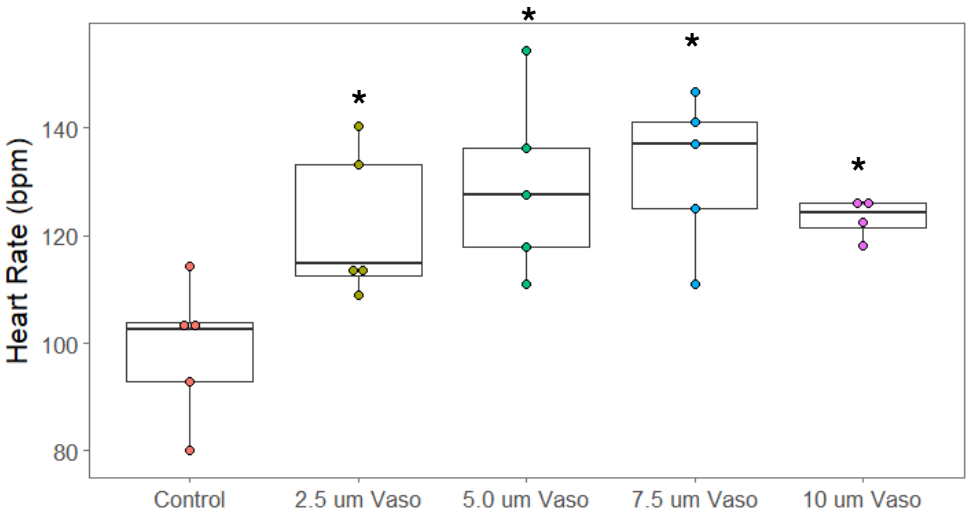

Supplemental Figure 1.6: Increasing concentrations of vasopressin produce increases in heart rate at 40 hpf. Dunnett's test was used to assess statistical significance. * indicates $p<0.05$. N=5 fish analyzed per treatment. Control vs 2.5 µM, p = 0.04; control vs 5 µM, p = 0.007; control vs 7.5 µM, p = 0.003; control vs 10 µM, p = 0.04.

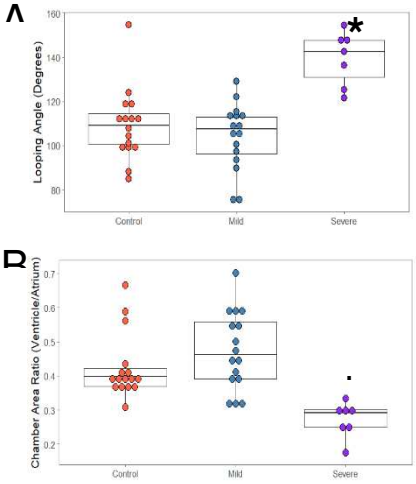

Supplementary Figure 1.7: A portion of the 10µM vasopressin-treated embryos demonstrate overt morphological defects. A) Looping angle is significantly increased in the "severe" group, but not in the mild group. P = 0.002 for control vs severe, p = 0.52 for control vs mild by Dunnett's test. B) Chamber area ratio is significantly decreased in severe group, but not in the mild. P = 0.002 for control vs severe, p = 0.25 for control vs mild by Dunnett's test. N= 15 control, 16 mild, and 7 severe.

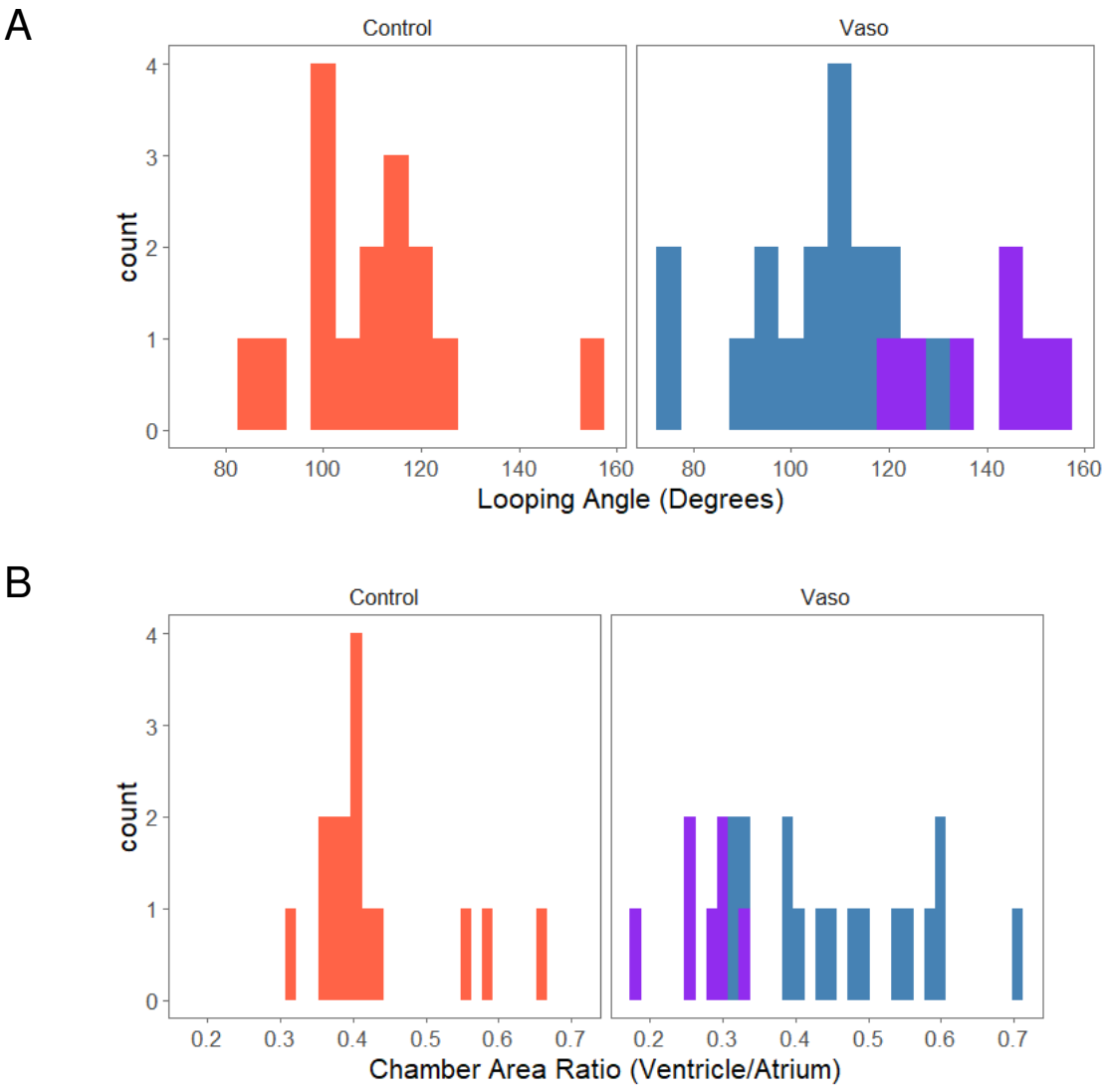

Supplementary Figure 1.8: In 10 um vasopressin treatments, the severely affected embryos cluster separately from the mildly affected group. A) Histograms of number of embryos vs looping angle or B) chamber area ratio in control and vasopressin-treated groups. Orange represents control embryos, blue represents mildly affected embryos, and purple represents severely affected embryos. N= 15 control, 16 mild, and 7 severe vasopressin-treated embryos.

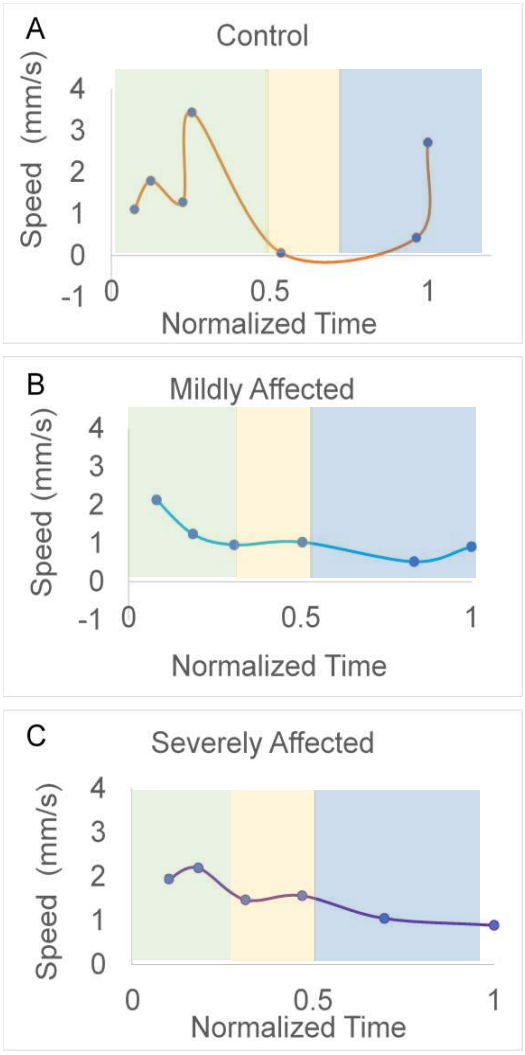

Supplementary Figure 1.9: Cardiac contraction patterns are altered similarly in mildly and severely affected embryos at 40 hpf. A) Contraction wave of a representative A) control, B) mildly-affected, and C) severely affected 10 µMvasopressin-treated embryo. n = 11 control , 15 mildly-affected, and 5 severely-affected embryos. 0 normalized time represents start of atrial contraction. Green shading represents the atrium, yellow represents the AVJ, and blue represents the ventricle.

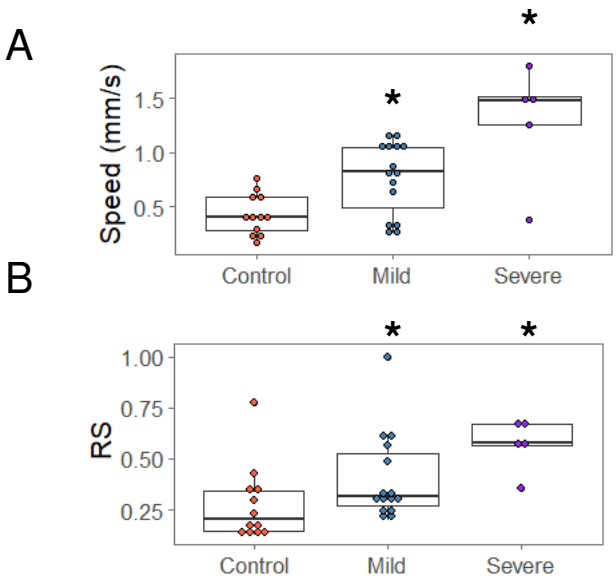

Supplementary Figure 1.10: The speed of the contraction through the AVJ is significantly increased in both mildly-affected, and severely-affected vasopressin-treated embryos. A) Speed of the contraction wave through the AVJ. B) Relative speed of the contraction wave – results have been normalized to the peak velocity of the contraction wave. N= 11 control, 15 mild, and 7-severe vasopressin-treated embryos. For the speed of contraction wave, p = 0.03 for control vs mild, and p =0.003 for control vs severe by Dunnett's test. For the relative speed, p =0.04 for control vs mild, p =0.003 for control vs severe.

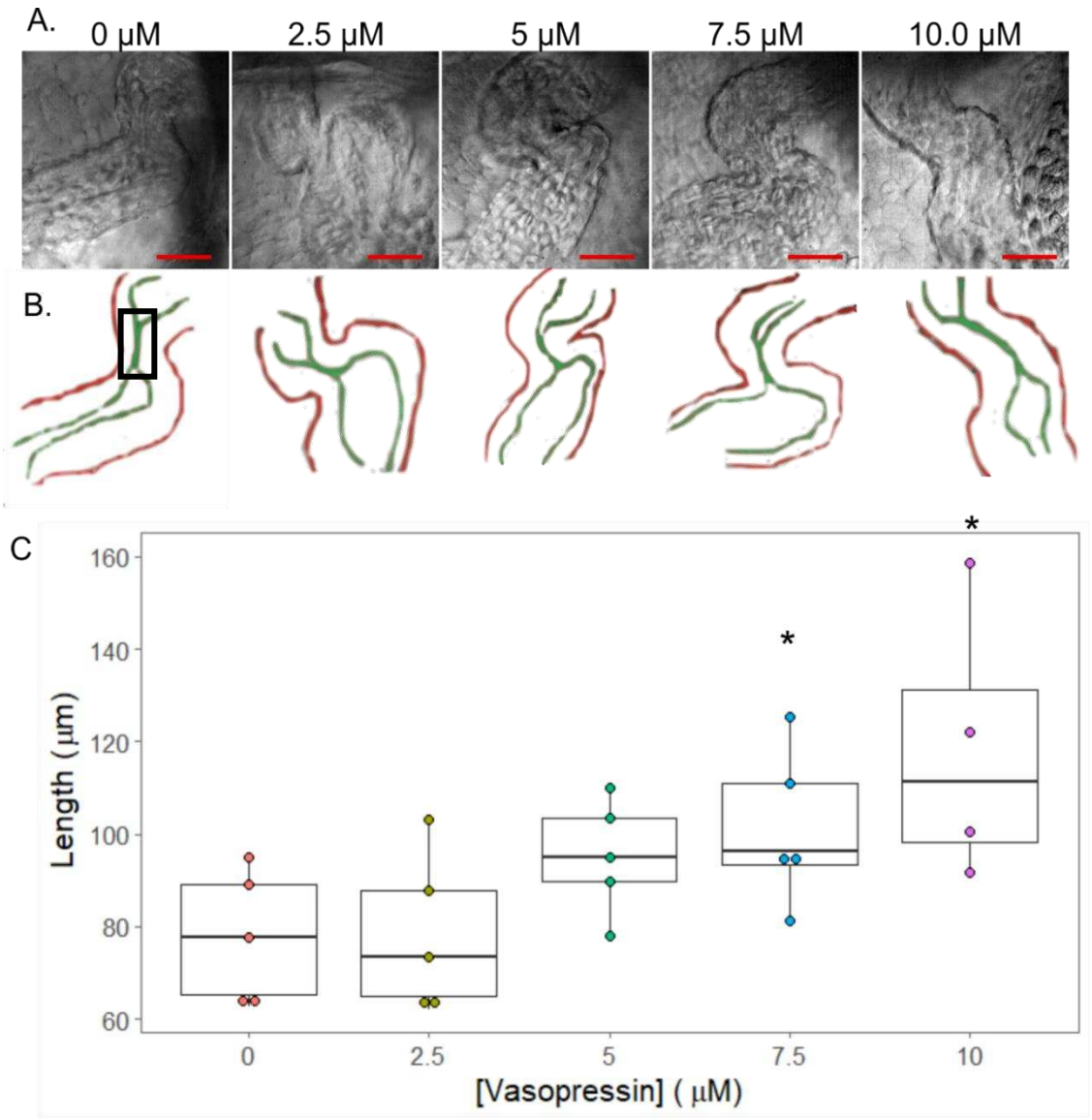

Supplementary Figure 1.11: Length of endothelial closure increases in a dose-dependent manner in response to afterload at 40 hpf. A) Endothelial closure at the end of ventricular systole at varying doses of vasopressin. B) Tracings of hearts. Red represents outer (myocardial) wall, green represents inner (endocardial) layer. The regions where the endocardial layers meet was quantified as the "length of endocardial closure" in C. Black box in control panel indicates the region being measured. C) Length of endothelial closure increases as vasopressin concentration increases. ANOVA was used to determine statistical significance, followed by Tukey's test. * indicates $p < 0.05$. Control vs 2.5 µM, $p = 0.99$; control vs 5 µM, $p = 0.57$; control vs 7.5 µM, $p = 0.04$, control vs 10 µM, $p = 0.01$.

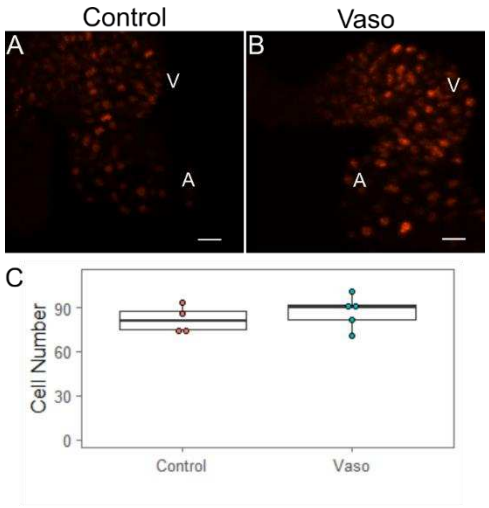

Supplementary Figure 1.12: Ventricular cardiomyocyte cell number is not affected by vasopressin-treatment. Maximum intensity projections of A) Control and B) vaso-treated embryos at 56 hpf. n = 4 control and 5 vaso-treated embryos. P = 0.48

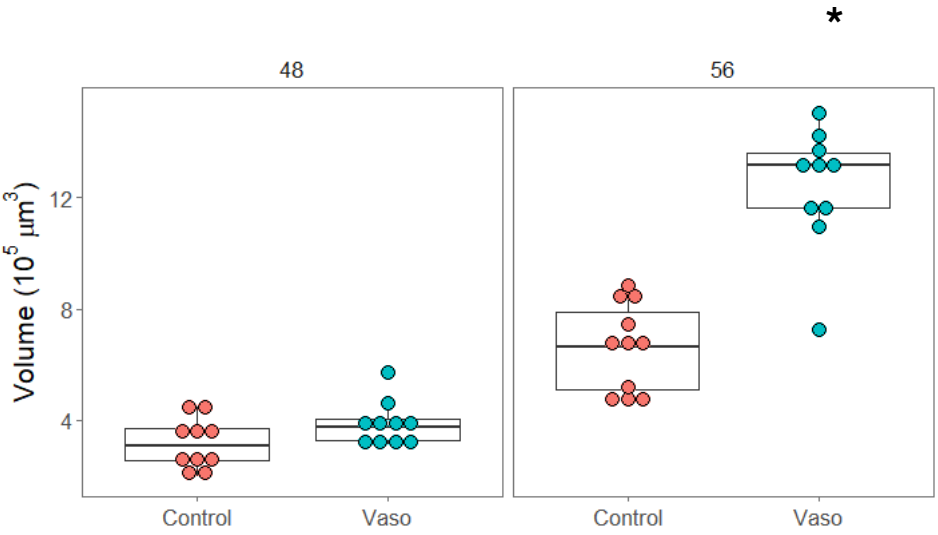

Supplementary Figure 1.13: Application of Vasopressin Mimics Known Effects of Increased Afterload. n = 10 fish per group (vasopressin treated or control) per time point. A Student's T-test was used to determine statistical significance, * indicates $p < 0.05$. Error bars represent standard deviations.

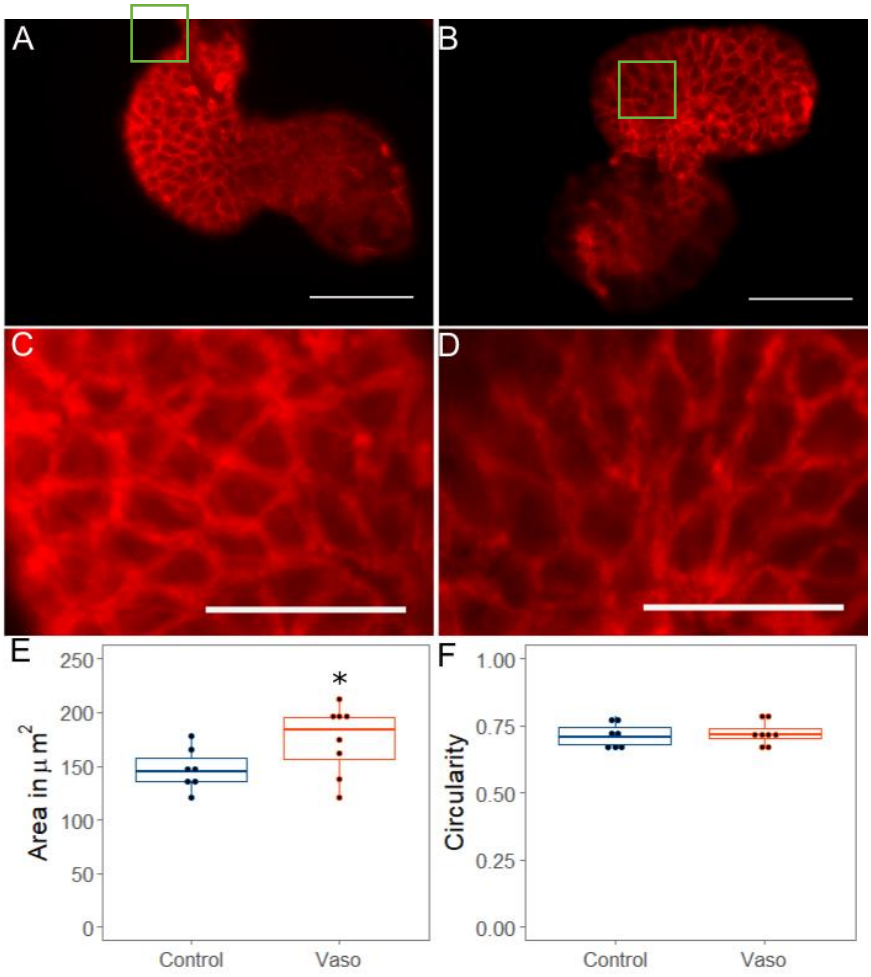

Supplementary Figure 1.14: Application of Vasopressin Mimics Known Effects of Increased Afterload. A) Control heart at 52 hpf. B) Vasopressin-treated heart at 52 hpf. Scale bar represents 20 µm. C) Control ventricle at 52 hpf. D) Vasopressin-treated heart at 52 hpf. Scale bar represents 20 µm. E) Area and F) Circularity of myocardial cells in the ventricle of control and vaso-treated hearts.N= 7 for wildtype hearts, n =7 for vasopressin-treated hearts. 5 myocytes were analyzed per heart. Student's T-test was used to determine statistical significance, * indicates $p < 0.05$.

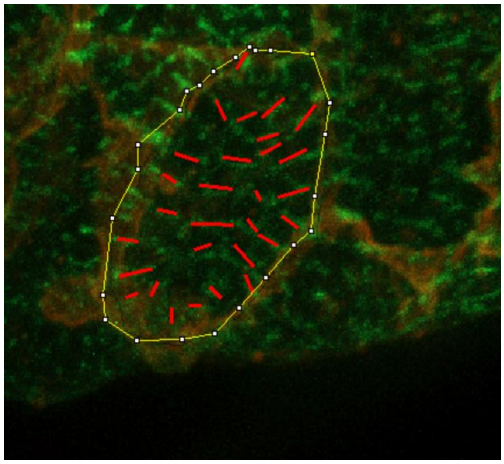

Supplementary Figure 1.15: Example of how total z-band size /cell (TBZ) was calculated. Red lines trace the GFP-labeled z discs, while the yellow line traces the myocardial cell border. Both the cross-sectional area of the cell and the length of each z- band was quantified in Image J. The individual lengths of z- band were summed together in each cell measured, this was termed "Total Z-band Size." Total z-band size was then divided by the area of the cell to normalize for cell size differences. Over 2000 z-bands were measured in both the control and vasopressin-treated groups.

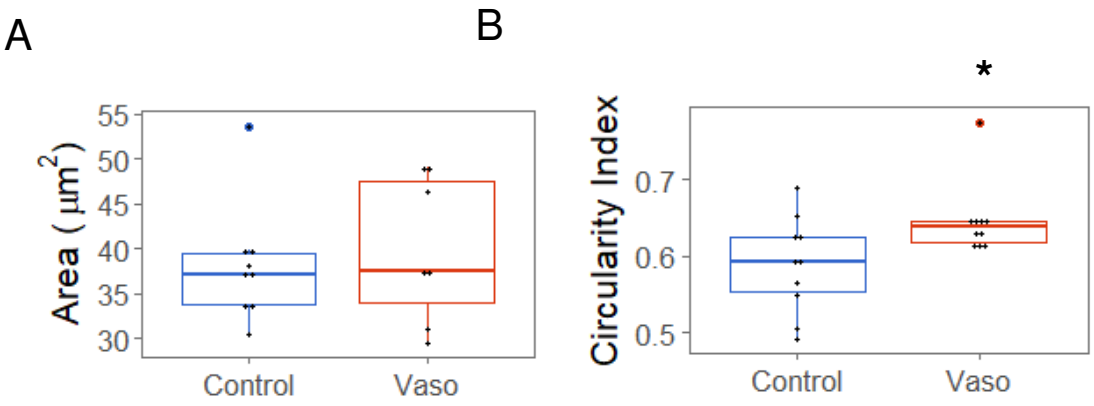

Supplementary Figure 1.16. Myocardial AVJ cells adopt altered morphology in response to high afterload. N = 11 wildtype hearts, 10 vasopressin treated hearts. Statistical significance was determined using Student's T-test; * indicates $p < 0.05$. A) and B) Analysis of myocardial cells. 5 cells were analyzed per location per heart, area was measured for each cell and averaged. AVJ myocardial cells were defined as myocardial cells located in the constriction between the atrium and ventricle.

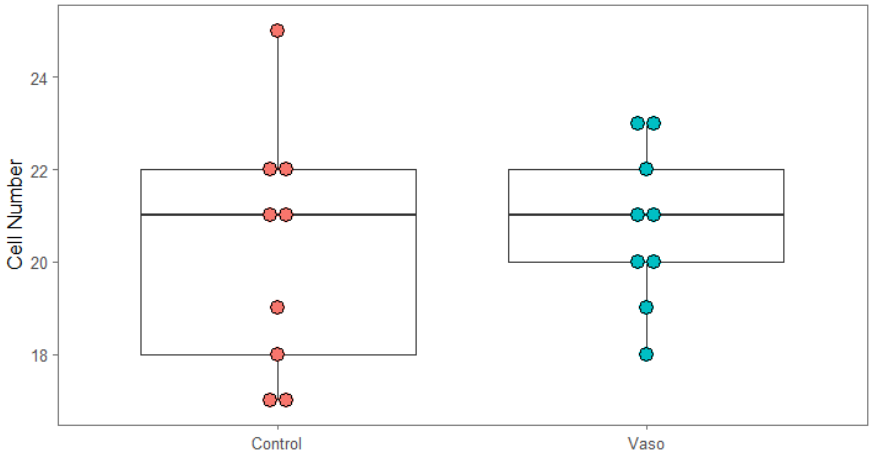

Supplementary Figure 1.17: Total endocardial cells located in AVJ is not affected by vasopressin-treatment at 72 hpf. AVJ endocardial cells were defined as fli-positive cells located in the constriction between the atrium and ventricle. P=0.60.

APPENDIX 2: Supplemental Material for Chapter 3

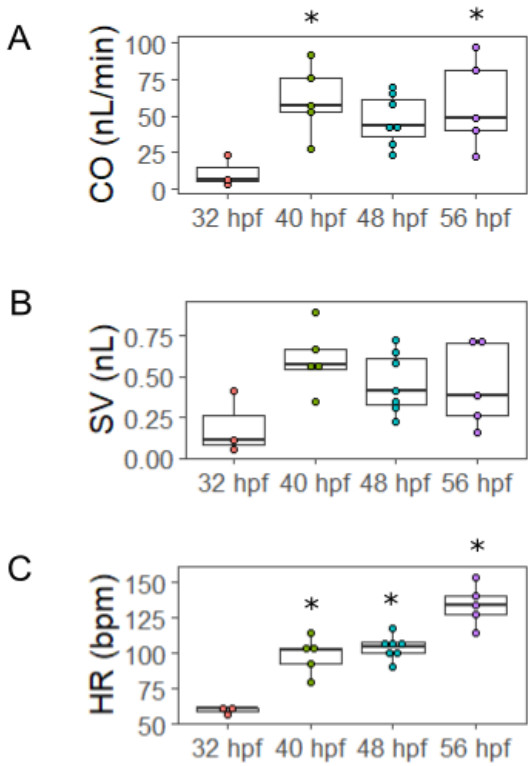

Supplementary Figure 2.1: Changes in heart rate mediate increases in cardiac output between 32 and 56 hpf. A) Cardiac ouput increases between 32 and 40 hpf. p = 0.02 for 32 v 40, 0.08 for 32 vs 48 hpf, 0.03 for 32 by 56 hpf (Dunnets test). B) Stroke volume does not significantly change between 32 and 56 hpf. C) Heart rate linearly increases through developmental time. p-value for 32hpf vs 40 hpf = 0.0005, p-value for 32hpf vs 48 hpf = 0.0001, 32hpf vs 56 hpf < 0.0001 by Dunnett's test. n =3 embryos at 32, 5 embryos at 40, 7 embryos at 48 hpf, and 5 embryos at 56 hpf;

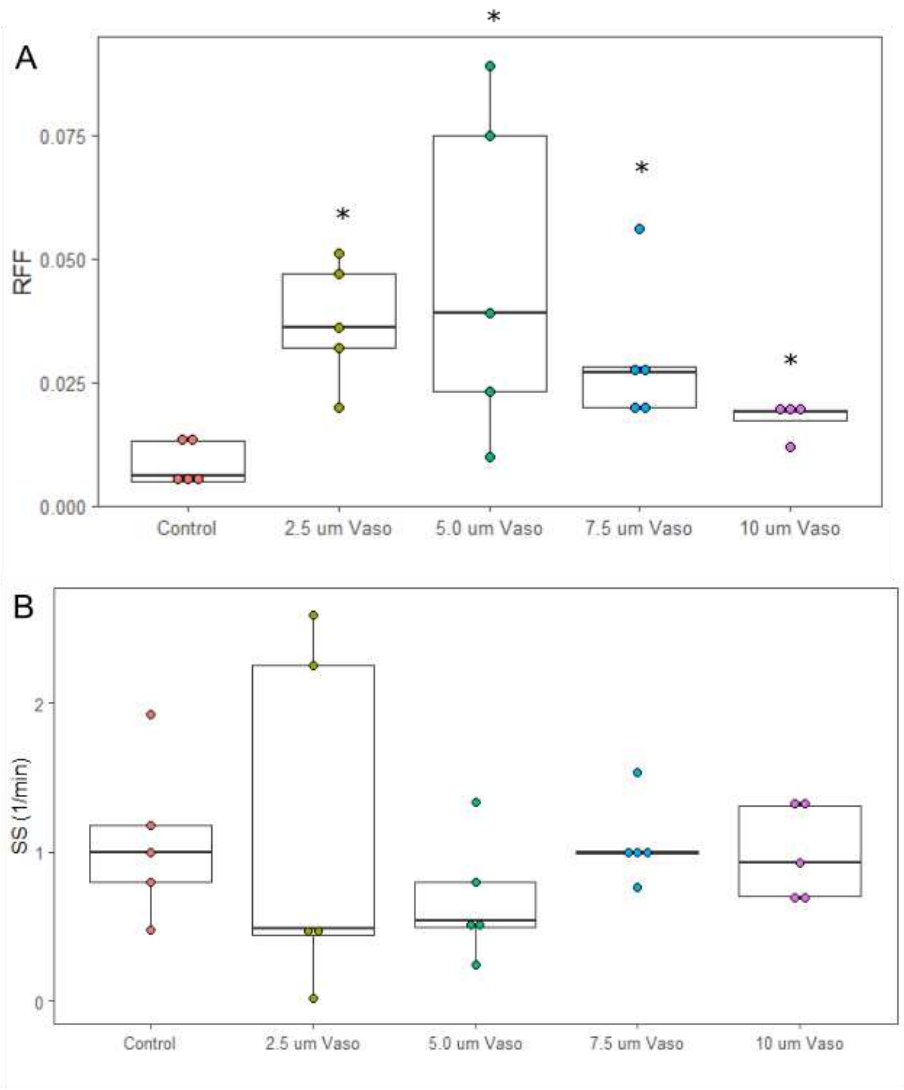

Supplementary Figure 2.2: Vasopressin-treatment increases RF, but not shear stress by 56 hpf. A) RFF increases with increasing vasopressin dose. p = 0.02 for control vs 2.5, 0.01 for control vs 5, 0.03 for control vs 7.5, 0.04 for control vs 10, by Dunn's Test B) Shear stress at the AVJ is not significantly altered. P =0.72 by anova.

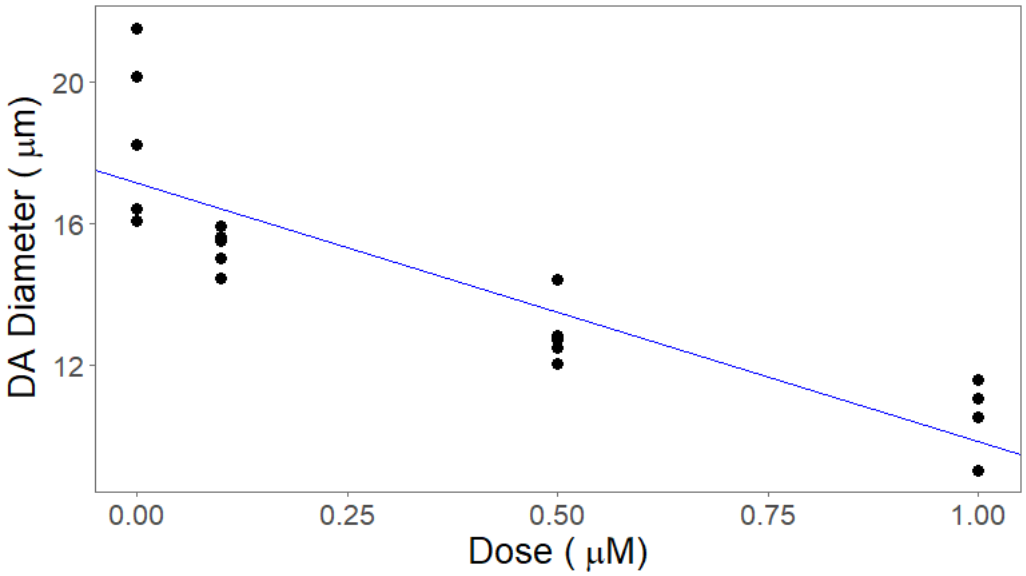

Supplemental Figure 2.3: Increasing the concentration of vasopressin produces a dose dependent vasoconstrictive effect at 72 hpf. Each dot represents one fish, blue line is line of best fit. R^2 = 0.77. Trendline equation determined in R.

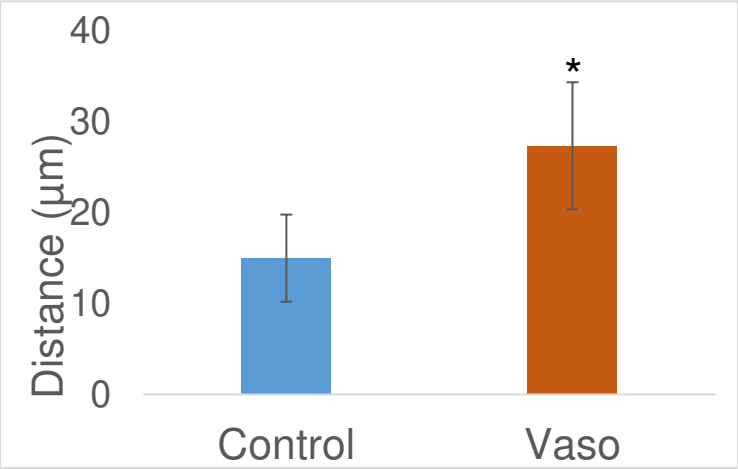

Supplemental Figure 2.4: Cardiac jelly production is expanded at the ventricle. Distance between myocardium and endocardium at the outer curvature of the ventricle. N= 9 vasopressin-treated, 7 control heats. Student's t-test was used to determine statistical significance. P=0.04.

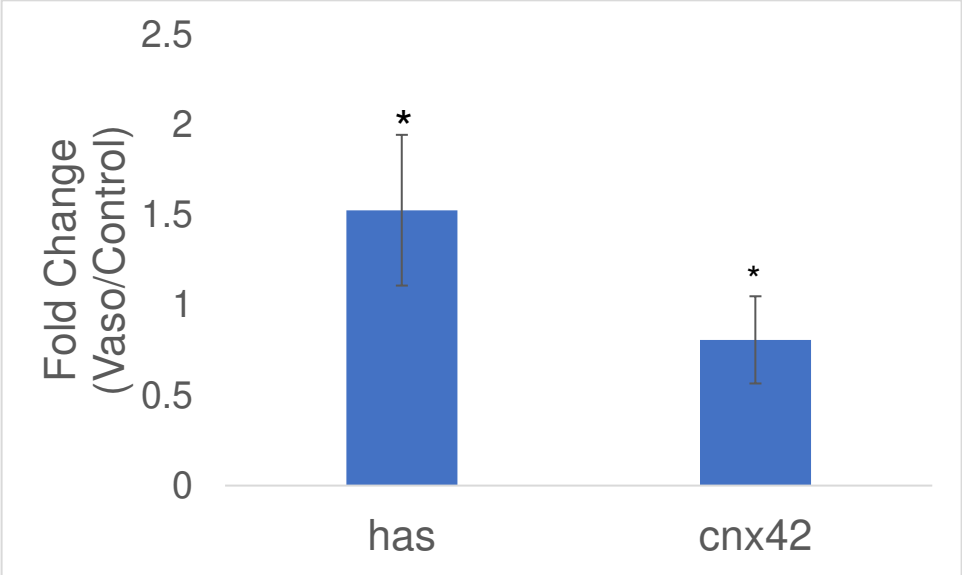

Supplemental Figure 2.5: Key cardiac jelly components and extracellular matrix genes are differentially expressed in cardiac tissue. Specifically, there is 1.4 fold increase in the production of has2, a primary component of cardiac jelly. There was no change in expression of control gene, cnx42. 10 hearts were pooled per condition, 2µg of RNA was extracted and reverse-transcribed into cDNA. *Efα* was used as a reference gene. Pfaffl analysis was performed to determine fold change.

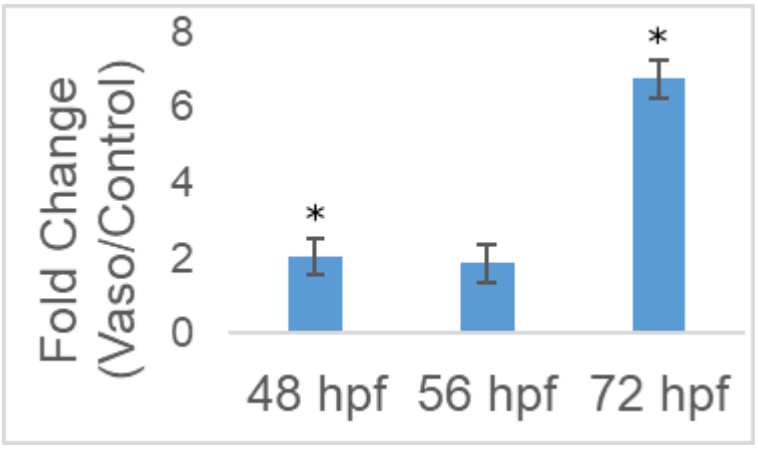

Supplemental Figure 2.6: Klf2a expression is increased in vasopressin-treated embryos. qRT-PCR of control and vasopressin treated hearts at 48,56,and 72 hpf. 10 hearts were pooled per condition, 2µg of RNA was extracted and reverse-transcribed into cDNA. *Efα* was used as a reference gene. Orange line represents a 1-fold change in expression (no difference between control and vaso). The Pfaffl method was to analyze data. Statistical significance was determined using a Student's T-test. P = 0.01 for 48hpf, 0.06 for 56 hpf, and 0.03 for 72hpf.

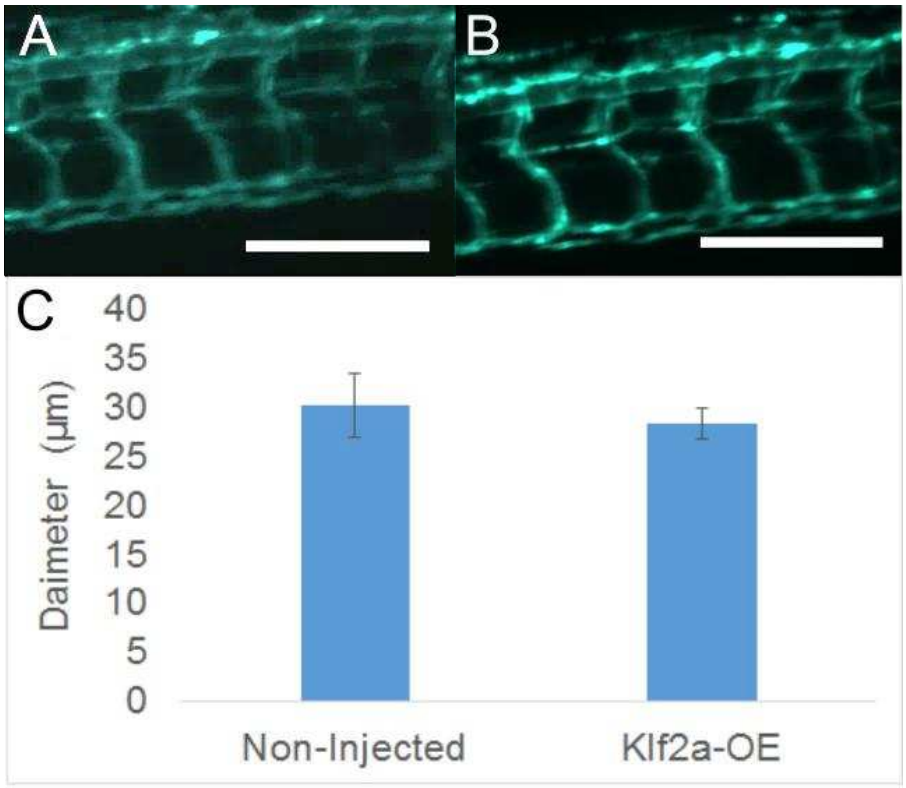

Supplementary Figure 2.7: Klf2a-OE does not significantly change the vasculature. A) Control and B) vaso-treated vessels at 72 hpf. Images were taken above the yolk extension as in Figure 1. C) Klf2a-OE does not cause a significant constriction at 72 hpf in the dorsal aorta. N=10 for both control and vasopressin-treated groups. P=0.4. Scale bar represent 50 um.

APPENDIX 3: Supplemental Material for Chapter 4

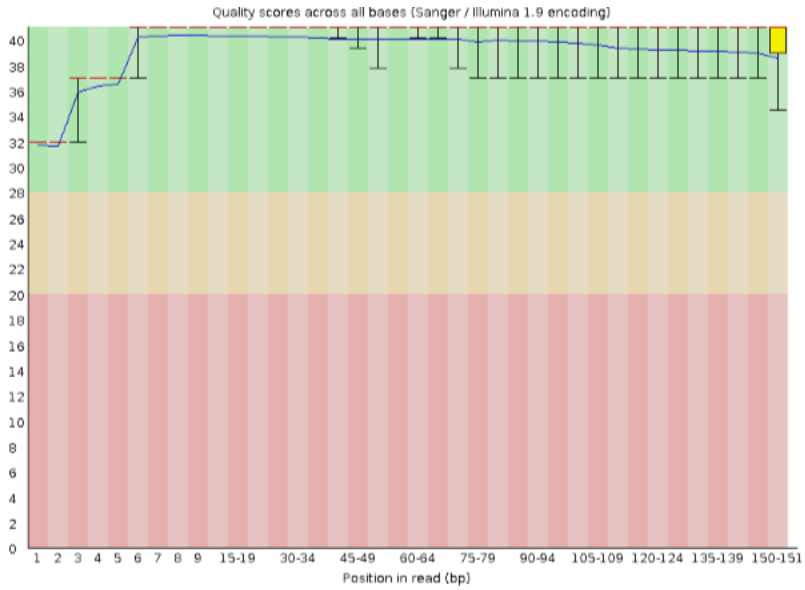

Supplemental Figure 3.1: Representative plot of quality scores (Phred) across a read post trimming. The average quality score is above 30 across the entire length of the read.

Supplemental Table 3.1: These 4 genes were commonly upregulated in chamber myocytes and AVJ myocytes as compared to immature myocytes.

ID	Gene Name	Function
ENSDARG00000063910	atp8	ATP synthase 8
ENSDARG00000080401	NC_002333	none
ENSDARG00000081938	NC_002333.13	none
ENSDARG00000082789	NC_002333.18	none

Supplemental Table 3.2: List of genes co-downregulated in AVJ and chamber myocytes.

NAME	DESCRIPTION
NUP155	nucleoporin 155 [Source:ZFIN;Acc:ZDB-GENE-040426-711]
PRKACBA	protein kinase, cAMP-dependent, catalytic, beta a [Source:ZFIN;Acc:ZDB-GENE-040426-1351]
PLK4	polo-like kinase 4 (Drosophila) [Source:NCBI gene;Acc:368390]
RAD52	RAD52 homolog, DNA repair protein [Source:ZFIN;Acc:ZDB-GENE-050731-10]
SELE	selectin E [Source:ZFIN;Acc:ZDB-GENE-041014-221]
ENPP2	ectonucleotide pyrophosphatase/phosphodiesterase 2 [Source:ZFIN;Acc:ZDB-GENE-040426-1156]
METTL21A	methyltransferase like 21A [Source:NCBI gene;Acc:541441]
MCM9	minichromosome maintenance 9 homologous recombination repair factor [Source:NCBI gene;Acc:555610]
IPO9	importin 9 [Source:ZFIN;Acc:ZDB-GENE-040426-2953]
RAD54L	RAD54 like [Source:ZFIN;Acc:ZDB-GENE-040426-968]
FGL2A	fibrinogen-like 2a [Source:ZFIN;Acc:ZDB-GENE-030131-9506]
NKX2.7	NK2 transcription factor related 7 [Source:ZFIN;Acc:ZDB-GENE-990415-179]
SLC4A1B	solute carrier family 4 member 1b (Diego blood group) [Source:ZFIN;Acc:ZDB-GENE-110215-2]
SUV39H1A	suppressor of variegation 3-9 homolog 1a [Source:NCBI gene;Acc:445198]
SLC2A15A	solute carrier family 2 member 15a [Source:ZFIN;Acc:ZDB-GENE-060531-109]
PARPBP	PARP1 binding protein [Source:NCBI gene;Acc:678635]
HSPA12B	heat shock protein 12B [Source:ZFIN;Acc:ZDB-GENE-070226-1]
ZGC:171776	zgc:171776 [Source:ZFIN;Acc:ZDB-GENE-071004-36]
ANAPC4	anaphase promoting complex subunit 4 [Source:ZFIN;Acc:ZDB-GENE-041212-10]
HS1BP3	HCLS1 binding protein 3 [Source:ZFIN;Acc:ZDB-GENE-131121-391]
ANKLE2	ankyrin repeat and LEM domain containing 2 [Source:ZFIN;Acc:ZDB-GENE-030131-6090]
NMRK1	nicotinamide riboside kinase 1 [Source:ZFIN;Acc:ZDB-GENE-050320-8]
ENTPD4	ectonucleoside triphosphate diphosphohydrolase 4 [Source:ZFIN;Acc:ZDB-GENE-040718-116]
SULF1	sulfatase 1 [Source:ZFIN;Acc:ZDB-GENE-030131-9242]
CEACAM1	CEA cell adhesion molecule 1 [Source:ZFIN;Acc:ZDB-GENE-010724-14]
ABRAXAS1	abraxas 1, BRCA1 A complex subunit [Source:NCBI gene;Acc:449820]
POLA1	polymerase (DNA directed), alpha 1 [Source:ZFIN;Acc:ZDB-GENE-030114-9]
GCM2	glial cells missing transcription factor 2 [Source:ZFIN;Acc:ZDB-GENE-050127-1]
DRAM1	DNA-damage regulated autophagy modulator 1 [Source:ZFIN;Acc:ZDB-GENE-041010-147]
S1PR5B	sphingosine-1-phosphate receptor 5b [Source:ZFIN;Acc:ZDB-GENE-061201-27]
MYB	v-myb avian myeloblastosis viral oncogene homolog [Source:ZFIN;Acc:ZDB-GENE-991110-14]
FBL	fibrillarin [Source:ZFIN;Acc:ZDB-GENE-040426-1936]
SLC29A1B	solute carrier family 29 member 1b [Source:ZFIN;Acc:ZDB-GENE-130415-4]
GHRA	growth hormone receptor a [Source:ZFIN;Acc:ZDB-GENE-070509-1]
FANCC	FA complementation group C [Source:ZFIN;Acc:ZDB-GENE-060510-2]

ZGC:110045	zgc:110045 [Source:ZFIN;Acc:ZDB-GENE-050706-149]
HAUS3	HAUS augmin-like complex, subunit 3 [Source:ZFIN;Acc:ZDB-GENE-060929-592]
NCAPH	non-SMC condensin I complex, subunit H [Source:ZFIN;Acc:ZDB-GENE-070112-652]
IGHMBP2	immunoglobulin mu DNA binding protein 2 [Source:ZFIN;Acc:ZDB-GENE-050419-258]
HOXC3A	homeobox C3a [Source:NCBI gene;Acc:30421]
ZGC:109744	zgc:109744 [Source:ZFIN;Acc:ZDB-GENE-050809-146]
SMYD5	SMYD family member 5 [Source:ZFIN;Acc:ZDB-GENE-040912-39]
SI:CH211-194M7.3	si:ch211-194m7.3 [Source:ZFIN;Acc:ZDB-GENE-131121-19]
ETAA1	ETAA1 activator of ATR kinase [Source:ZFIN;Acc:ZDB-GENE-080204-12]
APCDD1L	adenomatosis polyposis coli down-regulated 1-like [Source:ZFIN;Acc:ZDB-GENE-121022-3]
ZFYVE16	zinc finger, FYVE domain containing 16 [Source:ZFIN;Acc:ZDB-GENE-091116-62]
C9H3ORF38	si:ch211-261p9.4 [Source:ZFIN;Acc:ZDB-GENE-081104-205]
CEP70	centrosomal protein 70 [Source:ZFIN;Acc:ZDB-GENE-070705-311]
BLM	BLM RecQ like helicase [Source:ZFIN;Acc:ZDB-GENE-070702-5]
OAFB	OAF homolog b (Drosophila) [Source:ZFIN;Acc:ZDB-GENE-121017-2]
DNA2	DNA replication helicase/nuclease 2 [Source:ZFIN;Acc:ZDB-GENE-090313-71]
WDR90	WD repeat domain 90 [Source:ZFIN;Acc:ZDB-GENE-070424-67]
FAM117AB	family with sequence similarity 117 member Ab [Source:ZFIN;Acc:ZDB-GENE-080515-7]
LPXN	leupaxin [Source:ZFIN;Acc:ZDB-GENE-081105-159]
ZGC:85936	zgc:85936 [Source:ZFIN;Acc:ZDB-GENE-040426-2450]
ATXN7L1	ataxin 7-like 1 [Source:ZFIN;Acc:ZDB-GENE-131127-383]
RAD54B	RAD54 homolog B [Source:ZFIN;Acc:ZDB-GENE-060810-50]
SI:CH73-112L6.1	si:ch73-112l6.1 [Source:ZFIN;Acc:ZDB-GENE-091204-14]
SI:CH1073-186O8.3	si:ch1073-186o8.3 [Source:ZFIN;Acc:ZDB-GENE-131126-56]
CENPH	centromere protein H [Source:ZFIN;Acc:ZDB-GENE-081104-340]
MS4A17A.10	membrane-spanning 4-domains, subfamily A, member 17A.10 [Source:ZFIN;Acc:ZDB-GENE-080829-3]
CR354383.1	None
FP101861.1	None
SI:DKEY-195M11.8	si:dkey-195m11.8 [Source:ZFIN;Acc:ZDB-GENE-030131-3092]
ZGC:112970	zgc:112970 [Source:NCBI gene;Acc:541543]
CCNE1	cyclin E1 [Source:NCBI gene;Acc:30188]
GCH2	GTP cyclohydrolase 2 [Source:ZFIN;Acc:ZDB-GENE-001205-3]
CU915256.1	XK-related protein 8-like [Source:NCBI gene;Acc:100148479]
SI:DKEY-25O1.7	si:dkey-25o1.7 [Source:ZFIN;Acc:ZDB-GENE-091204-375]
SLC29A1A	solute carrier family 29 member 1a [Source:ZFIN;Acc:ZDB-GENE-050913-138]
HAUS6	HAUS augmin-like complex, subunit 6 [Source:NCBI gene;Acc:558814]
LAPTM5	lysosomal protein transmembrane 5 [Source:ZFIN;Acc:ZDB-GENE-170303-1]
ZGC:136410	zgc:136410 [Source:ZFIN;Acc:ZDB-GENE-060421-6071]
CRY2	cryptochrome circadian regulator 2 [Source:ZFIN;Acc:ZDB-GENE-010426-6]
CABZ01110379.1	None
CT978957.2	None
E2F1	E2F transcription factor 1 [Source:ZFIN;Acc:ZDB-GENE-131024-3]
CU929079.2	None

FOXI1	forkhead box i1 [Source:ZFIN;Acc:ZDB-GENE-030505-1]
ETF1A	eukaryotic translation termination factor 1a [Source:ZFIN;Acc:ZDB-GENE-080218-14]
CABZ01113599.1	None
SI:CH211-147M6.1	si:ch211-147m6.1 [Source:ZFIN;Acc:ZDB-GENE-131120-57]
FO834799.1	Fanconi anemia group A protein-like [Source:NCBI gene;Acc:110438398]
CABZ01080371.2	wu:fj30f06 [Source:NCBI gene;Acc:792477]
CABZ01072848.1	None

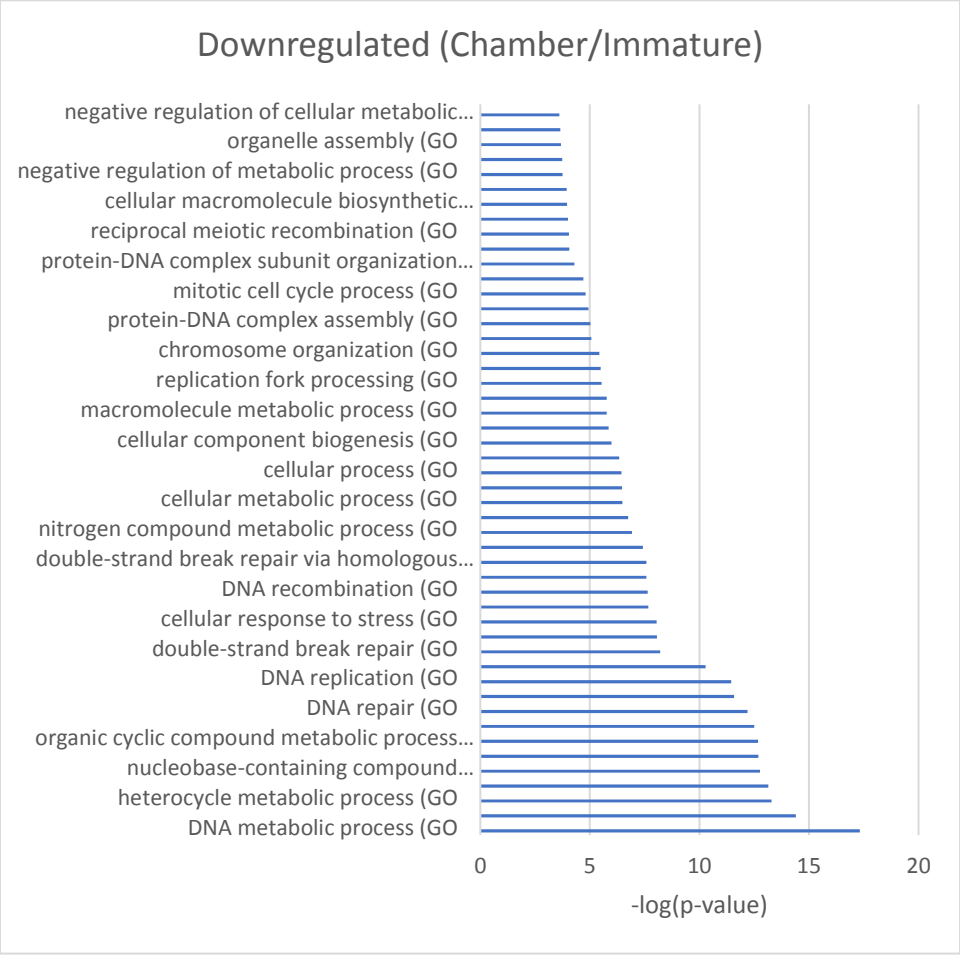

Supplemental Figure 3.2: Gene ontology analysis of genes downregulated exclusively in chamber myocytes as compared to immature myocytes.

Supplementary Table 3.4: 12 genes that were co-differentially expressed between AVJ/chamber and chamber/immature myocytes.

Gene	Name	Function	Heart Phenotype
ENSDARG00000009748	dffb	aptopsis factor	
ENSDARG00000009553	gng3	g-protein, involved in signal transduction	mutant mice have heart failure
ENSDARG00000013794	klf 11 b	transcription factor	downregulated in heart failure, overexpression prevents hypertrophy in adults
ENSDARG00000002509	zgc:153911	plasma membrane protein	
ENSDARG00000012684	apt2b1a	Ca2+ aptpase	
ENSDARG00000004954	grna	paracrine factor	involved in epicardial developemnt, heart failure
ENSDARG00000021113	ptma	prothymosin	expressed in heart
ENSDARG00000008986	e2f7	transcription factor	
ENSDARG00000014209	ODFl2	extracellular matrix protein	associated with coronary disease
ENSDARG00000019098	cd82a	prevents cell division	marks cardiomyocyte fated progenitors
ENSDARG00000012389	adar	RNA binding protein	Strongly associated with CHD
ENSDARG00000007359	UBL4a	ubiquitin like 4a	UBL4a

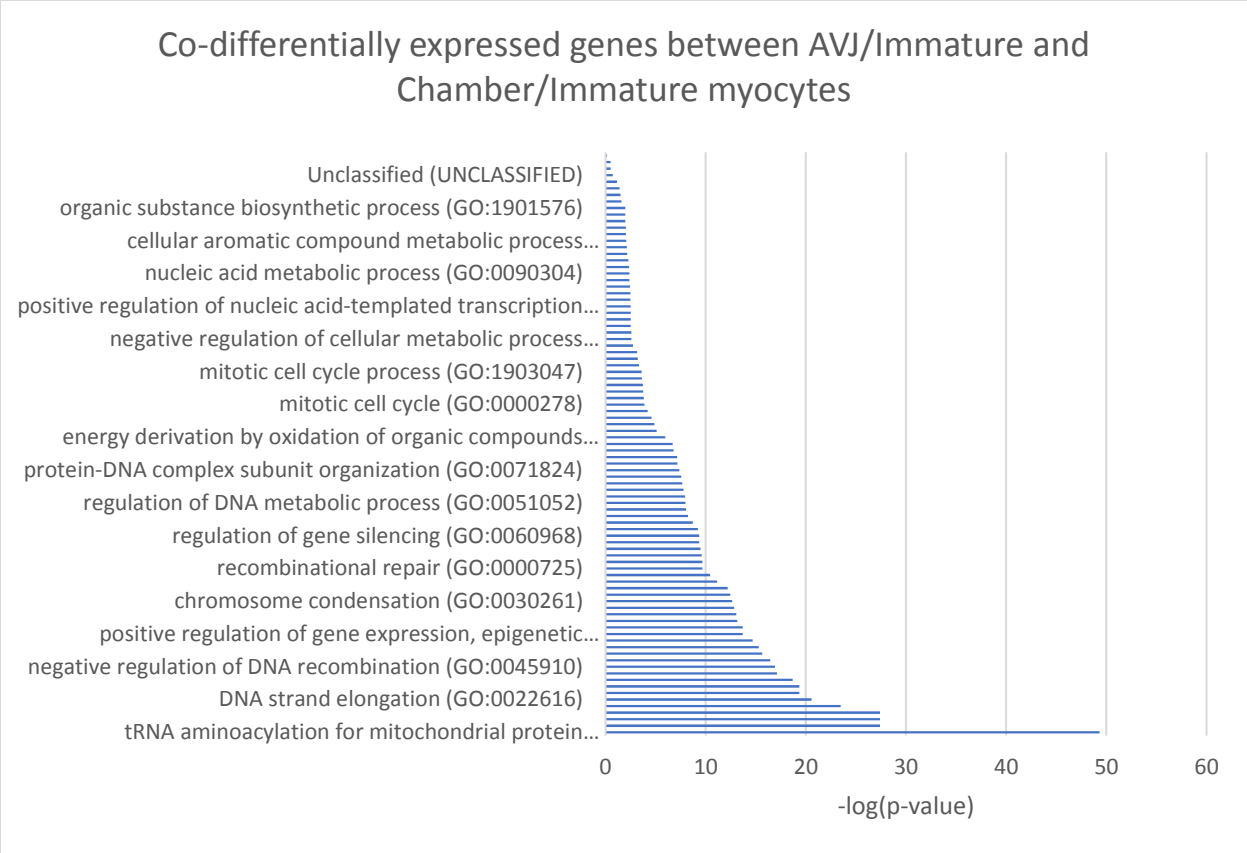

Supplementary Figure 3.3: Gene ontology analysis of genes co-differentially regulated in between chamber/immature and AVJ/immature myocytes.S